INVESTIGATION OF EPIDERMAL GROWTH FACTOR RECEPTOR IN LIVE CELLS BY VARIOUS FLUORESCENCE CROSS-CORRELATION SPECTROSCOPY MODALITIES

SIBEL YAVAS

(DIPLOMA, JOHANNES-GUTENBERG-UNIVERSITY;

MAINZ)

A THESIS SUBMITTED
FOR THE DEGREE OF DOCTOR OF PHILOSOPHY
DEPARTMENT OF CHEMISTRY
NATIONAL UNIVERSITY OF SINGAPORE
2016

Declaration

I hereby declare that this thesis is my original work and it has been written by me in its entirety. I have duly acknowledged all the sources of information which have been used in the thesis.

This thesis has also not been submitted for any degree in any university previously.

_____

Sibel Yavas

19 August 2016

Acknowledgments

I would firstly like to thank my supervisor Prof. Thorsten Wohland for his guidance, active support and constant motivation during my studies.

A special thanks also goes to Radek Machan, who helped me in during the period of my research. I am also thankful to my lab colleagues - Angela, Jagadish, Xue Wen, Kamal, Shuangru, Anjali, Andreas, Sarala and Saptha for their friendships, feedback and open discussions. The long days (which sometimes extended to nights) that I spent working in the lab together with CBIS members was a great experience and will always remain in my memory.

Outside the lab, I would also like to extend my thanks to all my friends that I met during my time in Singapore. Especially many thanks to my dearest friends Katja, Buse, Anurag and Erhan for their support and friendship during these four years. Thank so to my friend Erdinc for being so supportive.

And lastly to my parents Sevgi and Salih for believing in me, for their love and constant support.

Table of Content

Summary

The aim of this work was to investigate the effects of external factors on EGFR complex fractions, since substaintial discrepanies exist in preformed Epidermal Growth Factor Receptor (EGFR) levels. In this regard, we investigated the different experimental conditions, which influenced the dynamics of EGFR in living cells, by using various Fluorescence Cross-Correlation Spectroscopy (FCCS) modalities.

Chapter 1 provides an overview about the biological background of the EGFR. It summarizes important aspects about EGFR signaling pathways, dimerization of the receptor, the clinical relevance, the plasma membrane organization, EGFR ligands, alternative genetic tags and the scope of this study.

Chapter 2 focuses on the main techniques applied in this study. The principles of the single molecule techniques are introduced and discussed which includes Single Wavelength Fluorescence Cross-Correlation Spectroscopy (SW-FCCS), quasi Pulsed Interleaved Excitation (quasi PIE-FCCS), Dual Color FCCS (DC-FCCS) and Dual Color-Internal Total Illumination Reflection-FCCS (DC-ITIR-FCCS). The basics and the instrumental setup are described in this chapter.

Chapter 3 presents the materials and methods used in this work.

Chapter 4 describes the influence of the experimental factors on the receptor dimerization amount. We investigated here the influence of cell lines (HEK293, COS-7 and CHO-K1), temperature (room temperature and 37°C) and membrane localization on the quantitation of preformed dimers using SW-FCCS, DC-FCCS, quasi PIE-FCCS, and imaging FCCS. While measurement modality, temperature, and localization on upper or lower membrane have only a limited influence on the dimerization amount observed, cell line, and location to periphery versus centre of the cell can change dimerization results

significantly. The observed dimerization amount is strongly dependent on the expression level of endogenous EGFR in a cell line and also shows a strong cell-to-cell variability even within the same cell line. In addition, using imaging FCCS, we find that dimers have a tendency to be found at the periphery of cells compared to central positions.

Chapter 5 illustrates the cloning of alternative genetic tags to existing fluorescently labeled probes, which were used in the determination of EGFR complexes. The new receptor tags, as well as an improved red fluorescent protein were tested for its biological functionality and suitability for FCS measurements.

Chapter 6 is the conclusion and outlook section of this entire work. It presents the discoveries in this work and discusses possible future work to understand the proper EGFR activation.

List of Tables

List of Figures

List of Abbreviations and Symbols

3D1p1t	3-dimensional-1-particle-1-triplet
λ_{em}	Emission wavelength
τ	Delay time
τ_d	diffusion time
ω_0	Lateral distance from the centre of the laser focus to where the intensity has decay to 1/e2
ω_z	Axial distance from the centre of the laser focus to where the intensity has decay to 1/e2
n	Refractive index
Å	Angstrom
ACF	Auto-Correlation Function
ACP	Acyl carrier protein
A_{eff}	Effective area
AGT	Alkyltransferase
ALEX	Alternating laser excitation
APD	Avalanche photodiodes
ATP	Adenosine-5`-triphophate
BC	Benzylcytosine
BG	Benzylguanine
BSA	Bovine serum albumin
CCD	Charge coupled detector
Cbl	Casitas B-lineage lymphoma proto-oncogene
CCF	Cross-Correlation Function
CCP	Clathrin-coated pits
CHO	Chinese hamster ovary
CCF	Cross-correlation function
Cps	Counts per particle per second
D	Diffusion coefficient
DNA	Deoxyribonucleic acid
DC	Dual color
EGF	Epidermal growth factor
EGFR	Epidermal growth factor receptor
eGFP	(Enhanced) Green fluorescent protein
EMCCD	Electron multiplying Charge coupled detector
ER	Endoplasmic reticulum
$F_g(t)$	Fluorescence intensity of green labeled particles
$F_r(t)$	Fluorescence intensity of red labeled particles
F_{trip}	Fraction of particles in the triplet state
FCCS	Fluorescence cross-correlation spectroscopy
FCS	Fluorescence correlation spectroscopy
FIDA	Fluorescence intensity distribution analysis
FP	Fluorescent protein
fL	Femtolitres
FRET	Förster resonance energy transfer

G(τ)	correlation function
G(0)	Amplitude of the correlation function
GBM	Glioblastoma mulitforme
GFP	Green fluorescent protein
HGF	Hepatocyte growth factor
ILVs	Intraluminal vesicles
ITIR	Imaging total internal reflection
JM	Juxtamembrane
K	Structure factor
LAT-A	Latrunculin A
L_D	Liquid-disordered
L_0	Liquid-ordered
MAPK	Mitogen-activated protein kinase
mApple	Monomeric Apple
m*β*CD	Methyl-*β*-cyclodextrin
mRFP	Monomeric red fluorescent protein
N	Particle number
NA	Numerical aperture
NMR	Nuclear magnetic resonance
NSCLC	Non-small-cell-lung cancer
q	Cross-correlation amount
PBS	Phosphate Buffered Saline
PCH	Photon counting histogram
PCR	Polymerase chain reaction
PDGF	Platelet-derived growth factor
PI3K	Phosphatidylinositol 3-kinase
PIE	Pulsed interleaved excitation
PMT	Plasma membrane targeting
PSF	Point spread function
PTB	Phosphorylate tyrosine binding
PTP	Phosphatases
RT	Room temperature
sfGFP	Superfolder green fluorescent protein
spFRET	Single-Pair fluorescence resonance energy transfer
STAT	Signal transducers and activators of transcription
SW-FCCS	Single-wavelength excitation fluorescence cross-correlation spectroscopy
RTK	Receptor Tyrosine kinase
TCSPC	Time correlated single photon counting
TIR	Total Internal reflection
TIRFM	Total internal reflection fluorescence microscopy
TM	Transmembrane
TP	two-photon
V_{eff}	Effective volume

1 Introduction

The Epidermal Growth Factor Receptor (EGFR) is a cell surface protein from the transmembrane Receptor Tyrosine Kinase (RTK) family. It is also known as HER-1 and ErbB-1, and is a member of the ErbB receptor family (Yarden and Sliwkowski 2001, Hynes and Lane 2005). There are 58 human RTKs grouped in 20 subfamilies with the same structural features, consisting of an extracellular domain with ligand binding site, a transmembrane region, an intracellular region with tyrosine kinase domain (TK) with an attached Carboxyl (C)-terminus and a juxtamembrane (JM) region (Lemmon and Schlessinger 2010). Other members of the ErbB family are ErbB2 (Neu/HER2), ErbB3 (HER3) and ErbB4 (HER4).

EGFR is expressed in epithelial, mesenchymal and neuronal tissues of the body. Its activity is crucial to maintain and process different signaling cascades. Consequently, its proper functioning is responsible for tissue development and homeostasis.

The discovery of EGFR can be tracked back to the 1960s, when Stanley Cohen and Rita Levi-Montalcini almost coincidentally reported that a component of the salivary gland has induced early eyelid opening and tooth eruption in baby mice (Levi-Montalcini and Cohen 1960). Not long thereafter, Cohen (1962) identified the amino acid sequence of this component, which was later named epidermal growth factor or in short EGF (Cohen 1962). After discovering this ligand and identifying its physiological impact on baby mice, Cohen in collaboration with Carpenter focused further on its binding

properties (Carpenter and Cohen 1979). They succeeded to characterize EGFR by binding radiolabeled I^{125}-labeled EGF ligand in the human epidermoid carcinoma cell line A431. Cells stimulated with EGF responded with increased phosphorylation (Carpenter, King et al. 1978). Initial cloning of the complete cDNA from epidermal carcinoma cells revealed the sequence of EGFR. It gave a more detailed insight into the organization of the molecular receptor. EGFR functionality in mammalian cells has been identified from results obtained in studies involving transgenic mices with known receptor and ligand concentration. Further research on EGFR contributed to the understanding on receptor activation and downstream signaling. Moreover, the aberrant activity of this receptor was linked to the onset of cancer. Overexpression or hyperactivation of EGFR has been reported in a number of head, breast, lung and neck cancers (Seshacharyulu, Ponnusamy et al. 2012, Sasaki, Hiroki et al. 2013). It is well known today that EGFR and ErbB members control cellular proliferation and therefore show a significant relationship between ErbB receptor function and cancer pathology (Citri, Skaria et al. 2003). Hence, it is important to obtain insight into the underlying biological mechanisms of EGFR and ErbBs in order to develop alternative therapeutic approaches for anti-cancer treatment. EGFR is known to reside in the plasma membrane where important biochemical events were initiated. To understand the mechanism of EGFR activation, the localization of the receptor in the plasma membrane and the diversity of the plasma membrane are crucial and require a detailed investigation.

1.1 Characteristics of the plasma membrane

The semipermeable plasma membrane in the cell represents an important border between the extracellular and intracellular environment. The key constituents of plasma membranes are membrane proteins together with sterols, glycerophospholipids and sphingolipids (van Meer 2005). In aqueous solution, lipids induce spontaneous lipid bilayer formation, which is generated by the association of the hydrophobic features of lipids and by aggregation of hydrophilic parts of the lipids. Lipids are amphipathic molecules, which are asymmetrically distributed between the inner and outer leaflet. In mammalian cells, the lipids phosphatidylcholine and sphingomyelin are primarily placed in the outer monolayer, whereas nearly all phosphatidylethanolamine and all phosphatidylserine (PS) are in the inner leaflet (Verkleij, Zwaal et al. 1973, Zwaal and Schroit 1997). Fluid-Mosaic Membrane model introduced in 1972 had an important impact on the perception of dynamics in cell membranes (Singer and Nicolson 1972). Their concept hypothesizes that membranes are of two-dimensional fluid nature and the membrane proteins can diffuse easily in the lipid layers. Later on, this model has been expanded and modified in order to include other factors such as protein and lipid aggregation, lipid domains and cytoskeleton. A recent study demonstrated that phospholipids can do rapid spontaneous flip-flop between the two leaflets (van Meer, Voelker et al. 2008). This can be observed when newly synthesized phospholipids in the cytoplasmic leaflet need to be transported to the exoplasmic leaflet in order to maintain bilayer function (Gummadi and Kumar 2005).

All organelles are surrounded by cell membranes in order to isolate them from the extracellular milieu. This is important as many cellular processes, trafficking and machineries are located within the membrane, and because it controls a wide range of signaling events. The membrane surrounding cell organelles consists of 1000 different lipid species and varies between different kinds of organelles. Membrane diversity can be observed also between the apical and basal plasma membrane of the cell. Biological membranes show a lamellar organization, which is aligned by the association of polar headgroup of lipids and of hydrophobic lipid chains in 2-dimensional form (van Meer, Voelker et al. 2008). This formed asymmetric bilayer structure is important for maintaining functionality of the membrane proteins as they consume ATP as flipping of lipids across the lipid bilayer is an ATP-dependent process (van Meer 2011). The properties of lipids play an important role in maintaining a robust, resistant and dense structure as some signaling events may induce changes in pH or local compositions on the cell surface.

Different types of lipids, proteins and cholesterol are accumulated at certain areas in the cell membrane. These regions, enriched with cholesterol and glycosphingolipid, are referred to as lipid rafts. Their lipids seem to be highly saturated which enables close packing with sphingolipids and causes phase separation from the surroundings (Pike 2003). Much research has been focused on the elucidation of the nature of the rafts as it is involved in many signal transduction and processes of membrane proteins. The size of lipid

rafts was found to be around 50 nm in live fibroblasts by photonic force microscopy (Varma and Mayor 1998, Pralle, Keller et al. 2000). Lipid rafts are also known as liquid-ordered (L_0) phase; they contain high level of cholesterol and saturated lipids, which results in lower fluidity. On the cell membrane, lipid rafts are surrounded by non-raft regions, which are termed as liquid-disordered (L_D) phase. Some studies investigated the properties of cholesterol in mixtures; it has been demonstrated that the packing of cholesterol with saturated lipids activates phase separation in mixtures (Silvius, del Giudice et al. 1996, Polozov and Gawrisch 2006). Further studies found that tight lipid packing and phase separation cause their insolubility in nonionic detergents, e.g. 1% Triton-X (London and Brown 2000). Brown and Rose (1992) investigated 1% Triton X detergent-resistance membranes (DRMs) from MDCK cells. Their analysis revealed that the cholesterol and sphingomyelin amount in the DRMs was 32 mol% and 14 mol%, respectively, while only 12 mol% cholesterol and 1 mol% sphingomyelin occurred in the whole cell lysate (Brown and Goldstein 1992). However, extraction procedure disturbs many lipid-protein association and subsequently lead to a loss of a huge part of proteins from the DRMs. Therefore, DRMs do not reflect the actual composition of liquid-ordered regions in the cell membrane. Moreover, the highest content of cholesterol (30-50% of total lipids) was estimated to be in the plasma membrane in mammalian cells, whereas endoplasmic reticulum (ER) membrane revealed low cholesterol amount (3-6% of total lipids) (Lange 1991). A tightly maintained packing of cholesterol indicates its possible role in participation in signal transduction, regulation of

membrane fluidity and permeability and due to a possible role in building a platform for different proteins in the plasma membrane.

One of the lipid raft subgroups, called caveolae, have a similar composition to lipid rafts but with the difference that it also contains caveolin-1 (Murata, Peranen et al. 1995). This additional protein seems to be responsible for the formation of flask-shaped invagination on the membrane, observed as caveolae. Their sizes were determined to be around ~100 nm by electron microscopy (Murata, Peranen et al. 1995). In contrast, the size determination of lipid rafts is less straightforward as they cannot be discriminated by the neighboring membrane and can therefore be measured only indirectly. GPI-linked proteins are located in these domains and applied as references of lipid rafts (Brown and Goldstein 1992). Analysis of GPI-linked protein reported a size of around 70 nm in fluorescence depolarization studies (Varma and Mayor 1998). Studies with scanning electron microscopy revealed that the diameter of these domains are 60-80 nm, with a 10-50 nm diameter neck (McIntosh, Tan et al. 2002, Predescu, Predescu et al. 2007).

Moreover, studies show that lipid rafts are mostly concentrated in the apical plasma membrane in polarized epithelial cells and only a limited amount is present in the basal and dendritic membranes (Simons and Ikonen 1997).

Lipid rafts contain some important receptors such as EGFR and other RTKs (Pike, Han et al. 2005). However, the influence of these domains in EGFR signaling is quite complex. A line of evidence shows that the activation of EGFR that resides in these domains is prevented (Chen and Resh 2002,

Roepstorff, Thomsen et al. 2002). On the other hand, other reports suggest that lipid rafts enhance EGFR activation and signaling (Zhuang, Lin et al. 2002, Peres, Yart et al. 2003). A common method to explore the relationship between EGFR and lipid rafts is to disrupt the cholesterol content by drugs methyl-β-cyclodxtrin (mβCD) from the plasma membrane. For instance, studies with cholesterol depletion have demonstrated that EGFR signaling is disrupted (Orr, Hu et al. 2005). New evidence presented by Bag et al. (2015) have shown that EGFR reside in cholesterol-dependent as well as cholesterol-independent domains (Bag, Huang et al. 2015). It is well accepted that lipid rafts have a big impact in activation, mobility and localization of EGFR and therefore many researchers focus on the investigation of their influence in EGFR signaling. Moreover, it is important to take into account the experimental conditions when comparing different results of EGR localization in lipid rafts.

1.2 The architecture of EGFR

The human EGFR is a glycoprotein with a size of 170-kDA where the encoding gene is positioned at chromosome 7, 7p11.2 (Reiter, Threadgill et al. 2001). This receptor gene is composed of 28 exons and 27 introns, of which the first 16 encode the extracellular domain, exon 17 is responsible for the transmembrane helix, exons extending from 18 to 24 are involved in the tyrosine kinase domain and those from 25 to 28 in the formation of the C-terminus. When EGFR is in the form of a precursor, it contains 1210 amino

acids. However, after cleavage of the signal peptide, the receptor is made up of the remaining 1186 amino acids and is referred to be in the matured form. Among the ErbB receptor members, the tyrosine kinase domain shows the highest sequence identity (59-81%), while the lowest one can be found in the C-terminus (12-30%) (Nair 2005).

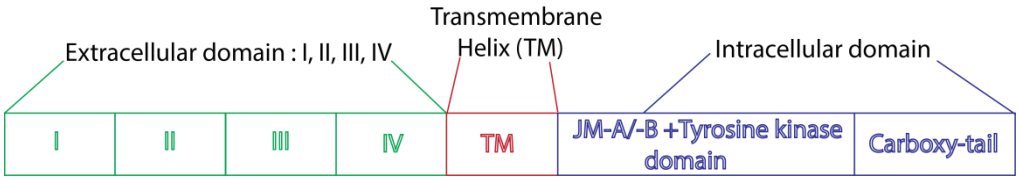

Figure 1.2.1 Domain organization of the EGFR. Extracellular domains (1-620): I (L1), II (CR1), III (L2) and IV (CR2). transmembrane helix (TM) (621-643), juxtamembrane segment (JM): JM-A/-B (644-685) and the intracellular domain: tyrosine kinase domain (TK) and C-tail (686-1186)

As shown in Figure **1.2.1**, the extracellular domain of EGFR is connected to the transmembrane (TM) helix, the juxtamembrane (JM) segment, followed by the intracellular tyrosine kinase catalytic domain, which contains the C-terminal tail. The extracellular part is composed of four functional domains, i.e. domain I (L1), III (L2), II (S1, CR1) and IV (S2, CR2). The first two are built with ß-helical folds showing 37% identical sequences and provide the ligand binding pocket. The other two are elongated and composed from many cysteine-rich residues, whichare held together by disulfide bonds. The function of the dimerization arm (domain II) is to establish EGFR dimers. EGFR can dimerize with another EGFR, which is known as homodimerization, whereas dimerization with other ErbB member is referred to be as heterodimerization. Ligand binding to homo-or heterodimers leads to

phosphorylation of the tyrosine residues in the C-terminus. The extracellular domain of all ErbB members is densely glycosylated in the N-terminus. There are twelve N-glycosylation compounds present in EGFR which is necessary for the localization of the receptor on the cell surface (Slieker, Martensen et al. 1986). In a pair of reports, the EGFR glycosylation mutant N420Q and N579Q led to an increase in ligand-independent dimerization. This led to the notion that glycosylation of the ectodomain prevents dimerization when the ligand is absent (Tsuda, Ikeda et al. 2000, Whitson, Whitson et al. 2005).

Nuclear magnetic resonance (NMR) analysis revealed that the transmembrane section of EGFR is a single helix (Rigby, Grant et al. 1998). The transmembrane helix is connected to the juxtamembrane (JM) segments JM-A and JM-B. Recently, the studies of Jura et al. (2009) has demonstrated that the JM is crucial for EGFR dimer stabilization (Jura, Endres et al. 2009). The direct contact of the two JM domains and the neighboring kinases lead to the stabilization of the active receptor. Deletion of the JM domain induced changes in EGFR dimerization (Jura, Endres et al. 2009). Other studies reported that deletion of JM the region resulted in aberrant ligand binding (Macdonald-Obermann and Pike 2009) and induced decreased phosphorylation (Thiel and Carpenter 2007). Furthermore, the impact of JM domain on the formation of asymmetric kinase has been approved by other groups as well (Thiel and Carpenter 2007, Hubbard 2009, Red Brewer, Choi et al. 2009, Arkhipov, Shan et al. 2013, Endres, Das et al. 2013).

The tyrosine kinase domain (TK) is divided in N-lobe and C-lobe. The first one is mostly made up of β-sheets, as for the second one, α-helical structure is prevailing. This active asymmetric EGFR dimer leads to the binding of adenosine-5`-triphophate (ATP) to the rift between these two lobes. This process catalyzes the trans-autophosphorylation reaction of the tyrosine residues located in the C-terminus, leading to triggering of specific signaling pathways. In particular, the dimerization partner of EGFR determines which specific signaling pathway will be activated. Interestingly, the activation of EGFR tyrosine kinase domains occurs in a similar way as the activation of other kinase groups, e.g. cyclin-dependent kinases (Zhang, Gureasko et al. 2006). The C-terminus equipped with multiple tyrosines as well as some serine/threonine residues, which will be phosphorylated upon ligand activation and leads to the recruitment of several effector proteins such as Grb2 or STAT, which control downstream signaling pathways. The complete functionality of the C-terminus is not well understood, but it was shown to possess regulatory impact on receptor activation (Gajiwala 2013); e.g. the residues 984-996 on the C-terminal have been found to be crucial for the interaction with actin (den Hartigh, van Bergen en Henegouwen et al. 1992).

Despite technical challenges to crystallize single-transmembrane proteins, the x-ray crystal structure (Figure **1.2.2**) of the extracellular domain of EGFR as well as of the other three ErbBs, have been solved in a liganded (EGFR and ErbB4) and unliganded state (all ErbBs) (Ogiso, Ishitani et al. 2002). Structural studies detected two principal conformations of the extracellular domains

within EGFR, ErbB3 and ErbB4 in the absence of the ligand. In the `tethered` conformation, the domain II and IV are very close to each other and folded by intramolecular interactions, thus obstructing the ligand binding. In contrast, in the open/extended form, the overall domain is stretched out and domain I and III provide the binding site for the ligand. Domain II, often called the dimerization arm, enables building receptor-receptor complexes. Ligand binding to extracellular domain promotes a ~130° rotation of domains I and II, leading to a transition from the tethered to the open extended configuration. Thus, these conformations promote a back-to-back dimerization that is stabilized by domain II.

Apart from the two possible configurations in the unliganded state described above, another proposed EGFR model is the rotation model of inactive dimers in the absence of a ligand. When a ligand binds to the receptor this will cause the extracellular domain to become flexible, inducing rotation of juxtamembrane and reorganization of the kinase domains in an asymmetric manner (Moriki, Maruyama et al. 2001).

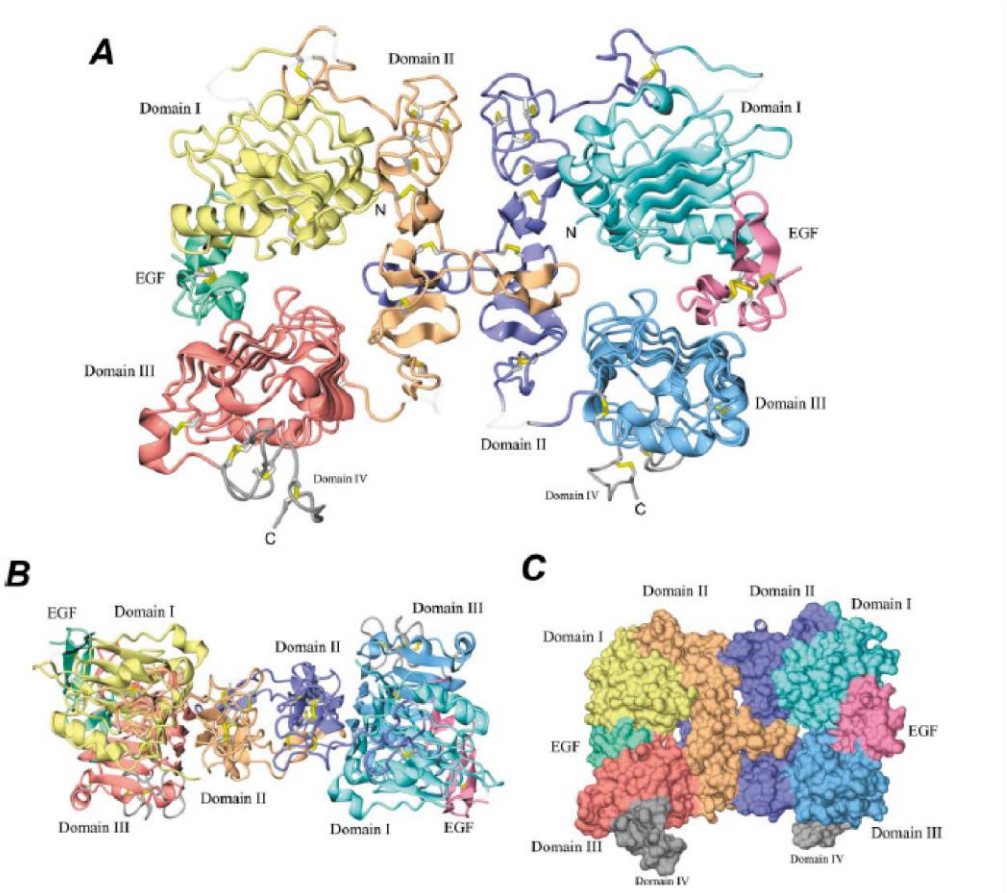

Figure 1.2.2 The crystal structure of the 2:2 EGFR-EGF complexes. **(A)** Ribbon diagram illustrates the extracellular domain of EGF-EGFR complexes. The two ligands are colored pink and pale green. Organization of domain I (yellow), II (orange), III (red) and IV (gray) are shown of the receptor 1 and the domain I (cyan), II (dark blue), III pale blue and IV (gray) of the receptor 2. disulfide bonds are marked in yellow **(B)** Ribbon diagram in the top view **(C)** Surface model of the EGF-EGFR complexes of **(A)** Figure taken from (Ogiso, Ishitani et al. 2002)

The ErbB-2 extracellular domain was also crystallized in the unliganded state. The structure of ErbB-2 is unique and it is the only receptor that was detected in the extended conformation even in the absence of a ligand. Moreover, this receptor did never exhibit the tethered mode in structural analysis. Until now, the structure of liganded Heterodimer of ErbB2 has not been solved yet.

1.3 Receptor ligands and affinity

Eleven ligands are known to bind with different specificity and affinity to their respective receptors, namely EGF, transforming growth factor (TGF-a), heparin-binding EGF-like growth factor (HB-EGF), amphiregulin, betacellulin, epiregulin, epigen and neuregulin (NRG1-4) (Harris, Chung et al. 2003, Schneider and Wolf 2009). A large part of these ligands is found as type I single-pass membrane proteins as an integral part of the cell surface. When proteolytic cleavage by proteins from the ADAMs (disintegrin and metalloproteases) and MMPs (matrix metalloproteinases) family occur, ligands float in the extracellular milieu and subsequently bind to the respective receptors. This proteolytic processing of the ligands is also known as protein ectodomain shedding.

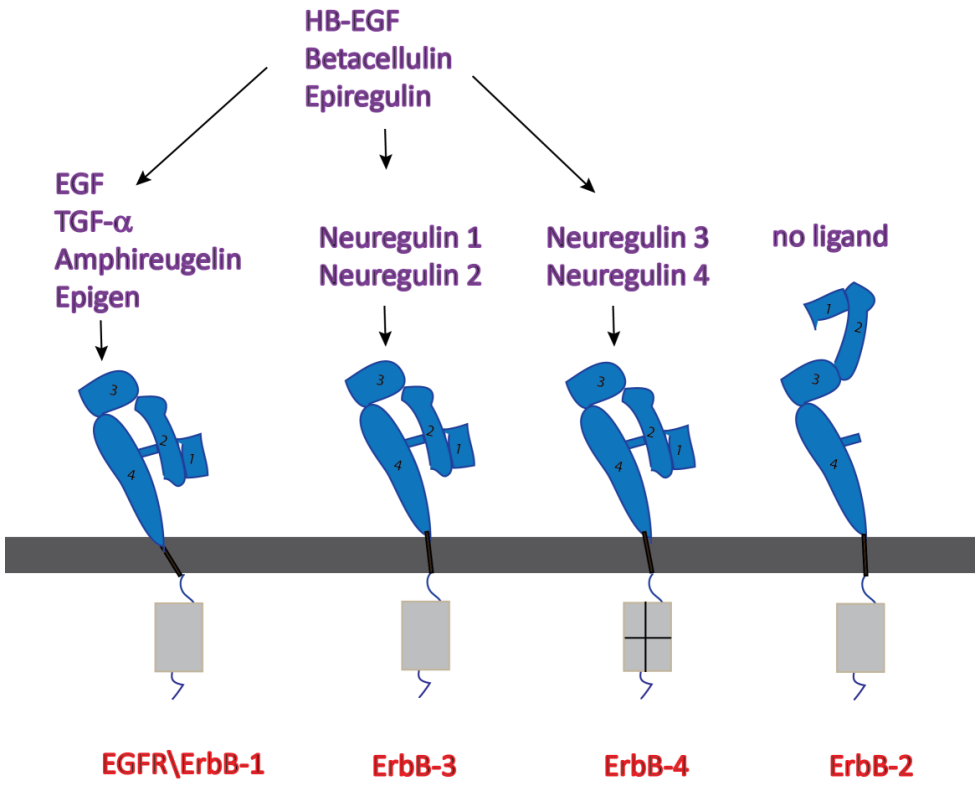

Figure 1.3.1 ErbB family members and ligands

When released ligand binds to the extracellular domain of ErbB receptors, the monomeric receptors will either homo-/hetero-dimerize or already existing preformed dimers will undergo a rearrangement. This receptor activation is then followed by intracellular auto-phosphorylation of tyrosine residues. Depending on which ligand has bound to EGFR, different downstream signaling will be triggered. Some studies suggest that distinct biological outcomes are caused by specific ligand binding and can be correlated to certain phosphorylated residues in the C-terminus of EGFR (Saito, Okada et al. 2004, Wilson, Mill et al. 2012). An interesting study was shown by Sako et. al (2000); fluorescently labeled EGF bound mostly to preformed dimers (Sako, Minoghchi et al. 2000). Ligand binding to receptor dimers leads to rearrangement of existing dimers and subsequent clustering. Researchers also found that these ligands exhibit high or low binding affinity to EGFR. High receptor affinities, ranging from 0.1–1 nM, are achieved by EGF, TGF, BTC and heparin-binding EGF, whereas AREG, epiregulin, and epigen show affinities which are 10- to 100-fold lower (Jones, Akita et al. 1999, Wilson, Gilmore et al. 2009). The first discovered and well characterized EGF ligand is a polypeptide consisting of 53 amino acids and associated with the regulation of different cellular processes. It shows three disulfide bonds which are formed by six cysteine residues. According to a previous study, the N-terminus of EGF and TGF-α is responsible for binding it to the L1 domain in the ectodomain of EGFR (Garrett, McKern et al. 2002, Ogiso, Ishitani et al. 2002). No ligand is known which can bind to ErbB2 (Wada, Qian et al. 1990, Qian, LeVea et al. 1994). A study conducted by Daub

et al. (1996) showed that EGFR can be activated not only by ligand, but also by G-protein coupled receptors (GPCR) (Daub, Weiss et al. 1996). However, later on, this mechanism was contradicted by Prenzel et al. (1999) (Prenzel, Zwick et al. 1999). Their study reported that EGFR could not be activated by the GPCR as previously concluded. Although GPCR plays a role in EGFR activation, it only induces cleaving of HB-EGF from the membrane, which consequently binds to the receptor (Prenzel, Zwick et al. 1999).

Extensive research has been conducted to reveal the properties of low and a high binding process of EGF to EGFR. In order to investigate these bindings, King et al. (1982) used I^{125}-labeled EGF and EGFR (King and Cuatrecasas 1982). The findings showed a concave-up curvilinear Scatchard plot. The initial slope of the curve refers to apparent high affinity receptors and the shallow slope indicates receptors with low affinity. Among the populations, those with high affinity represent only 2-5% (K_D ~300 pM), whereas the rest of 95-98% has a low affinity (K_D ~2-5 nM) (King and Cuatrecasas 1982). In a later study, the model of low-and high affinity receptors has been explained by the occurrence of monomeric receptors and preformed dimers, respectively (Yarden and Schlessinger 1987). In contrast, a mathematical approach by Klein et al. (2004) suggests that the results obtained from Scatchard plots are incomplete. They claim that the external site, which is the cause of the two different binding affinities, has not been taken into account (Klein, Mattoon et al. 2004). However, it must be emphasized that these hypothesizes are yet to be proved experimentally. On the contrary, the experiments performed by the group of Ogiso et al. (2002) shows the

crystallographic structure of EGFR as tethered and open/extended form. Moreover, the first configuration is assumed to represent monomeric receptors with low ligand affinity and the latter preformed dimers with high ligand affinity. Rees et al. (1984) characterized the properties of these two different receptor groups and found that some immobile receptors and low diffusion coefficients are the ones accounting for high affinity classes, whereas the low-affinity receptors showed to be more mobile with higher diffusion coefficients (Rees, Gregoriou et al. 1984). Depending on whether the binding affinity of the ligand to the receptor is low or high, different signaling pathways will be activated (Krall, Beyer et al. 2011). Another study described the origin of the two distinct receptor classes through the localization of the receptors in different regions on the heterogeneous membrane (Mayawala, Vlachos et al. 2005).

In opposition to King et al (1982), who showed a positive cooperativity by using Scatchard plots, the model of Macdonald and Pike explains the occurrence of two distinct states by negative cooperativity (Macdonald and Pike 2008). Their hypothesis predicts that depending on its low or high ligand concentration, EGFR exist as single occupied dimers or/and double occupied dimers, respectively. Further evidence of negative cooperativity is provided in the studies of *Drosophila* EGFR (Alvarado, Klein et al. 2010).

The difficulties in the investigation of low-and high affinity receptor population rely on the fact that both are encoded from the same gene. Therefore, it is not possible to interfere in these two distinct populations.

One potential experimental approach to investigate these affinities is the insertion of a mutation in EGFR transcript in order to explore the receptor classes. For instance, an addition of cysteine residues in EGFR resulted in an increase of preformed dimers, which consequently shifted the equilibrium from the fraction of low affinity to the high affinity receptors (Sorokin, Lemmon et al. 1994). The study conducted by Garret (2002) provides additional evidence for the existence of the high affinity population. EGFR with CR1 loop deletion showed only low affinity binding and no high affinity state (Garrett, McKern et al. 2002). Moreover, the insertion of a cysteine bridge between domain II and IV reduced significantly the fraction of high affinity receptors (Walker, Orchard et al. 2004). However, EGFR mutations with a defective domain II, essential to form a back-to-back dimer, shows that more complex autoinhibtory mechanisms are involved (Mattoon, Klein et al. 2004).

1.4 Cycle of EGFR signaling

Homo-or heterodimerization of EGFR is an important step for activation of different signaling cascades. Ligand binding promotes dimerization of receptors or conformational changes on existing preformed dimers, allowing activation of tyrosine kinase domains and subsequently trans-autophosphorylation of several tyrosine residues in the C-terminus. Receptor activation is essential to main cell functions, for example cell differentiation, survival, apoptosis and proliferation. Among all ErbB members, there is no

known ligand that can bind to ErbB2. However, the ligandless receptor is important as it participates in dimerization with other ErbBmembers (Garrett, McKern et al. 2003). The dimerization of ErbB2 with EGFR appears to be stronger than EGFR homodimerization resulting in a longer lifetime in the membrane and elongated receptor activation (Li, Macdonald-Obermann et al. 2012). ErbB3 is equipped with a defective or very low tyrosine kinase activity (Citri, Skaria et al. 2003, Shi, Telesco et al. 2010). Regardless, ErbB3 is still efficient to conduct signaling cascades by dimerization with ErbB2. In this ErbB2/ErbB3 heterodimer, the ligandless ErbB2 has adequate kinase activity to phosphorylate ErbB3 (Schulze, Deng et al. 2005). Interestingly, a recent study has demonstrated that ErbB2/ErbB3 must be in a tetrameric form in order to phosphorylate each other. It has been found that ErbB2 from one dimer phosphorylates ErbB3 in the second dimer (Zhang, Park et al. 2012). Activated ligand-receptor complexes then promote trans-autophosphorylation of tyrosine kinase residues in the C-terminus. These phosphorylated residues in turn recruit and bind to the intracellular proteins such as Src homology 2 (SH2) and phosphotyrosine binding (PTB) domains. Consequently, relief of these proteins from the C-terminus will induce stimulation of distinct cellular signaling pathways, i.e. mitogen-activated protein kinase (MAPK), phosphatidylinositol 3-kinase (PI3K)/AKT, signal transducers and activators of transcription (STAT) signaling pathways (Figure **1.4.1**). Another unique feature of EGFR is the fact that it can function as an oncogene through stimulation of the Ras oncoprotein, as it promotes the conversion of inactive GDP-bound Ras to its active GTP-bound form (Margolis

and Skolnik 1994). Ligand induced EGFR activation plays an important role in signaling due to its location in the center of many distinct cellular signaling pathways. Activated EGFR complexes are spatially well controlled by receptor internalization, ubiquitination and degradation, referred to as down-regulation of EGFR (Wells, Welsh et al. 1990). Signal termination of ligand-activated receptors is primarily achieved by internalization of EGFR complexes from the cell membrane and forwarded to the endosomes. The major endocytosis clathrin-dependent pathway is the translocation of activated EGFR complexes to the early endosomes via clathrin-coated pits (CCP) which are released as vesicles from the membrane (Roepstorff, Grøvdal et al. 2008). Once this complex reached this compartment, it will be either recycled back to the cell surface or further transferred to the lysosomes. During the last few years, alternative possible endocytosis pathway, the clathrin-independent, has been reported. In the studies conducted by Sigismund et al. (2005) it has been observed that the presence of high EGF ligand concentration (20 ng/ml) results in clathrin-independent endocytosis via flask-shaped oligomerized caveolae to the early endosomes (Sigismund, Woelk et al. 2005). The same group demonstrated that clathrin-dependent endocytosis is preferred at low EGF ligand concentration (1-2 ng/ml) (Sigismund, Woelk et al. 2005). In the current model of endocytosis, ubiquitination is an essential step where ubiquitin polypeptide interacts with lysine residues in the C-terminus of ErbB receptors. EGFR was one of the first receptors in which this process was discovered. It was recently hypothesized that ubiquitination is a common process among RTKs (Goh and Sorkin 2013).

However, it has been only indirectly proved by mutations or down-regulation of its elements. In the presumed model of the clathrin-dependent pathway, the ligand-receptor complex located inside of clathrin-coated pits will be released from the cell surface and transported to the early endosomes. The studies of Goh et al. (2010) reported that clathrin element AP-2 adaptor protein identifies activated receptors for internalization on their motifs located in the C-terminus (Goh, Huang et al. 2010). Contrarily, a pair of reports has shown that AP-2 is unimportant for recognition of EGFR complexes in clathrin-coated carriers (Hinrichsen, Harborth et al. 2003, Motley, Bright et al. 2003, Huang, Khvorova et al. 2004).

Another possible internalization pathway compared to the clathrin-dependent and independent pathway of EGFR is through circular dorsal ruffles. These are membrane protrusions consisting of actin structures (Hoon, Wong et al. 2012).

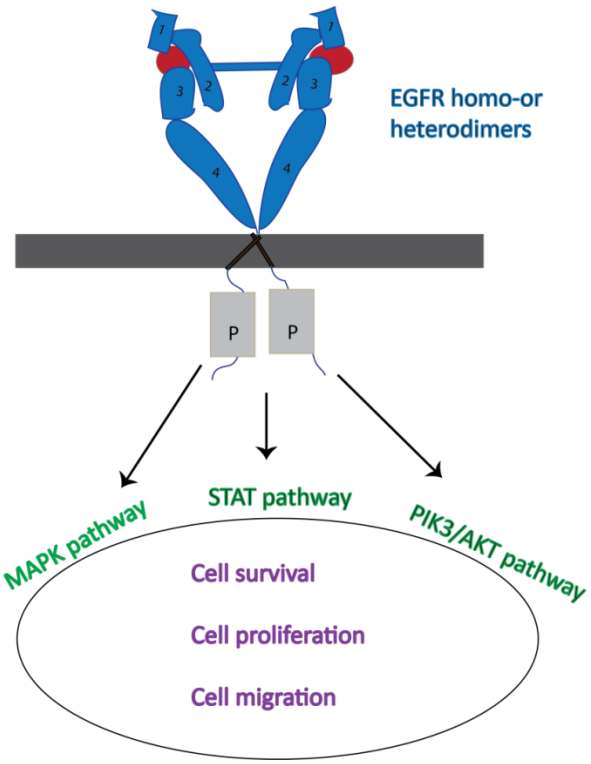

Figure 1.4.1 Main signaling pathways triggered by EGFR

The circular dorsal ruffles are accumulated on the apical cell surface and are activated by growth factors as EGF, hepatocyte growth factor (HGF), and platelet-derived growth factor (PDGF) (Buccione, Orth et al. 2004, Orth and McNiven 2006, Hoon, Wong et al. 2012). However, the participation of the actin cytoskeleton in the formation of circular dorsal ruffles and its signaling remains unclear. Nevertheless, Orth et al. (2006) showed that clathrin-independent internalization via circular dorsal ruffles enables intake of a large amount of EGFR (~50%) (Orth, Krueger et al. 2006). Once the liganded receptor complex reaches the early endosomes, the complex will be either recycled back to the cell membrane or transported via intraluminal vesicles (ILVs) to lysosomes for degradation. Dependent on homo-or heterodimerization by ErbB members, the type and concentration of the

ligand determines the destination of the internalized receptor complexes. Sorkin et al. (1991) reported that high EGF and EGFR concentration led to recycling back 80% of internalized receptors from endosomes to the cell surface (Sorkin, Krolenko et al. 1991). Furthermore, after fragmentation of EGFR complexes, the unoccupied EGFRs were transported back to the cell surface (Masui, Castro et al. 1993). Another study showed that the rate of recycling is much slower for ligand-receptor complex than for ligandless one (Resat, Ewald et al. 2003). A unique feature of EGFR is that it starts to initiate signaling from the cell membrane and reaches the nucleus instead of ending up in the early endosomes. In this possible pathway, EGFR and its ligands can function as a transcription factor of the cyclin D1 gene (Lin, Makino et al. 2001, Brand, Iida et al. 2011) or associate as a cofactor of STAT3 and E2F1 transcription factors (Seshacharyulu, Ponnusamy et al. 2012). However, the exact mechanism of how EGFR is transported to the nucleus has yet to be elucidated. Apart from the functioning of EGFR in the nucleus, the EGFR will be transported to the early endosomes by ongoing different steps. Ligand activated EGFR complexes enable some binding sites on the C-terminus and interacts with proteins such asGrb2 and Casitas B-lineage lymphoma proto-oncogene (Cbl). Cbl is an ubiquitin ligase that attaches mono or polyubiquitins to EGFR (Jiang and Sorkin 2003). This Cbl-EGFR binding has been considered to be important for internalization of the early endosomes. There, the receptor complexes will be forwarded to late endosomes and ubiquitinated EGFR will undergo degradation in lysosomes (Barriere, Nemes et al. 2007). In addition, the acidic environment in the endosomes is critical,

influencing whether the activated receptor complexes will remain ubiquinated and end up in the lysosomes. For instance, ErbB2/ErbB1 heterodimers are tagged by some proteins for recycling back to cell surface, whereas ErbB1 homodimers are destined for degradation in lysosomes. Interestingly, EGFR ligands also determine which endocytosis pathway will be taken. EGF-EGFR complex will end up in lysosomes for degradation and the TGF-α-receptor will be recycled back to the cell surface. Recent studies performed by Bag et al. (2015) reported that low EGF concentration (10 ng/ml) promotes the EGFR homodimers to be transported back to the cell membrane (Bag, Huang et al. 2015). Low pH in the endosomes also determines if certain ligand-receptor complex will be further degraded in lysosomes or recycled back to the cell membrane. Another possible inactivation process of ligand-EGFR complexes is the process of dephosphorylation by phosphatases (PTP), which can bind covalently to EGFR and induces dephosphorylation and hydrolysis (Zhang and VanEtten 1991, Barriere, Nemes et al. 2007).

1.5 Dimerization and clustering of EGFR

According to the traditional model of EGFR activation, the receptor in the membrane of resting cells exists in monomeric form. Upon binding of its ligand (epidermal growth factor, EGF), the receptor undergoes a conformational change into an open conformation allowing association of two EGFR molecules into a dimer (Cochet, Kashles et al. 1988) (Figure **1.5.1**).

Consequently, dimerization leads to auto-phosphorylation of tyrosine residues in the intracellular domain (Schlessinger 2002, Lemmon and Schlessinger 2010). Neverthless, EGFR can be activated by auto-phosphoprylation even in in the absence of ligand (Ma, Ahmed et al. 2011) and the suppression of spontaneous activation of EGFR has been investigated (Baumdick, Bruggemann et al. 2015). This traditional model has been supported by crystal structures of the extracellular domain of EGFR (Garrett, McKern et al. 2002, Ogiso, Ishitani et al. 2002) as well as by reports of EGFR dimerization following stimulation with EGF. However, numerous studies have also shown the presence of EGFR dimers or even larger oligomers in the membranes of resting cells (Gadella Jr and Jovin 1995, Sako, Minoghchi et al. 2000, Martin-Fernandez, Clarke et al. 2002, Clayton, Walker et al. 2005, Saffarian, Li et al. 2007, Clayton, Orchard et al. 2008, Hofman, Bader et al. 2010, Hiroshima, Saeki et al. 2012, Needham, Hirsch et al. 2013, Needham, Zanetti-Domingues et al. 2014, Valley, Lidke et al. 2014, Gao, Wang et al. 2015). In *C.elegans,* the extracellular domain of EGFR (named as LET-23) has been found in dimeric form in the absence of ligand (Freed, Alvarado et al. 2015). Historically, the existence of preformed dimers and oligomers were initially demonstrated by immunogold labeling of the EGFR in the absence of ligand using electron microscopy (Webb, Roberts et al. 2008). In this research, approximately 40% of the receptor population was found as preformed dimers and approximately 10% as oligomers in A431 cells. When ligand was added, there was a noticeable increase in the fraction of oligomers (~30%) and a decrease in monomeric EGFR (~30%). However, the

amount of preformed dimers remained similar (~40%). These findings were further shown by the techniques of chemical cross-linking and co-immunoprecipitation (Moriki, Maruyama et al. 2001, Yu, Sharma et al. 2002, Zhu, Iaria et al. 2003). The studies of Hofmann et al. (2010) found that the amount of preformed dimers was around 40% in resting cells by the method of Homo-FRET (Hofman, Bader et al. 2010). This technique can measure the energy transfer between identical fluorescence proteins in order to quantify receptor dimerization. The structural studies conducted by Jura et al. (2009) demonstrated that activity of the tyrosine kinase domain is inhibited by the dimerization of the C-terminus in the absence of ligand (Jura, Endres et al. 2009). Moreover, Clayton et al. (2008) have shown the occurrence of higher order EGFR oligomers. In unstimulated cells, all receptors are in the form of dimers or trimers, while EGF addition increased the cluster size to four receptors (Clayton, Orchard et al. 2008). The presence of clusters and oligomers of EGFR has been also reported by using different technologies (Needham, Zanetti-Domingues et al. 2015, Zanetti-Domingues, Hirsch et al. 2015, Needham, Roberts et al. 2016), although the macromolecular structure of EGFR remains elusive.

EGFR resides in lipid rafts in the plasma membrane which is enriched with different kind of lipids, cholesterol and proteins (Pike and Miller 1998, Pike 2005, Lajoie, Partridge et al. 2007). Depletion of cholesterol from the plasma membrane enhanced the binding of EGF to EGFR (Pike and Casey 2002). A

recent work showed the presence of EGFR in cholesterol-dependent and cholesterol-independent domains (Bag, Huang et al. 2015).

Two populations of EGFR, which differ by their affinity for EGF, have been identified and attributed by some authors to monomers and preformed dimers, respectively (Macdonald and Pike 2008). The preformed dimers have a higher affinity for EGF and thus allowing faster signaling (Gadella Jr and Jovin 1995, Chung, Akita et al. 2010). This is supported by the different pathways taken at low and high signal doses (Sigismund, Argenzio et al. 2008, Krall, Beyer et al. 2011). However, the studies on Drosophila EGFR revealed that these low and high affinity classes for EGF do not show evidence for two populations and the scatchard plot was derived from negatively cooperative EGF binding (Alvarado, Klein et al. 2010). Nevertheless, the existence of preformed dimers, their relative amount in resting cells and their role in EGFR signaling present an open question as the findings of individual studies differ considerably (Jovin 2014, Valley, Lidke et al. 2014). While some authors reported negligible amounts of preformed dimers (Endres, Das et al. 2013, Yamashita, Yano et al. 2015), others have found mostly EGFR molecules in dimeric form (Moriki, Maruyama et al. 2001, Lemmon and Schlessinger 2010, Valley, Lidke et al. 2014, Sarabipour and Hristova 2015). For instance, spatial intensity distribution analysis revealed ~90% monomeric EGFR in unstimulated cells (Swift, Godin et al. 2011). Similar findings were observed by Nagy et al. (2010); preformed dimers could be detected only at high expression levels of approximately 600.000 receptors per cell (Nagy, Claus et

al. 2010). Furthermore, another research group found monomeric EGFR at low expression levels in COS-7 cells in the absence of the ligand (Huang, Bharill et al. 2016). In contrast to that, our previous study has shown that dimerization to be independent of receptor expression levels in the range from 20.000 to 260.000 copies in individual CHO-K1 cells and the average dimer amount was ~60% (Liu, Sudhaharan et al. 2007). Here, the dimer fraction was calculated by considering monomers in dimers divided by total the number of monomers. According to the single particle tracking studies of EGFR, the receptor forms transient dimers in the absence of EGF (Chung, Akita et al. 2010, Low-Nam, Lidke et al. 2011, Cutler, Malik et al. 2013).

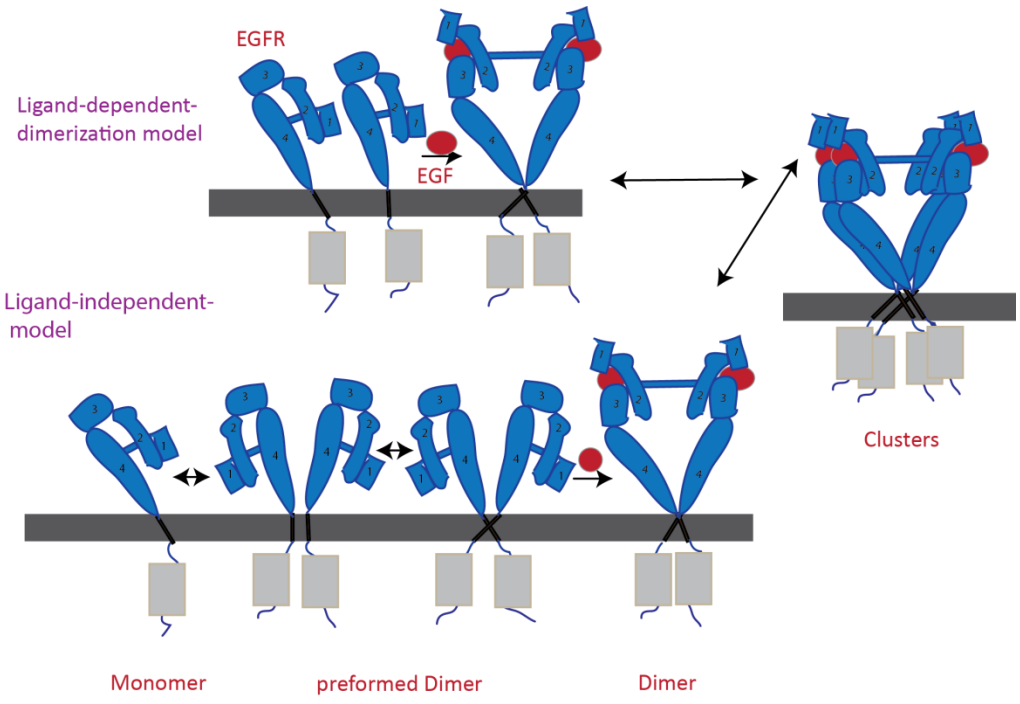

Figure 1.5.1 Traditional activation model of dimerization and the ligand-independent model

On the other hand, results presented by Tao and Maruyama indicate that EGFR dimers are already formed in the endoplasmic reticulum, which would suggest a much more stable association (Tao and Maruyama 2008). The structural studies of Jura et al. (2009) demonstrated that activity of the tyrosine kinase domain is inhibited by the dimerization of the C-terminus in the absence of t ligand (Jura, Endres et al. 2009).

Among possible explanations for the contradictory findings, those addressing the intrinsic differences between cell lines as well as differences in the state of the cells used in the individual studies are the most promising. It has been, for instance, suggested that fixed cells frequently used in super-resolution microscopy studies can display a higher abundance of receptor oligomers due to aggregation artificially promoted by fixation (Kusumi and Suzuki 2005). Insufficient starvation of cells and the use of phosphatase inhibitors have also been proposed as potential sources of elevated levels of receptor dimers (Nagy, Claus et al. 2010). EGFR dimerization has been found to depend strongly on temperature (Gadella Jr and Jovin 1995). Other factors which should be considered include specific artifacts and limitations of the experimental techniques used. Techniques differ in the efficiency with which they can detect short-lived transient dimers as well as in their ability to distinguish true functional receptor dimers from groups of receptors in close proximity due to co-localization in membrane domains (Lidke, Nagy et al. 2003, Yeow and Clayton 2007, Anikovsky, Dale et al. 2008, Szabo, Horvath et al. 2008).

Fluorescence lifetime correlation spectroscopy has been deployed to investigate the interaction of antagonist antibody with EGFR (Chen and Irudayaraj 2010) which resulted in initiation of receptor internalization.

EGFR is frequently misregulated in cancer cells. For instance, the EGFR mutant L858R showed dimerization in the absence of ligand (Wang, Longo et al. 2011). Many anti-cancer treatmtents aim to interfere in improper receptor activation in order to stop malignant cell survival and proliferation.

1.6 Clinical relevance of EGFR

As previously mentioned, EGFR can be found in epithelial human tissues and it is crucial in cellular processes, e.g. differentiation, proliferation and development (Carpenter 1987, Ullrich and Schlessinger 1990). Misregulation of downstream signaling induced by EGFR occurs in different carcinomas (head, neck, breast, bladder ovarian, renal, colon, non-small-cell-lung cancer (NSCLC)) and plays an important role in the formation, survival and progression of a number of diseases (Klapper, Kirschbaum et al. 2000, Baselga 2002, Ciardiello and Tortora 2008). Around 10% to 30% of NSCLC diagnosed patients show either mutations in EGFR or EGFR, which is mostly overexpressed (Siegelin and Borczuk 2014). The most common one was observed to be Exon 19 and L858R. The latter mutation is based at exon 21, where leucine is substituted by arginine, accounting for 43% EGFR mutations in lung tumors.

These mutations, known also as activating mutations, are leading to uncontrolled ligand-independent activation of EGFR and prolonged kinase phosphorylation (Greulich, Chen et al. 2005, Okabe, Okamoto et al. 2007). Besides mutations, misregulation of EGFR can also be caused by EGFR overexpression in epithelial tumors as a response to its hypoxic microenvironment or by gene amplification (Franovic, Gunaratnam et al. 2007). A previous study suggests that EGFR overexpression can lead to a high production level of autocrine signaling such as TGF-α and EGF (Sizeland and Burgess 1992), which induces activation of different signaling pathways.

Glioblastoma mulitforme (GBM) is the most common aggressive brain tumor, which is caused by EGFRvIII mutation (Padfield, Ellis et al. 2015). GBM diagnosis has been associated with poor prognosis and a maximum of 15 months' survival time (Gan, Cvrljevic et al. 2013). This variant has an in-frame deletion of 801 base pair (bp) of the coding sequences in exon 2-7, leading to the loss of 267 amino acids in the extracellular domain and being consequently only 145 kilo Dalton (kD). Interestingly, this mutated EGFR is characterized by an additional junction site and a novel glycine residue. A previous study has reported that dimerization of transient EGFRvIII with itself and wild-type EGFR may be a crucial factor for altered signaling downregulation and GBM cell proliferation (Pillay, Allaf et al. 2009). Furthermore, the stabilization of this transient homodimers is facilitated by disulfide bonds through free aminoterminal cysteines.

Over the last decades, a lot of improvements has been achieved in targeting EGFR in carcinomas with anti-EGFR agents to interfere with downstream signaling. Monoclonal antibodies (Mabs) and Tyrosine kinase inhibitors (TKIs) are two of the most common classes of agents used to target EGFR signaling (Dassonville, Bozec et al. 2007). These drugs differ in their specificity and mechanisms. Cetuximab is a Mab used to prevent binding of endogenous ligand to EGFR by occupying the binding pocket in the extracellular domain and by inducing internalization of EGFR-cetuximab complexes. This will reduce the amount of EGFR on the cell surface. In contrast to Mabs, TKIs compete with adenosine triphosphate (ATP) and bind to the intracellular domain of tyrosine kinase in order to inhibit auto-phosphorylation and downstream signaling. Another class of TKIs available on the market is Gefinitib, Erlotinib and Lapatinib. The disadvantage of using TKIs is that ATP competitors are not specific to EGFR. Consequently, Gefinitib can be also prescribed to inhibit the growth of ErbB2-overexpressing tumor cells (e.g. breast cancer). In clinical studies, Gefinitib has been shown as the most effective in around 10% of NSCLC patients. However, therapeutic approaches are limited and sometimes ineffective; after initially good responses to TKI treatments, the drug has shown to be widely ineffective, associated with increased patient resistance to the targeted therapy. Moreover, researchers found that long-term intake of drugs might cause a second mutation, T790M, which was present in around 50% of TKI resistant patients (Kobayashi, Boggon et al. 2005, Pao, Miller et al. 2005). However, in most cases, this

T790M mutation disappears after interrupting TKI therapy (Sequist, Waltman et al. 2011).

Drawbacks of available drugs targeting EGFR dysregulation are many side effects (rash, acne, nausea, and diarrhea) and patients often acquired drug resistance. Indeed, there is a need for improvement and new alternatives in cancer therapy to be explored.

In this study, we aim to investigate the experimental effects on EGFR dimerization in the absence of a ligand. Imaging and tracking of EGFR were enabled by its labeling with Fluorescent Proteins (FP) in order to address the question to which extent experimental factors influence the amount of EGFR dimers and to obtain insights into EGFR function. Results in this field will help to develop new intervention strategies to overcome current limitations.

1.7 Improvements of the fluorophores and validation of this approach

Genetic labeling of a target molecule with FPs is routinely used in cell biology to investigate protein function and interaction. .Many FPs have been isolated from distinct organisms or the first discovered green fluorescent protein (GFP) has been modified by mutagenesis in order to evolve a wide range of FPs starting from the blue until yellow regions (Day and Davidson 2009, Kremers, Gilbert et al. 2011). Although the usage of mutated FPs faces some challenges. It was reported that some of them show fast photobleaching,

limited quantum yield, incomplete maturation and restricted spectral properties which limit its usage in the investigation of molecular interaction (Wiedenmann, Oswald et al. 2009). Consequently, there is a need for improved fluorophores especially in the red region with specific properties e.g. brightness, photostability and a wide range of spectral features. In our previous and recent work, it has been shown that the cross-correlation of the positive control mRFP-EGFR-eGFP never reaches 100% due to a non-fluorescent fraction of mRFP (Foo, Naredi-Rainer et al. 2012).The cross-correlation amount is a measure to evaluate whether distinct labeled molecules interact with each other. This limitation comes from the restricted maturation of the mRFP. Protein folding and the formation of chromophore are the two important processes. The tertiary structure of the FPs is in the form of β-barrel, which protects the chromophore from quenching by the solvent (Day and Davidson 2009). The incomplete folding of these proteins is due to the trapping of a protein fraction as nonfluorescent green species and defective shielding of the fluorophore by the surrounding cylindrical shell of β-strands. In addition, low extinction coefficient and quantum yield of mRFP (44,000 M^{-1} cm^{-1} and 0.25, respectively) contribute to low brightness and consequently reduces the precision of dimerization amount (Yang, Cheng et al. 1996, Campbell, Tour et al. 2002). Therefore, an improved version of a red FPs, namely, mApple has been cloned into EGFR plasmid and tested for its functionality. This FP shows an extinction coefficient of 75 000 M^{-1} $cm^{-1}$and a quantum yield of 0.49 (Shaner, Lin et al. 2008).

A number of alternatives to the traditional FPs have been developed, known as chemical tags. These small polypeptides were fused to the molecule of interest and need to be covalently labeled with organic dyes or fluorophores. In this work, ACP-tag on EGFR was studied to determine the receptor interaction in order to compare it with the results obtained by FPs. In addition, the variant SNAP-tag and CLIP-tag were additionally cloned and investigated as they show improved selectivity and high signal-to-noise ratios. There is a wide range of substrates for SNAP-tag labeling available, for example, dyes, fluorophores, beads or biotin.

1.8 Scope of this study

Despite more than 35 years' research on EGFR dimerization and signaling, the underlying molecular mechanism is not yet solved and requires further investigation. The exact knowledge of EGFR activation and signaling will help in order to develop effective therapeutic interventions to target aberrant EGFR activity. Especially the mechanism of EGFR dimerization in the absence of a ligand and in ligand stimulated cells will help to get insight in EGFR misregulated cancer cells.

EGFR exists as a mixture of monomers and dimers even in the unliganded state (section **1.8**). A pair of studies have been conducted in order to quantify the dimerization of EGFR in the absence of EGF but have demonstrated inconsistent results in dimerization amount (Moriki, Maruyama et al. 2001, Chung, Akita et al. 2010, Hofman, Bader et al. 2010, Nagy, Claus et al. 2010,

Valley, Lidke et al. 2014). This made it necessary to investigate distinct possible misleading sources for this inconsistency as already a huge range of EGFR dimers and monomers reported in the literature are not insightful in receptor dynamics. The question addressed in this thesis is whether these huge discrepancies in results are related to the sample preparation method or to the application of distinct techniques. The first scope of this work was to systematically investigate the experimental factors, which could have impact in the determination of EGFR dimerization. For that reason, the experiments were performed under various conditions at different temperature ranges, in distinct cell lines and membrane position as each single study´s result arised using distinct temperature and cell lines. Room and physiological temperature were chosen individually in previous studies and we aim to investigate the temperature factor on the outcome of EGFR dimers. In addition, three different cell lines with distinct proportions of endogenous EGFR were used for the determination of EGFR dimerization in unliganded state. Furthermore, the amount of EGFR dimers was examined and focused to the basal and apical membrane in all cell lines. The second part was to compare the dimerization results obtained by different Fluorescent Correlation Spectroscopy (FCS) methods. To solve these inconsistencies, the fraction of EGFR molecules present in the form of homodimers in the plasma membranes has been performed at physiological as well as at room temperature and on the apical and on basal membranes in different cell lines by using EGFR constructs labeled with fluorescent proteins EGFP and/or mRFP. In addition, we compared CHO-K1 cells, selected as an

example of a cell line lacking endogenous EGFR, with two lines of fibroblasts which express endogenously intermediate and low levels of EGFR (COS-7 approximately 100.000 EGFR/cell (Tong, Taylor et al. 2008) and HEK293 20.000 EGFR/cell (Carter and Sorkin 1998). The measurements of EGFR dimerization have been performed bySingle Wavelength Fluorescence Cross-Correlation Spectroscopy (SW-FCCS). In addition, selected experiments were repeated using other Fluorescence Cross-Correlation Spectroscopy (FCCS) modalities, namely Dual-Color FCCS (DC-FCCS), quasi Pulsed Interleaved Excitation FCCS (quasi PIE-FCCS) (Padilla-Parra, Auduge et al. 2011) and Dual-Color imaging Total Internal Reflection FCCS (DC-ITIR-FCCS). Moreover, the influence of cholesterol and the cytoskeleton on EGFR dimerization has been investigated by means of methyl-β-cyclodextrin (mβCD) and Latrunculin-A (LAT-A) treatment in resting cells.

Lately, a series of new constructs with chemical tags (ACP, SNAP and CLIP) and an improved version of the red Fluorescent Protein (FP) mRFP, namely mApple, were cloned and tested for their suitability for FCS measurements.

2 Single-molecule techniques

2.1 Fluorescence Correlation Spectroscopy (FCS)

Single-molecule techniques have become important tools in life science, providing access to complex biological molecular systems. Fluorescence Correlation Spectroscopy (FCS) is a powerful technique with a single-molecule sensitivity that is routinely used to investigate protein conformation

dynamics, aggregation, kinetics of chemical reactions, diffusion and photophysical properties of molecules. For instance, FCS has been applied for drug screening, enzyme kinetic bindings and diffusion measurements on membranes (Weidemann 2014). FCS was initially developed by Magde and Elson in the seventies (Magde, Elson et al. 1972). In that study, FCS was successfully used to investigate the binding of ethidium bromide with DNA. The application of this tool increased fast when FCS was successfully coupled to confocal detection, which enabled measurements with high signal to noise ratio (Rigler, Mets et al. 1993). This combination delivered several advantages; it suppressed background fluorescence and scattered light and provided dramatic improvement of detection efficiency of fluorophores. Other important advantages are the wide range of time scales of FCS from nanoseconds to seconds and that it works at sub-nanomolar to micromolar concentrations, which is similar to the physiological expression level of membrane receptors. The underlying principle of FCS is based on monitoring the fluorescence fluctuations caused by the movement of the fluorescently labeled molecules through an observation volume due to Brownian motion. These fluctuations come from noise and chemical and physical properties of the fluorophores and are recorded as a function of time. Autocorrelation of these fluctuations results in an autocorrelation function, which decays in time. It allows one to extract physical parameters of molecular processes. For that reason, FCS enables to monitor important chemical kinetics, quenching, complexation and diffusion of fluorophores. Hence, it has found massive applications in the life sciences. FCS is non-invasive and experiments can be

performed in live cells. By using sensitive detectors, it establishes detection at the single-molecule level with high accuracy, which in turn helps to resolve fundamental undiscovered cellular processes in living systems. However, this technique is based on the recording of fluorescence fluctuations and therefore requires probes, labeled with fluorescent tags.

One of the most important achievements in cell biology is the discovery of green fluorescent protein (GFP) (27kD) in jellyfish *Aequorea victoria*. Molecular cloning allows genetic labeling of any protein with GFP by fusion to its N-or C-terminus. GFP serves as a molecular marker in cells, which enables the investigation of dynamics at the molecular level *in situ*. In addition, GFP and other fluorescent proteins sustain the biological function and cellular localizations of many chimeric proteins. Fluorescent proteins are commonly used in single molecule techniques. For instance, it allows measurement of local concentrations and diffusions that would not be possible by conventional techniques. Particularly, mutant versions of GFP, known as enhanced GFP (eGFP) and superfolder GFP (sfGFP) have been cloned which show improved spectral properties. Other homologs over a broad range of different colors are available for the application in fluorescence spectroscopy. Fluorescently tagged probes are used in many variants of single molecule techniques. Another advanced single molecule technology is Förster resonance energy transfer (FRET) which is known to be a powerful method to detect molecular interactions. However, for high efficiency and accurate results, it requires a close distance in the range of 10-100 Angstrom (Å)

between molecules of interest to transfer energy from the donor (excited fluorophore) to the acceptor.

Nowadays, FCS has been applied to determine various diffusion modes such as Brownian diffusion (Mets and Rigler 1994, Di Rienzo, Piazza et al. 2014), anomalous diffusion (Metzler, Jeon et al. 2016), rotational and translational diffusion (Oura, Yamamoto et al. 2016) and flow (Magde, Webb et al. 1978, Gosch, Blom et al. 2000, Ashdown, Pandzic et al. 2015). Additionally, FCS was used to determine the kinetic rate constants of distinct reactions (Brandao, Sangji et al. 2014, Kanno and Levitus 2014, Bi, Yin et al. 2016, Ye, Luo et al. 2016) and found application in clinical research (Torres, Genzen et al. 2012, Olson, Torres et al. 2013, El-Shaheny 2014).

Complementary methods to FCS are photon counting histogram (PCH) (Chen, Muller et al. 1999, Müller, Chen et al. 2000)and fluorescence intensity distribution analysis (FIDA) (Kask, Palo et al. 2000, Palo, Brand et al. 2002) in which the brightness of the fluorophores is evaluated.

An extended version of FCS is the Fluorescence Cross-correlation Spectroscopy (FCCS), which is based on measuring temporal fluctuation of the movements of differently labeled molecules. This variant allows one to measure molecular interactions and dynamics and will be further discussed in section **2.3**. In this work, different versions of FCCS have been used to investigate EGFR interaction in living cells. This method provides the possibility to measure receptor dynamics and dimerization in real time in living systems. Investigation of EGFR interaction in live systems provides

temporal and spatial information, which makes it attractive especially in cell biology and cancer research.

2.2 Theory of FCS

As mentioned in the previous section, FCS is based on the measurements of the movement of fluorophores in an observation volume and works in nanomolar up to high micromole rconcentrations. The observation volume in a confocal setup is generated by a focused laser beam. The pinhole positioned in front of the detection channel creates a small detection volume of less than a femtolitre (fl). Fluorophores move in and out through the observation volume and induce temporal fluctuations. The statistical analysis of the average fluorescence fluctuations provides information on physical parameters such as concentration, association/dissociation kinetics and motion of the molecules. To get physical information about the molecules, the intensity trace is correlated with itself at time shift $\tau$and transformed into an autocorrelation function (ACF). At zero time shift $\tau_{0,}$ intensity traces overlap with each other to 100%; this is reflected by the highest correlation value in the autocorrelation curve. The correlation value decreases by increasing τ. Autocorrelation of the intensity traces allows the derivation of an autocorrelation curve, which enable the quantification of the average diffusion time by the width of the curve and to determine the underlying processes by the shape of the curve. Additionally, the amplitude of the curve represents the particle numbers in the observation volume.

The fluorescence fluctuations at a certain time t is presented as

$$\delta F(t) = F(t) - \langle F(t) \rangle \tag{2.2.1}$$

F(t) is the fluorescence intensity, ⟨ ⟩ represents the average fluorescence intensity. ⟨F(t) ⟩ is calculated by

$$\langle F(t) \rangle = \frac{1}{T} \int_0^T F(t) dt \tag{2.2.2}$$

The normalized ACF is defined as

$$G(\tau) = \frac{\langle F(t) \cdot F(t+\tau) \rangle}{\langle F(t) \rangle^2} \tag{2.2.3}$$

τ stands for the lag time.

Substitution of equation **2.2.1** into **2.2.3** results in

$$G(\tau) = \frac{\langle (\delta F(t) + \langle F \rangle)(\delta F(t+\tau) + \langle F \rangle) \rangle}{\langle (\delta F(t) + \langle F \rangle) \rangle^2} \tag{2.2.4}$$

$$= \frac{\langle \delta F(t) \delta F(t+\tau) + \langle F \rangle^2 \rangle}{\langle F \rangle^2}$$

$$= \frac{\langle \delta F(t) \delta F(t+\tau) \rangle}{\langle F(t) \rangle^2} + 1$$

Given in this form, the ACF decays to 1 at infinite $\tau_\infty (G(\infty) = 1)$.

The autocorrelation amplitude G(0) is inversely proportional to the average particle number (N) in the confocal volume and is given by

$$G(0) = \frac{1}{N} + G_\infty \tag{2.2.5}$$

The autocorrelation curves are fitted with different mathematical models to extract the diffusion time and numbers of molecules in the observation

volume. Organic dyes diffuse freely solution. The fitting of free diffusing particles was performed by 3-dimensional-1-particle-1-triplet (3D1p1t) model, in which the function is expressed as

$$G_{3D1p1t}(\tau) = \frac{1}{N}\left(1+\frac{\tau}{\tau_D}\right)^{-1}\left(1+\frac{\tau}{\tau_D}K^{-2}\right)^{-\frac{1}{2}} f_{trip}(\tau) + G_\infty \quad (2.2.6)$$

$f_{trip}(\tau)$ Is defined as

$$f_{trip}(\tau) = \left(\frac{F_{trip}}{1-F_{trip}}\right)^{-1} exp\left(-\frac{\tau}{\tau_{trip}}\right) + 1 \quad (2.2.7)$$

$\tau_D$is the average diffusion time of the fluorophores in the detection volume and defined as $\tau_D = \frac{\omega_0^2}{4D}$. ω_0^2 is the radial distance at which the maximum intensity is decreased by a factor of $1/e^2$. F_{trip} stands for the fraction of particles in the triplet state and τ_{trip} is the triplet state relaxation time.

The structure factor K of the confocal volume is mathematically defined as

K= ω_z/ω_0 (height over its waist of the confocal volume).

2.3 Principles of Fluorescence cross-correlation spectroscopy (FCCS) and Single-Wavelength Fluorescence Cross-Correlation Spectroscopy (SW-FCCS)

Fluorescence Cross-Correlation Spectroscopy (FCCS), an extension of FCS, is commonly used to explore molecular interactions and is the focus of this thesis. The theory of Dual-Color Fluorescence Cross-Correlation Spectroscopy (DC-FCCS) was initially introduced by Eigen and Rigler (Eigen and Rigler 1994) and first successfully applied on the measurement of the interactions of

fluorescently labeled DNA in 1997 (Schwille, Meyer-Almes et al. 1997). The application of this tool has increased rapidly to monitor protein-protein interactions and dynamics in the cytosol and membrane of cells in a predefined confocal volume. In confocal FCS, the evaluation of molecular complexes is limited by the diffusion coefficients and mass (Meseth, Wohland et al. 1999). The development of FCCS has increased the sensitivity and resolution of the traditional FCS. In addition, this method does not require a certain spatial distance between the molecules as in the case of FRET. In DC-FCCS, two different lasers are used to excite distinctly labeled molecules; fluorescence fluctuations are recorded in two different emission channels and auto- and cross-correlated. FCCS evaluates molecular interactions by means of a cross-correlation curve without any restriction. The cross-correlation curve will rise up if molecules interact or/and are co-localized and move together.

However, FCCS in general and DC-FCCS show some artifacts. The major problem in FCCS is spectral cross-talk in which the photons are wrongly assigned to the detection channels. The long tail of the emission spectrum of the green molecule GFP causes photons to arrive in the green channel and some in the red channel. Accordingly, it leads to a false positive cross-correlation and reduces the sensitivity of the method. Fortunately, a modality of FCCS, namely pulsed interleaved excitation FCCS (PIE-FCCS) can get rid of cross-talk. The principle of this technique will be further discussed in the next subsection.

The main drawback in DC-FCCS is the imperfect overlap of the detection volumes. The origin of this problem arises with the usage of two distinct laser beams with different beam waists resulting in different sizes of the confocal volumes. If the volumes are shifted along the axis and do not overlap perfectly, the cross-correlation amplitude is reduced and the dynamic range decreases. The dynamic range of the experiments strongly depends on the calibration of the two laser beams. Thus, a new modality of FCCS, Single wavelength cross-correlation spectroscopy (SW-FCCS) was developed (Hwang and Wohland 2005, Liu, Sudhaharan et al. 2007). This simplified technique uses only one laser (514 nm) to excite differently labeled fluorophores simultaneously and cancels out the difficult calibration of two laser spots which is the case in DC-FCCS. Another similar tool to SW-FCCS is two-photon excitation FCCS (TP-FCCS) which can also excite fluorophores with one laser, but uses two-photon excitation (Swift, Burger et al. 2007). However, the count per particle per second (cps) of TP-FCCS is much lower (Berland and Shen 2003)than that of DC-FCCS due to strong photobleaching and saturation present in TP-FCCS (Dittrich and Schwille 2001). In TP-FCCS, a wider range of fluorophores can be used, while in SW-FCCS only selected fluorophores with overlapping excitation spectra and large distances between their emission spectra are adequate.

SW-FCCS was developed by our group and is the main technique used in this thesis besides other FCCS modalities. The proteins of interest are labeled with enhanced green fluorescent protein (eGFP) and monomeric red fluorescent protein (mRFP). The fluorescence fluctuations of eGFP and mRFP

are recorded in the green and red channels, respectively and the auto- and cross-correlation curves are calculated. The normalized cross-correlation function (CCF) is given by

$$G_x(\tau) = \frac{\langle F_g(t) \cdot F_r(t+\tau)\rangle}{\langle F_g(t)\rangle\langle F_r(t)\rangle} = \frac{\langle \delta F_g(t) \cdot \delta F_r(t+\tau)\rangle}{\langle F_g(t)\rangle\langle F_r(t)\rangle} + 1 \qquad (2.3.1)$$

$F_g(t)$ stands for the fluorescence intensity of green labeled molecules and $F_r(t)$ of red labeled molecules. Compared to auto-correlation, here, the fluorescence fluctuations of two distinctly labeled molecules are cross-correlated at different time points.

2.3.1 Curve fitting of 2-dimesional systems

The auto-and cross-correlation functions (ACFs and CCFs) were fitted with a model for 2-dimensional diffusion with the reversible switching of the fluorophores to a dark (triplet) state. The model (equation **2.3.1.1**) contains five unknown parameters: the apparent particle number N_{app}, the diffusion coefficient D, the fraction of fluorophores in the dark state F_{trip}, the characteristic time of switching to the dark state τ_{trip} and the asymptotic value for long correlation times G_{inf}. The switching to the dark state is, in this case, most likely a combination of photophysical processes (triplet transitions, isomerization) and a protonation-deprotonation equilibrium (Widengren 2010, Sun, Guo et al. 2015). While a single exponential may not be the correct description of the correlation function of such processes, it provides a reasonably well parametrization of the correlation curve, thanks

to a sufficient difference between τ_{trip} and the characteristic diffusion time, where the actual choice of the parametrization of the initial decay of the correlation function has only limited effect on its diffusional part. The asymptotic value for long correlation times G_{inf} is in the ideal case of a perfectly stationary process equal to 0. However, in practice, small non-zero values are commonly encountered due to the finite length of the sampled intensity time-trace or due to non-stationarity of the time-trace caused by photobleaching. Therefore, we leave G_{inf} as a free fitting parameter. The radius of effective detection area ω_0 was determined by calibration with a dye with known value of D. The fitting was performed by a self-written module in Igor Pro (WaveMetrics, Portland, OR).

$$G(\tau) = \frac{1}{N_{app}} \frac{\omega_0^2}{\omega_0^2 + 4D\tau}\left[1 + \frac{F_{trip}}{1-F_{trip}} \exp\left(\frac{-\tau}{\tau_{trip}}\right)\right] + G_{inf} \qquad (2.3.1.1)$$

To estimate the receptor interaction amount measured in the confocal volume, the particle numbers N_{app} were extracted by fitting both the ACF and CCF curves. Background-corrected particle numbers N were obtained from N_{app} as described previously (Koppel 1974, Hess and Webb 2002). The background was measured in cells not expressing any fluorescent proteins and illuminated by excitation light of the same intensity as used in the actual SW-FCCS recordings. The typical background levels were between 500-800 cps.

The amount of cross-correlation q (the ratio of the concentration of the double-labelled species to that of all the particles carrying the less abundant

label) was calculated according to equation **2.3.1.2** and used as a measure of the amount of molecules existing in the form of complexes (Kohl, Haustein et al. 2005). *q* is written as

$$q = \frac{\max\ (N_{g;}\, N_r)}{N_x} \tag{2.3.1.2}$$

The formula above is derived from

$$G_G(0) = \frac{1}{N_G} = \frac{N_g + N_{gr}}{(N_g + N_{gr})^2}; \qquad G_R(0) = \frac{1}{N_R} = \frac{N_r + N_{gr}}{(N_r + N_{gr})^2} \tag{2.3.1.3}$$

$$G_X(0) = \frac{1}{N_X} = \frac{N_{gr}}{(N_g + N_{gr})(N_r + N_{gr})} \tag{2.3.1.4}$$

$$q = \frac{N_{gr}}{\min\left[\left(N_g + N_{gr}\right); \left(N_r + N_{gr}\right)\right]} = \max\left[\frac{N_{gr}}{N_g + N_{gr}}; \frac{N_{gr}}{N_r + N_{gr}}\right]$$

$$= \max\left[\frac{G_X(0)}{G_R(0)}; \frac{G_X(0)}{G_G(0)}\right] = \frac{\max[N_G; N_R]}{N_X} \tag{2.3.1.5}$$

N_g, N_r and N_x are the backgrounds corrected particle numbers extracted from the ACFs in the green and the red channel and from the CCF, respectively.

The mean values and standard deviations of or standard errors of the *q* mean are calculated from all measurements performed under given conditions. We measured in at least four cells, typically maximal nine measurements per cell. The numbers of individual cells and measurements for each type of experiment are provided in the tables or in the text together with the respective results.

2.3.2 Instrumentation and calibration of SW-FCCS system

The SW-FCCS instrumentation was described in previous publications (Pan, Foo et al. 2007). Briefly, the setup consists of an Olympus FV300 confocal microscope (Olympus, Tokyo, Japan) equipped with two avalanche photodiodes (SPCM-AQR-14; PerkinElmer, Canada) as light detectors for FCS measurements. The Argon ion 514 nm laser line (Melles Griot, Albuquerque, NM) was focused by a 60x, NA 1.2 water immersion objective (UplanApo, Olympus, Japan) into a diffraction limited spot. Laser power (measured at the back aperture of the objective) was 20 µW in all experiments. The emitted fluorescence passed a 488/514 major dichroic (Omega Optical, Brattleboro, VT), a 150 µm pinhole, was split by a560 DCLP emission dichroic mirror (Omega Optical, Brattleboro, VT), passed through emission band-pass filters (545AF35 or 615DF45), respectively, Omega Optical, Brattleboro, VT) and reached the avalanche photodiodes. The output of the avalanche photodiodes was processed by a hardwarecorrelator (Flex02-01D, www.correlator.com, Bridgewater, NJ) to obtain the auto- and cross-correlation functions. The inbuilt photomultipliertubes (PMTs) of the FV300 were used for confocal imaging of the cells. The schematic setup is shown in the Figure **2.3.2.1**.

The effective detection volume was calibrated with a 20 nM aqueous solution of Rhodamine 6G (Sigma-Aldrich, St. Louis, MO) which has a known diffusion coefficient of 382 $\mu m^2/s$ at room temperature and 555 $\mu m^2/s$ at 37°C (as calculated from values and equation (temperature and viscosity dependent) given in (Kapusta 2010, PicoQuant, Berlin). Each channel, correction collar

and the position of the pinhole is optimized to detect the highest fluorescence count rate. The autocorrelation curve is fitted with a 3D1p1t model equation **2.2.6**. FCCS measures the diffusion time of the membrane receptor and the diffusion coefficient is calculated by solving the following equation

$$D_{target\ molecule} = \frac{(\tau_{D\ Rhodamine\ 6G} \cdot D_{Rhodamine\ 6G})}{\tau_{D\ molecule}} \qquad (2.3.2.1)$$

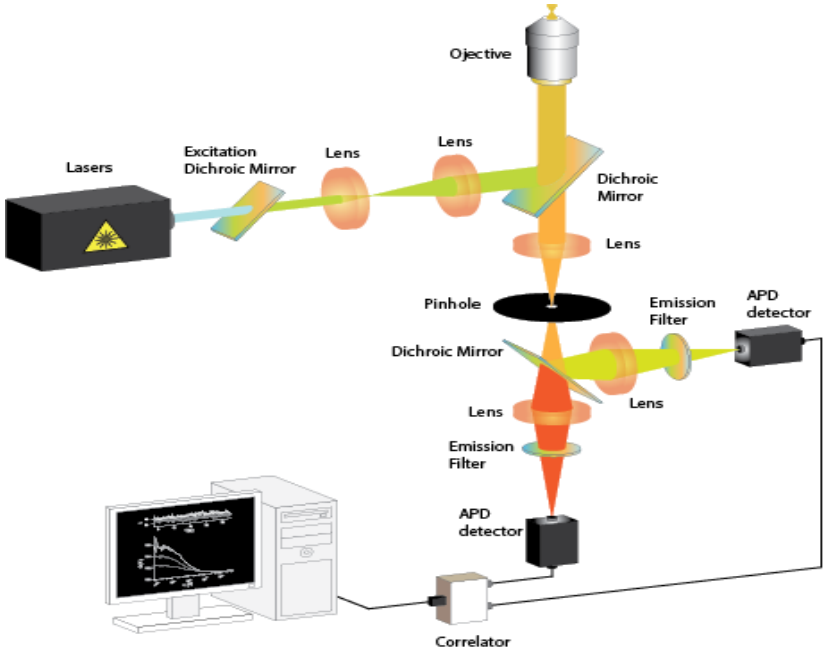

Figure 2.3.2.1 Schematic setup of SW-FCCS (image taken from Yong Hwee Foo)

The 37°C temperature during the measurements was maintained by a non-stage incubator (TempContro 37-2, Pecon, Erbach, Germany) and the corresponding temperature of the objective by an objective heating ring (TC-124A, Warner Instruments, Hamden, CT). The room temperature was 22°C,

as maintained by the air-conditioning system in the laboratory. Three 30 s data acquisitions were run consecutively in each selected point.

2.4 Dual-color fluorescence cross-correlation spectroscopy (DC-FCCS) and quasi pulsed interleaved excitation fluorescence cross-correlationspectroscopy (quasi PIE-FCCS)

DC-FCCS and quasi pulsed interleaved excitation fluorescence cross-correlation spectroscopy (quasi PIE-FCCS) are modalities of FCCS, which have been implemented to investigate molecular interactions and co-localizations in biological samples and solutions. In DC-FCCS, two different continuous lasers are used to excite spectrally separated fluorescent proteins. The emission is split by a dichroic mirror and forwarded to two distinct detectors. However, the main concern of FCCS arises from the non-perfect overlap of the detection volumes and wrong assignment of photons in the non-corresponding channel. This spectral crosstalk of emission in distinct detectors reduces the sensitivity and specificity of the method. More recently, alternating laser excitation (ALEX) source has been combined with FCCS (Kapanidis, Lee et al. 2004). The two excitation lasers are interleaved at time frame between 25 to 3000 milliseconds. The excitation lasers are alternatively operated in a time rate faster than the diffusion time of the molecules of interest. An important component in ALEX-FCCS is the time correlated single photon counting (TCSPC) module in which individual channel`s photons are detected. The exact arrival time of each photon in

TCSPS enables the generation of a fluorescence decay curve.By using ALEX as an excitation source, it is possible to obtain a cross-talk free correlation curve which prevents false positive cross-correlation. The studies of Lee et al. (2005) have demonstrated that the precision of single-pair fluorescence resonance energy transfer (spFRET) has been increased by combining it with ALEX (Lee, Kapanidis et al. 2005). In the same year, Mueller et al. developed the concept of pulsed interleaved excitation and increased the alternation time scale from microseconds to nanoseconds (Müller, Zaychikov et al. 2005). Importantly, the usage of this improved interleaved excitation source in FCS enables one to operate with submicro second resolution. The major advantage of PIE is the capacity to remove spectral crosstalk from cross-correlation curves and therefore increases the accuracy of FCCS. In addition, the cross-correlation function can be corrected for input of detector afterpulsing and background signal (Böhmer, Wahl et al. 2002, Kapusta, Wahl et al. 2007). PIE was used to investigate complexes which undergo FRET (Müller, Zaychikov et al. 2005). In these experiments, the amplitude ratios of correlation curves provide the FRET efficiency. As the arrival time of the photon is known, additional information such as the lifetime of the fluorophore can be extracted.

Besides using SW-FCCS, the modalities DC-FCCS and the variant of PIE-FCCS, quasi PIE-FCCS, were used to conduct receptor interaction experiments. This method of crosstalk elimination in FCCS is based on similar principles as PIE-FCCS (Müller, Zaychikov et al. 2005); however, it requires only a single pulsed

laser (485 nm), the second laser being continuous wave (543 nm). We therefore named it as quasi PIE-FCCS.

2.4.1 Instrumentation of quasi PIE-FCCS and DC-FCCS

DC-FCCS and quasi PIE-FCCS experiments were carried out in CHO-K1 cells at room temperature on a confocal microscope (FV1200, Olympus, Tokyo, Japan) equipped with a time-resolved FCS upgrade kit (PicoQuant, Berlin, Germany). For DC-FCCS, the cells were illuminated by two continuous wave laser lines of 488 nm and 543 nm (GLG 3135 and GLG 7000 respectively, Showa Optronics, Japan) through a 60x, NA 1.2 water immersion objective (UplanSApo, Olympus, Japan) to excite eGFP and mRFP, respectively. The same 543 nm laser was used for quasi PIE-FCCS together with a pulsed 485 nm laser (LDH-D-C-488, PicoQuant, Germany) operated at 20 MHz repetition rate. 20 μW of laser power for each individual laser line was used in all measurements. The fluorescence emission passed through a 405/488/543/635 major dichroic mirror (Chroma Technology, Bellows Falls, VT), a 120 μm confocal pinhole and, after being split by a 560DCXR (Chroma Technology, Bellows Falls, VT) emission dichroic, through a 600/50 (Chroma Technology, Bellows Falls, VT) or 513/17 (Brightline, Semrock, Rochester, NY) band-pass emission filter, respectively, to be detected by avalanche photodiodes (SPCM-AQR-14; PerkinElmer,Canada). The photon counts from the detectors were registered by aTimeHarp 260 time correlated single photon counting board (PicoQuant,Berlin, Germany) and processed by the SymPhoTime 64 software (PicoQuant,Berlin, Germany); the same software

was also used to calculate the correlation functions. Those were then analyzed in the same manner as the correlation functions obtained by SW-FCCS. As in the case of SW-FCCS, the dimensions of the effective detection volumes were determined by calibration of FCS measurements in solutions of reference dyes. Atto-488 (Atto-Tec, Siegen, Germany) was used for the 488 nm and 485 nm laser lines and Rhodamine 6G for the 543 nm line. The diffusion coefficient of Atto-488 was taken as 369 $\mu m^2/s$ at 22°C, based on values in Kapusta 2010, PicoQuant, Berlin. Each data acquisition lasted 30 s in the case of DC-FCCS and 60s in the case of quasi PIE-FCCS. When analyzing data acquired with the pulsed 485 nm laser, we used statistical filtering (Machan, Kapusta et al. 2014) to eliminate detector after-pulses and spectral crosstalk between the two detection channels as described previously (Padilla-Parra, Auduge et al. 2011).

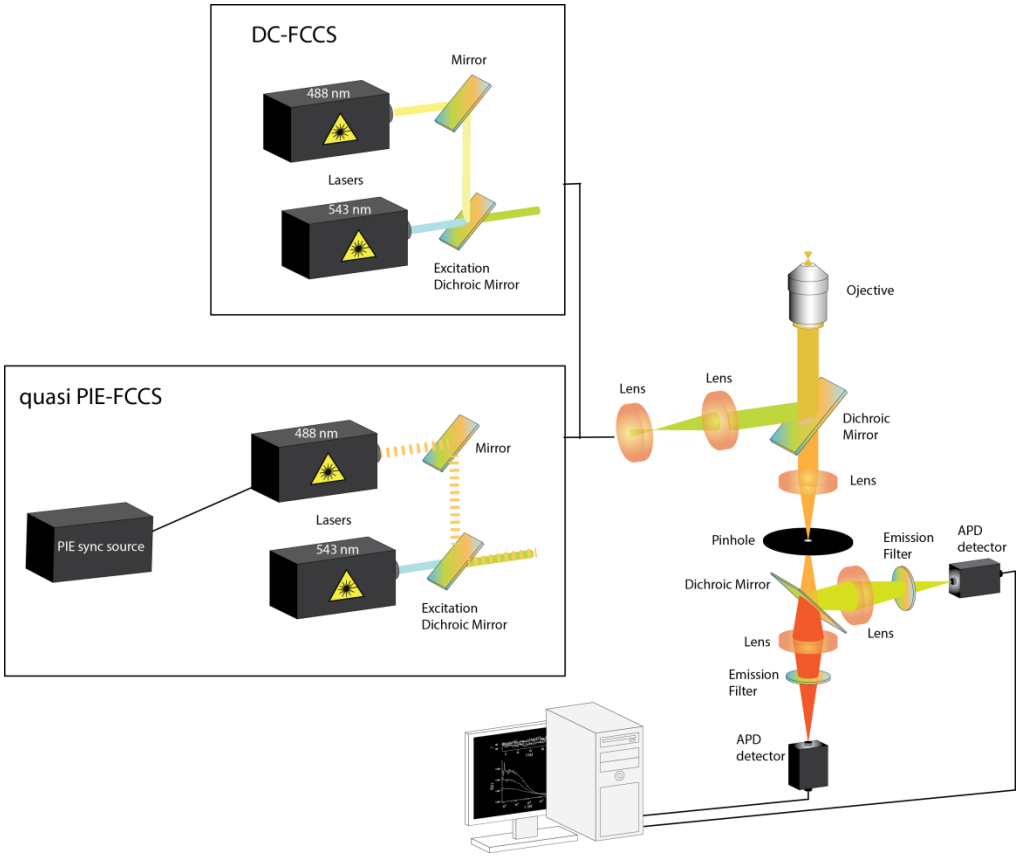

Figure 2.4.1.1 Schematic setup of quasi PIE-FCCS and DC-FCCS (adapted from Yong Hwee Foo image)

2.5 Total Internal Reflection Fluorescence Microscopy (TIRFM)

Historically, Axelrod (1981) first suggested that Total internal reflection fluorescence microscopy (TIRFM) is an efficient method to investigate cells-substrate contact (Axelrod 1981, Axelrod, Thompson et al. 1983). When the light passes from a higher refractive index medium to a lower refractive index medium, it will be refracted. In the case of refraction, the light path bends at the boundary of the two different media. Snell`s Law of refraction is expressed as

$$n_1 sin\theta_1 = n_2 sin\theta_2 \qquad (2.5.1)$$

$n_1$and n_2 indicate the refractive index of the two different media ($n_1 > n_2$) and $\theta_1$and$\theta_2$are the incident and refractive angles, respectively.

When the light beam passes from a denser medium to a less dense medium, it undergoes bending. However, if the angle of incident is bigger than the critical angle θc, the light is internally reflected and does not go beyond the boundary of these two media.θc is expressed as

$$\theta_c = sin^{-1}(n_2/n_1) \quad (2.5.2)$$

This internal reflection causes an evanescent field on the boundary. The energy of the evanescent field is strong enough to excite the fluorophores within this location. The intensity of the evanescent field is distance-dependent and shows an exponential decay from the boundary. Depth d can be calculated by

$$d = (\lambda_0/4\pi) \cdot (n_2^2 sin^2\theta - n_1^2)^{-1/2} \quad (2.5.3)$$

λ_0 is the wavelength of the light and $n_2 sin\theta$ indicates the numerical aperture (NA) of the objective. The depth of the evanescent field can reach around 100 nm and depends on several factors such as refractive indexes, incident angle, and wavelength.

TIRFM is a powerful imaging tool to detect fluorophores adherent to the cell surface and at the meantime, it reduces background signal significantly. Thus, it increases the signal to noise ratio and protect the living organism from photodamage. The total internal reflection illumination in FCS (ITIR-FCS) has shown to be an efficient and very sensitive method in studying membrane organization.

As shown previously, confocal FCS is a very effective method and it is usually combined with either photomultiplier tubes (PMTs) or avalanche photodiodes (APDs) as detectors. Unfortunately, the measurements are

performed on a selected small spot at a certain time and therefore misses to capture multiple spots at the same time. To extend the single spot measurements to a region of an image, TIRF has been equipped with cooled charge coupled detector (CCD) or electron multiplying (EM) CCDs dependent on the needs. Using EMCCD in ITIR-FCS has been successfully applied in monitoring of molecular dynamics in living organisms (Kannan, Har et al. 2006, Kannan, Guo et al. 2007, Sankaran, Manna et al. 2009, Sankaran, Shi et al. 2010, Sankaran, Bag et al. 2013, Singh, Krieger et al. 2013). In ITIR-FCS, every pixel in an image will be correlated and it enables to collect many positions at the same time. The effective detection area (A_{eff}) is defined as a convolution between the pixel area (axa) and the point spread function (PSF) of the microscope and expressed as $A_{eff} = a^2 \otimes PSF$. The PSF can be approximated as a Gaussian function with center x_0 and width w, the result of PSF (Bag, Sankaran et al. 2012) is given in **2.5.4**

$$PSF\ (x, x_0) = \frac{1}{\sigma\sqrt{2\pi}} e^{\frac{(x-x_0)^2}{2\sigma^2}} \tag{2.5.4}$$

where

$$\sigma = \sigma_0 \cdot \frac{\lambda_{em}}{NA} \tag{2.5.5}$$

λ_{em} is the emission wavelength and NA the numerical aperture of the objective. σ_0 was calculated to be 0.4 (Bag, Sankaran et al. 2012) .

2.5.1 Instrumentation of DC-ITIR-FCCS

Measurements in CHO-K1 cells at 37°C were also performed by DC-ITIR-FCCS. The setup consisted of an inverted epi-fluorescence microscope (IX83,

Olympus, Japan) equipped with a motorized TIRF illumination combiner (IX3-MITICO, Olympus, Japan), an image splitter (OptoSpilt II, Cairn Research, Faversham, UK) and an electron multiplying charge-coupled device (EM-CCD) camera (Evolve 512, Photometrics, Tucson, AZ). 491 nm and 561 nm lasers (LAS/491/100 and LAS/561/100, Olympus, Germany) were connected to the TIRF illumination combiner in which the incidence angles for individual laser lines were adjusted to give 110 nm penetration depth of the evanescent field. The laser power measured at the back aperture of the objective was 0.6 mW for the 491 nm laser and 0.9 mW for the 561 nm laser. A 60x, NA 1.49 oil immersion objective (ApoN, Olympus, Japan) was used to illuminate the sample and collect the fluorescence image. The fluorescence light then passes through a major dichroic (Di01-R488/561, Semrock, Rochester, NY) and was split by the image splitter into the two halves of the camera chip. The image splitter was fitted with an emission dichroic (FF560-FDi01, Semrock, Rochester, NY) and band-pass filters (510AF23 and 615DF45 respectively, Omega Optical, Brattleboro, VT). A bright-field image of a stage micrometer was used to align the image splitter following a procedure described previously (Kohl, Haustein et al. 2005). The camera was controlled by Micro-Manager 1.4 (Edelstein, Tsuchida et al. 2014) and in each measurement, a stack of 30000 frames with 3.4 ms per frame was acquired. The captured region of interest consist of 20 lines (to allow sufficiently fast read-out) spanning the whole width of the camera chip (to include corresponding images in both the green and the red spectral region). The chamber with imaged cells was placed in an on-stage incubator (Chamlide TC,

Live Cell Instrument, Seoul, Korea) maintaining the temperature of 37˚C and 5% CO_2 atmosphere.

The image stacks were then analyzed by a self-written FIJI (Schindelin, Arganda-Carreras et al. 2012) plug-in (Sankaran, Shi et al. 2010), which calculates the ACF from intensity fluctuations in each pixel as well as the CCF for each pair of corresponding pixels in the two halves of the image. In order to correct for gradual changes in fluorescence intensity caused by bleaching or membrane undulations, correlations were calculated in sliding windows of 2500 frames and then averaged to avoid distortion of correlation functions due to intensity changes caused by photo-bleaching or whole cell movement. The plug-in is analogous to our previously described program ImFCS (Sankaran, Shi et al. 2010). The correlation functions were fitted with a model for 2-dimensional diffusion derived previously (Sankaran, Manna et al. 2009) to extract values of apparent particle numbers N, diffusion coefficient D and asymptotic correlation G_{inf}. The size of the microscope point spread function (PSF) was calibrated by measurement in supported lipid bilayers as described earlier (Bag, Sankaran et al. 2012). The background was set at 500 counts based on recordings in samples of cells not expressing any fluorescent protein. 2x2 pixels were binned for the analysis.

Since the EM-CCD camera is not a true photon counting detector, recovering absolute particle numbers is not straightforward (Unruh and Gratton 2008). We, therefore, did not attempt to determine the absolute dimer fractions but instead characterized the level of dimerization by cross-correlation amount *q* defined by equation **2.3.1.2**, in line with a previous work on dual-color

imaging FCCS (Kohl, Haustein et al. 2005). By performing the analysis for every pair of corresponding pixels, we obtained a map of the distribution of *q* in the imaged cell.

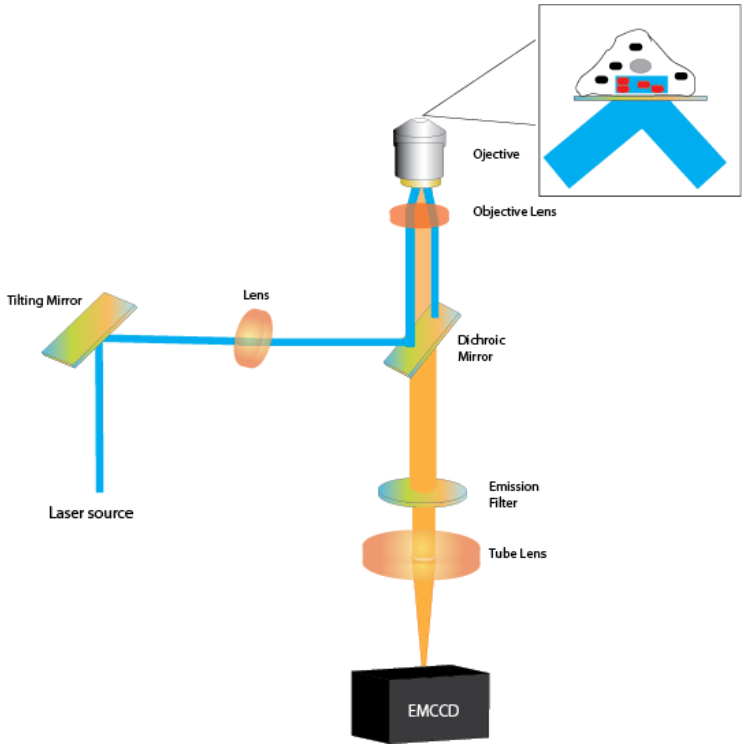

Figure 2.5.1.1 Schematic setup of ITIR-FCS. The laser beam passes through the lens in order to focus it to the dichroic mirror and is forwarded to the sample. In ITIR-FCCS, two lasers are used to illuminate the sample. The emissions are collected by the objective and forwarded to the EMCCD camera

3 Materials and Method

To investigate the factors influencing the dimer amount, the construct EGFR labeled with fluorescent proteins has been used for our measurements. Additionaly, the protein plasma membrane target (PMT) labeled with fluorescent proteins were included in the experiment plan to perform negative control on the FCCS system. PMT is derived from N-terminal (15 amino acids) of the X-linked retinitis pigmentosa protein RP2. Palmitoylation of this N-terminal is responsible for targeting of the protein to the plasma membrane localization (Chapple, Hardcastle et al. 2002). Therefore, PMTs were selected as a plasma membrane protein for conducting negative controls as they did not show any interactions when using FCCS.

3.1 Cloning of mApple-EGFR

The cloning of mApple-EGFR includes several steps. First, the insert mApple (a gift from Dr. David Piston, Washington University, St. Louis) was amplified by polymerase chain reaction(PCR) with Q5® High-Fidelity PCR Kit (New England BioLabs® Inc.,Ipswich, MA) using following primers (NewEnglandBioLabs® Inc., Ipswich, MA): Forward primer XhoI 5-3'AAACTCGAGATGGTGAGCAAGGG and Reverse primer XhoI 5-3'AAACTCGAGCTTGTACAGCTCGTC (Integrated DNA TechnologiesPte. Ltd, SG) in Eppendorf Mastercycler ep Gradient S (Hamburg, Germany). The PCR product was seperated by gelelectrophoresis and afterward extracted with GeneJET gel extraction kit (Thermo Scientific, Waltham, MA). The purified

PCR product was digested with XhoI enzyme. mRFP-EGFR plasmid (pNUT backbone, Figure 3.10.1) has been digested by XhoI to cut out mRFP, purified by gelelectrophoresis and dephosphorylated withFastAP Thermosensitive Alkaline Phosphatase (Thermo Scientific, Waltham, MA). Furthermore, the vectorbone was cleaned up by precipitation. Finally, EGFR vectorbone was ligated with mApple to the final construct mApple-EGFR (N-terminus). Ligated product was transformed to DH-5αcompetent cells, successfully cloned mApple-EGFR has been amplified for further measurements.

3.2 Cloning of SNAP-EGFR, EGFR-CLIP, PMT-SNAP, PMT-CLIP and SNAP-EGFR-CLIP

The inserts for the cloning were amplified by PCR using Q5® High-Fidelity PCR Kit (New England BioLabs® Inc. (NEB)) and the optimal annealing temperatures for a given set of primers were calculated in NEB T_m calculator online. Following primers were designed for the particular insert: SNAP to fuse it as N-terminus SNAP-EGFR: forward primer 5-3' AAACTCGAGATGGACAAAGACTGCG and reverse primer 5'-3' AAACTCGAGACCCAGCCCAG, EGFR for the fusion protein EGFR-CLIP forward primer 5'-3'AAAACCGGTATGCGACCCTCCG and reverse primer 5'-3' GAAACCGGTTGCTCCAATAAATTCACTGCTTTG, PMT for SNAP-PMT forward primer 5'-3' AAAGGATCCATGGGCTGCTTCTTCAGC and reverse primer 5'-3' AAAGGATCCTTAGCTCTCCTTGTCGGCC, PMT for PMT-CLIP forward primer 5'-3'AAAACCGGTATGGGCTGCTTCTTC and reverse primer 5'-3'

AAAACCGGTGCTCTCCTTGTCG, SNAP for SNAP-EGFR-CLIP forward primer 5'-3' AAAGATATCATGGACAAAGACTGCG and reverse primer 5'-3' AAAGATATCACCCAGCCCAGG. To get the final product SNAP-EGFR, SNAP were amplified by PCR using the primers mentioned above, digested with XhoI and precipitated. The vectorbone mRFP-EGFR was also digested with XhoI to remove mRFP and afterward dephosphorylated with FastAP Thermosensitive Alkaline Phosphatase (Thermo Scientific, Waltham,MA). The insert and vectorbone were purified by gelelectrophoresis. Finally, the SNAP and EGFR vectorbone were ligated for 5 minutes (min) at room temperature with Quick Ligase (New England BioLabs® Inc.). Ligated product was transformed and successful clones amplified. To clone the construct EGFR-CLIP (C-terminus), EGFR has been amplified using the given primers above, digested with AgeI and purified. The vectorbone CLIP (purchased from New England BioLabs® Inc.) were digested with AgeI, dephosphorylated and purified with gelelectrohporesis. The final substrates were ligated at room temperature for 5 minutes. The same procedure was used to clone the constructs SNAP-PMT and PMT-CLIP with the appropriative primers and enzymes. BamHI and AgeI were used to digest the PCR products and cut the vectorbone for SNAP-PMT (SNAP-vectorbone, Figure **3.10.3**) and PMT-CLIP (CLIP-vectorbone, Figure **3.10.2**). The cloning of the positive control SNAP-EGFR-CLIP were conducted in the plasmid EGFR-CLIP. SNAP were amplified by PCR, digested with EcoRV and cloned using same cloning protocol mentioned above.

3.3 Cloning of EGFR (I706Q, V948R)

The plasmid EGFR (1706Q, V948R) was a gift from Professor Tony Ng, King`s College London. Three PCR reactions have been conducted to get the insert EGFR (1706Q, V948R)-eGFP. In the first PCR, EGFR (1706Q, V948R) was amplified using DNA template EGFR (1706Q, V948R) and the forward primer 1 5'-3': (AgeI) AAAACCGGTATGCGACCCTCCGGGA and reverse primer 2 5'-3': AAATCCTCGCCCTTGCTCACCATACTTCCTCCTCCTGCTCCAATAAATTCA. The first PCR product contained EGFR (1706Q, V948R) and the protein linker (GGGS) with eGFP starting sequence. In the second PCR reaction, eGFP (linker and EGFR part) were amplified from the template PMT-eGFP with the following forward primer 35'-3': (underlined: codon of protein linker GGGS) AAATGAATTTATTGGAGCAGGAGGAGGAAGTATGGTGAGCAAGGGCGAGGAGC and reverse primer 4 5'-3' (NotI) AAAGCGGCCGCTTACTTGTACAGCTCGTCCAT. In the last PCR, the PCR product EGFR (1706Q, V948R) and the EGFP were used as a template with the forward primer 1 (from the first PCR reaction) and reverse primer 4 (from the second PCR reaction) to construct the insert EGFR (1706Q, V948R)-eGFP. The final product was cut by the restriction enzyme AgeI, precipitated, digested with NotI and gelelectrophoresis purified. The plasmid PMT-mRFP (vectorbone YFP, Figure **3.10.4**) were cut by AgeI and NotI to remove PMT-mRFP and purified by gelectrophoresis. In the last step, the vectorbone and insert were ligated using T4 Ligase (Thermo Scientific, Waltham, MA) at 16°C overnight. Afterward, the ligated product was transformed into DH-5α cells and amplified.

3.4 Cell culture and plasmid transfection

COS-7 (monkey kidney, fibroblast), HEK293 (human kidney, fibroblast) and CHO-K1 (Chinese hamster ovary, epithelial) cells purchased from ATCC (Manassas, VA) were cultured in DMEM (Hyclone Dulbecco's Modified Eagle's Medium, GE Healthcare, UK) containing 10% FBS (Hyclone fetal bovine serum, GE Healthcare, UK) and 1% PS,penicillin G and streptomycin (PAA, Austria) at 37˚C in 5% CO_2 atmosphere. Cells to 90% confluence were trypsinized with 0.5-1 ml 0.25% trypsin-0.03% EDTA solution (BSF, the Biopolis Shared Facilities, SG) for 3 min and ~5-10% of them were resuspended in 5 ml DMEM and placed back into the flask and incubator. Around $6x10^5$ - $1x10^6$ (CHO-K1 and COS-7) and ~5×10^6 (HEK293) splitted cells were centrifuged for 3 min and resuspended in ~8 µl electroporation buffer R when using 10 µl transfection system or ~90 µl R buffer at 100 µl transfection system. I used for COS-7 and CHO-k1 10 µl and for Hek293 cells 100 µl transfection system as Hek293 cells give better results when using 100 µl system. In general, ~3 µg EGFR-eGFP/mRFP, ~5 µg mRFP-EGFR-eGFP or 0.3 µg PMT-eGFP/mRFP were used in 10 µl transfection system or ~7 µg EGFR-eGFP/mRFP, ~13 µg mRFP-EGFR-eGFP or ~4 µg PMT-eGFP/mRFP in 100 µl transfection system. To do analysis at lower receptor concentration, only 1.5-2 µg labeled EGFR were transfected. With the aid of electroporation (Neon^R Transfection system, Life Technologies, Carlsbad, CA) appropriative amounts of EGFR constructs and plasma membrane targeting sequence (PMT) tagged with enhanced green fluorescent protein (eGFP) or monomeric red fluorescent protein (mRFP) were introduced into the cells using

manufacturer`s electroporation parameters for certain cell lines. The cells seeded on coverslips (30 mm in diameter; Lakeside, Monee, IL) or glass dishes (MatTek Corporation, Ashland, MA) submerged in DMEM with 10% FBS were kept in the incubator at 37˚C in 5% CO_2 atmosphere. After an overnight incubation, the transiently transfected cells were serum-starved for minimum 4 hours and incubated for 30 min with the following three inhibitors with the final concentrations of 2 mM for NaF, 10 mM for NaN_3 and 5 mM for 2-deoxy-D-glucose (all inhibitors from Sigma-Aldrich, St. Louis, MO). Finally, the coverslip with the cells was washed with PBS and mounted to an imaging chamber in the case of using glass slides filled with 1 ml PBS containing the three inhibitors. To analyze phosphorylated receptors, ~5-6 x 10^6 cells were transfected in 100 µl system with ~5-6 µg plasmid and seeded on a glass dish.

3.5 Western Blotting of phosphorylated chimera ErbB receptors

Cells were transfected with ~5-6 µg plasmid (wt-EGFR, mApple-EGFR, SNAP-EGFR, EGFR-CLIP, SNAP-EGFR-CLIP) in CHO-K1 cells and kept in the incubator overnight. Next day, the cells were starved for minimum 4 h and later on stimulated with a final concentration of 100ng/ml EGF for 30 minutes on ice(Moriki, Maruyama et al. 2001). The cells were washed three times with cold 1xPBS and lysed with RIPA buffer supplemented with phosphatase and protease inhibitor cocktail (Thermofischer, Waltham, MA) for 5 minutes on ice. After 15 min centrifugation at 4.000 g at 4 °C, the supernatant has been

stored at -80°C until its usage. Around 20 µl 2x Laemmli buffer (Bio-Rad, CA), supplemented with mercaptoethanol, were added to 25 µl cell aliquot and boiled for 10 min at 95 °C. The samples were loaded into the wells of a 7% SDS- polyacrylamide gel and were run at 100 V for ~1.20 h. The gel was blotted onto PVDF membrane (pore size 45 um, GE Healthcare, Little Chalfont, UK) at 100V for 1h. Afterward, the membrane was blocked in 3% BSA in 1xTBST solutionovernight at 4°C. Next day, the membrane has been washed three times with 1xTBST for 5 min and incubated with the primary antibody anti-pTyr (PY20) (sc-508; Santa Cruz Biotech., Santa Cruz, CA) in 1%BSA 1xTBST for 3-4 h. Afterward, the membrane has been washed three times with 1xTBST and incubated with sheep anti-mouse IgG conjugated with horseradish peroxidase (HRP) as a secondary antibody in 1% BSA for 1-2 h. Finally, the membrane waswashed with 1xTBST three times. The proteins were visualized by incubation the membrane in ECL substrate solution using manufactures recommendation (Clarity Western, ECL substrate, Bio Rad, CA). Finally, the membrane was analyzed in ImageQuant LAS4000 (GE Healthcare, Little Chalfont, UK).

3.6 Labeling procedure of ACP-EGFR with CoA-Atto488, CoA-OregonGreen and CoA-Cy3

ACP-EGFR was a gift from gift from Dr. Donna J Arndt-Jovin, Germany. Before covalently labeling of the receptors, CHO-K1 cells expressing the fusion protein were serum-starved for at least 4 h and to reduce the activity of EGFR

fusion protein (Bosch, Correa et al. 2014). Afterward, 1 µM CoA-label (CoA-Atto488, CoA-OregonGreen or CoA-Cy3) and 1 µM ACP Synthase (New England BioLabs® Inc.) were added to the cells in colorless DMEM supplemented with 1% 1 mg/mL bovine serum albumin (BSA) (Sigma Aldrich) at 37 °C, 5 % CO_2 for 30-40 min. Cells were washed three times with phenolred-free DMEM supplemented with 1% BSA and incubated with three inhibitors with the final concentrations of 2 mM NaF, 10 mM NaN_3 and 5 mM 2-deoxy-D-glucose (all inhibitors from Sigma-Aldrich).

3.7 Labeling of the constructs SNAP-EGFR, EGFR-CLIP and SNAP-EGFR-CLIP

The transfected cells with SNAP-EGFR were serum-starved and incubated with ~5-7 µM SNAP-Surface®488 substrate (New England BioLabs® Inc.) in colorless DMEM supplemented with 0.5% 1 mg/mL BSA at 37 °C, 5% CO_2 for 30 min. For the EGFR-CLIP construct, ~1.8µM CLIP-Cell™ TMR-Star (New England BioLabs® Inc.) substrates were added for 30 min. After labeling, the cells were after washing incubated for another 30 min as CLIP-Cell™ TMR-Star is cell-permeable. This step is necessary to remove unreacted substrates. Dual-labeling of SNAP-EGFR-CLIP were conducted in a similar way; first SNAP-tag were labeled with 7 µM SNAP-Surface®488 substrate, washed several times with DMEM and afterward labeled with~1.8µM CLIP-Cell™ TMR-Star solution. The labeling solution were replaced by DMEM and incubated for

another 30 min to remove uncreated CLIP substrates. All measurements were performed in the presence of internalization inhibitors as mentioned before.

3.8 Drug treatment and Ligand stimulation

Methyl-β-cyclodextrin (mβCD, Sigma) is routinely used in membranes tudies to extract cholesterol from lipid rafts. mβCD s capable to form a complex with cholesterol (Nishijo, Moriyama et al. 2003). Itwas solved in PBS buffer and kept at -20ºC. Transfected cellswere treated with a final concentration of 3 mM in serum-free media 1 ml 1xPBS. After 25 min incubation time, the cells were measured in the time frame until 10 min. Latrunculin A (LAT-A, Calbiochem) is obtained from red sea sponge Latrunculiamagnifica. In cell biology, it is used to inhibit actin polymerizationand destroy cytoskeleton. A stock solution of LAT-A in DMSO witha concentration of 10 mM was stored at -20ºC. For the experiments, a final concentration of 3 µM in 1ml 1xPBS was used to destroy cytoskeleton and the measurements were done within 15 min. The transfected cells with EGFR were stimulated with a final concentration of EGF (100ng/ml) or (10 ng/ml).

3.9 Estimation of number of labeled receptors per cell

We used the sum of background-corrected particle numbers from both the channels ($N_s = N_g + N_r$) to estimate the number of EGFR copies per cell. N_s is the number of labeled receptor molecules within the observation area $\pi\,\omega_0^2$

defined by the focus of the confocal microscope. The radius of the observation area ω_0 is determined by the calibration of the confocal volume. To obtain the number N_c of receptors per cell we need to estimate the area of the whole cell membrane A_c and then $N_c = N_s A_c/(\pi \omega_0^2)$. The area of the basal cell membrane A_b can be directly determined from the confocal images of the cells in which we performed the measurements. Approximating the shape of the apical membrane as a spherical surface, we can write $A_c = 2A_b + \pi h^2$, where the height of the cell h can be estimated as the typical difference in axial focus position between the basal and the apical membrane. The average calculated cell surface of CHO-K1, HEK293 and COS-7 were 691 μm^2, 602 μm^2 and 1501 μm^2, respectively. The calculated surface area of CHO-K1 is consistent with the literature value ~632 μm^2 (Kluba, Engelborghs et al. 2015).

3.10 Plasmid maps of different constructs

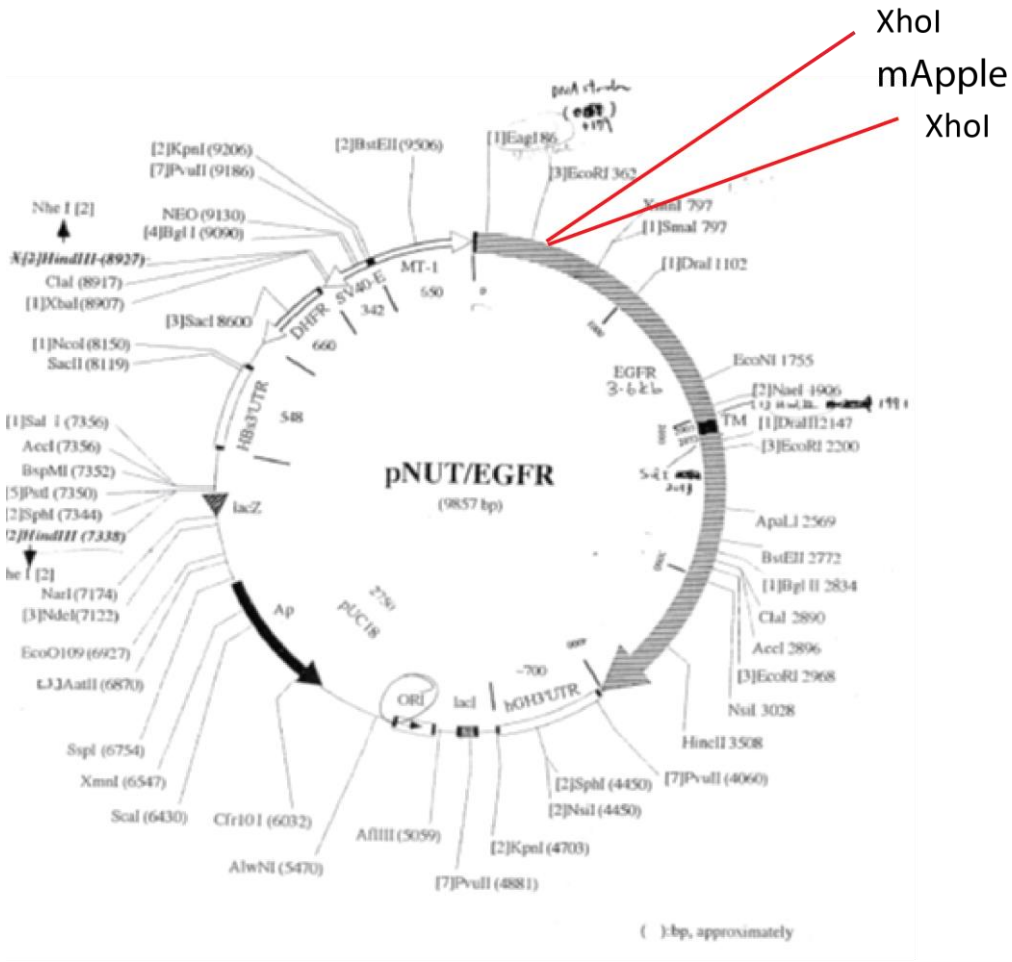

Figure 3.10.1 Plasmid map of mApple-EGFR

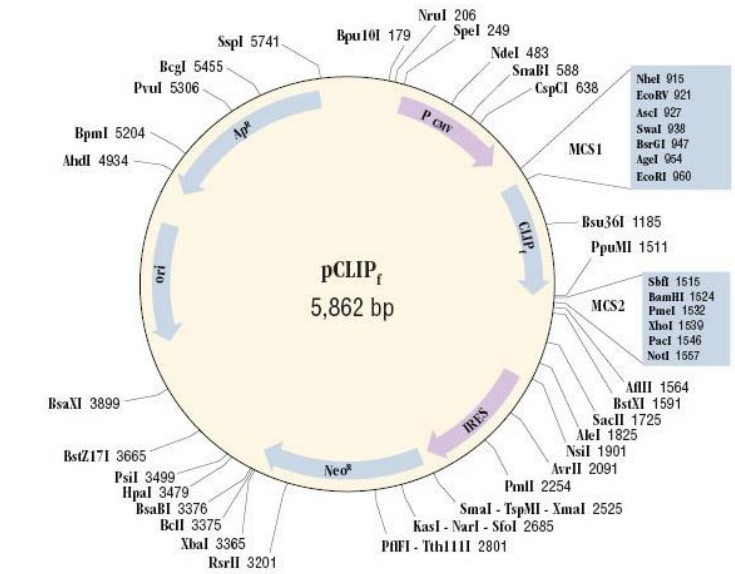

Figure 3.10.2 pCLIPf vectorbone (NEB website)

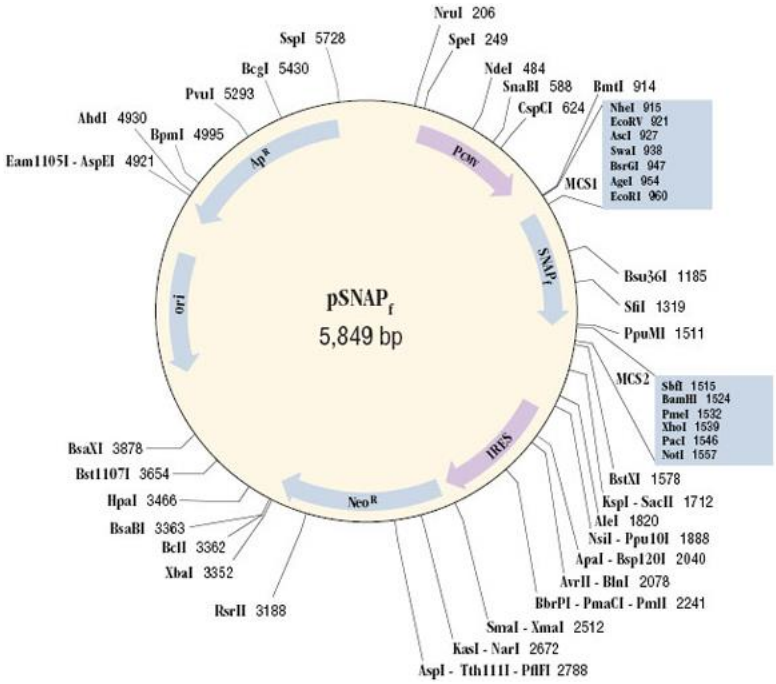

Figure 3.10.3 pSNAPf vectorbone (NEB website)

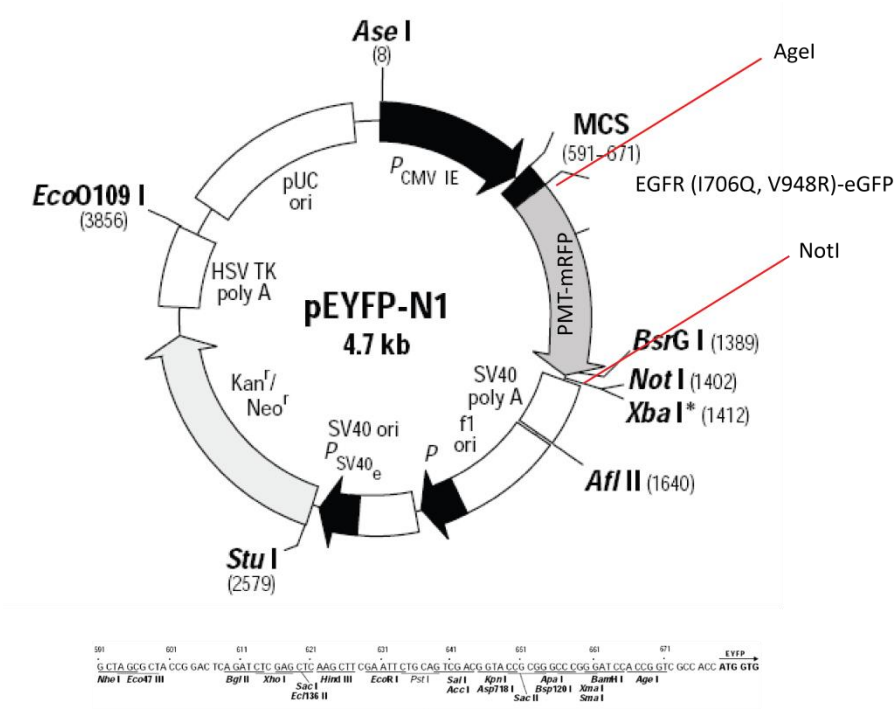

Figure 3.10.4 Plasmid map of EGFR (1706Q, V948R)-eGFP

4 Quantification of EGFR dimers in resting cells by using different FCCS modalities

After more than 35 years' research, uncertainty about the receptor dimerization in the absence of ligand still exists. We and other groups attempt to determine the amount of preformed dimers on the cell surface by using different technical and experimental approaches, but the results deviate extremely among the studies.

In this chapter, we address the question to which extent the experimental conditions influence the presence of receptor dimerization. In the second part, we perform the measurements on different FCCS modalities to test whether the results remain consistent.

In addition, some experiments on EGFR have been repeated to verify the consistency with our previously shown results (Liu, Sudhaharan et al. 2007, Ma, Ahmed et al. 2011).

4.1 Determination of Diffusion coefficient

It is thought that plasma membrane associated signaling relies on the surrounding of receptor localization. Therefore, three distinct cell lines CHO-K1, COS-7 and HEK293 have been chosen to evaluate the dimerization amount. Epithelial cells (CHO-K1) consist of distinct apical and basal membrane domains which are divided by tight junctions (Tanos and Rodriguez-Boulan 2008). Some evidence shows that the distinct lipid composition in the apical membrane makes it robust (Brasitus and Schachter

1980, Simons and van Meer 1988). However, fibroblasts as COS-7 do not contain characteristic apical basal polarity. In our experimental design, the transfected cells on the glass side named as lower membrane refers to basal membrane and the upper membrane on the top of the cell refers as apical membrane even in cell lines with no basal-apical polarity. Furthermore, the experiments were conducted in CHO-K1, COS-7 and HEK293 as they possess a different amount of endogenous EGFR. CHO-K1 does not express any endogenous EGFR.COS-7 and HEK293 have ~100,000 and ~20,000 receptors per cell, respectively. The temperature was set to room and physiological temperature during the experiments to examine the extent of physiological and non-physiological conditions on EGFR dynamics. This temperature was selected as it was frequently used in the past studies.

The cells were transiently transfected with mRFP-EGFR and EGFR-eGFPand kept in the incubator overnight. Usually, the glass dishes were covered up to with~50-60% confluent cells during experiments. Next day, the cells have been starved for minimum 4 h and afterward incubated with internalization inhibitors for 30 min. The localization of EGFR-eGFP was in the apical and basal plasma membrane. Healthy cells with firm attachment have been selected for FCCS measurements and analysis. To avoid artifacts on the correlation functions, the count rate of the fluorescence intensity did not exceed 300 kHz and the ratio between the two distinct intensity traces was between 0.5 to 2. The measurements were carried out on the apical and basal membrane to determine the diffusion coefficient *D*. To obtain *D*, the diffusion time τhas been extracted from the fitting and calculated using

equation **2.3.1.** The average *D* of the transmembrane EGFRat the apical and basal membrane was approximately $0.3 \pm 0.2\ \mu m^2/s$ (mean ± standard deviation (SD) at room temperature and showed no differences between these two membrane locations (t-test (one tail, type 1 for all data in this section), p=0.32) (Figure **4.1.1**). *D* is consistent with previously reported value (Chung, Akita et al. 2010, Kluba, Engelborghs et al. 2015) in resting cells. At the physiological temperature of 37°C, *D* reaches a higher value of approximately $0.7 \pm 0.3\ \mu m^2/s$ (t-test, p=0.0016). All correlation curves were successfully fitted with a model with a single diffusive component (2D1p1t); this is in agreement with the Saffman-Delbrueck model, which predicts only a negligible difference in *D* between a monomer and a dimer of a membrane protein (Weiß, Neef et al. 2013). In general, the *D* of mRFP-EGFR and EGFR-eGFP was in the same range in the apical and the basal membranes of all studied cell lines. In all cases, *D* increases with the increase of temperature as expected. In addition, we observed an increase of the standard deviation of *D* with temperature which is probably due to increased heterogeneity in local membrane organization at physiological temperature; similar effects have been observed previously (Ries, Chiantia et al. 2009). Consistently, *D* of EGFR measured by DC-FCCS and quasi PIE-FCCS at room temperature was also in the range $0.3 \pm 0.2\ \mu m^2/s$ in agreement with SW-FCCS results.The average *D* at 37°C determined by DC-ITIR-FCCS in both the green and the red detection channel was approximately $0.6 \pm 0.3\ \mu m^2/s$. A detailed description of the results obtained from quasi-PIE-FCCS, DC-FCCS and DC-ITIR-FCCS will be given in the sections **4.7** and **4.8**.

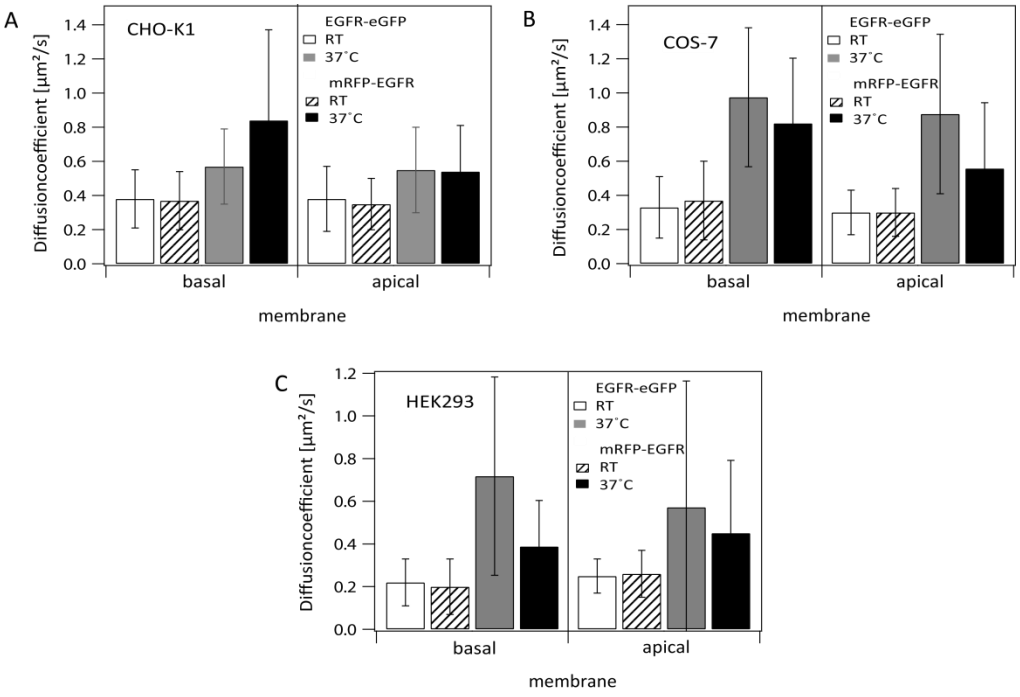

Figure 4.1.1 Diffusion coefficient in different cell lines. Diffusion coefficient D ± SD of EGFR-eGFP (white bar at RT, grey bar at 37°C) and mRFP-EGFR (striped bar at RT, black bar at 37°C) in the apical and the basal membranes of CHO-K1 **(A)** COS-7 (t-test:p=0.053 (basal/apical, RT), p=0.00005 (basal, RT/37°C) **(B)** and HEK293 cells (t-test:p=0.45 (basal (red and green EGFR, RT), p=0.00053 (apical, RT/37°C, mRFP-EGFR) **(C)** D values are similar in all three cell lines. (t-test: one tail, type 1).

4.2 EGFR complex fractions in resting cells using SW-FCCS

EGFR complex formation has been investigated under certain experimental conditions in three different cell lines. To investigate the cross-correlation amount *q*, transiently transfected labeled EGFR were measured for 30 seconds to obtain auto-and cross-correlation curves. An interaction of the receptors will result in an elevated cross-correlation curve, while non-interaction will lead to a flat cross-correlation curve (Figure **4.2.2**). The amount of factor *q* was calculated by using equation **2.3.1.2**. The measurements were initially performed on SW-FCCS. Control experiments as positive and negative were conducted for each cell line and each

temperature in order to determine the dynamic range of our method. Double labeled receptor mRFP-EGFR-eGFP as a positive control gave a cross-correlation amount *q* of 58% ± 1% in CHO-K1 cells; the value is the average from measurements on both membranes and at both temperatures, errors are given as the standard error of the mean (SEM) unless stated otherwise(t-test, p=0.44 (RT group), p=0.0002 (37˚C)). The average values of *q* of the controls are presented in Figure **4.2.1**, determined on different membrane location, temperature and cell lines.

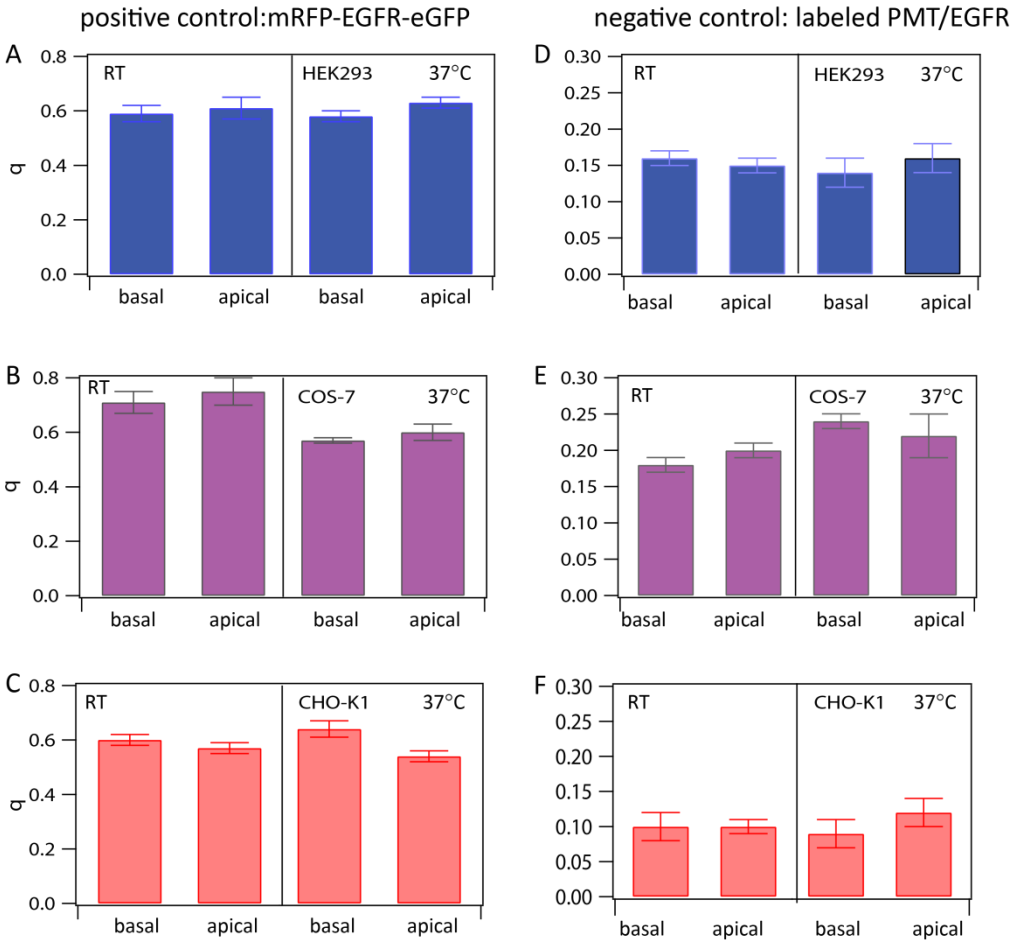

Figure 4.2.1 Results of positive and negative controls. **(A-C)** positive control mRFP-EGFR-eGFP *q* (± SEM) **(D-F)** negative control labeled PMT/EGFR *q* (± SEM) in HEK293, CHO-K1 and COS-7. The positive control set the upper limit of the system; the average *q* is similar in each cell line.

In COS-7 and HEK293 cells, the apparent complex fraction of mRFP-EGFR-eGFP was 68% ± 2% (t-test (one-tail, type 1 for all data used in this section), p=0.16 (RT group), p=0.15 (37˚C)) and 58% ± 1% (t-test, p=0.45 (RT group), p=0.28 (37˚C)), respectively. Consistently, the values *q* of the positive control is similar in all examined cell lines. The apparent complex fraction lower than 100% can be explained by the incomplete maturation of mRFP and its prolonged residence in dark or dim states (Hillesheim, Chen et al. 2006, Foo, Naredi-Rainer et al. 2012). In a previous study, the labeled plasma membrane targeting sequence (PMT) did not show protein interaction in CHO-K1 cell (Liu, Sudhaharan et al. 2007), making them a suitable negative control for FCCS measurements in cell membranes. Surprisingly, when using these labeled PMTs to determine the lower limit of our method, different behavior of these proteins was observed in COS-7 and HEK293. In these cell lines, a considerably higher amount of cross-correlation was found. A possible explanation for the increased cross-correlation is the partitioning of PMT into membrane microdomains. This will be discussed in section **4.8**. Hence, we selected monomeric labeled PMT and EGFR as the negative control for all three cell lines. We obtained the following cross-correlation amounts *q*: 10% ± 2% (t-test, p=0.45 (RT group), p=0.11 (37˚C)) in CHO-K1, 15% ± 0.5% (t-test, p=0.18 (RT group), p=0.41 (37˚C)) in HEK293 and 21% ± 1% (t-test, p=0.17 (RT group), p=0.25 (37˚C)) in COS-7 cells (Figure **4.2.1**). The apparent complex fraction is significantly higher than in the other cell lines; possibly caused by partitioning of PMT and EGFR into the same domains and makes detection of low levels of EGFR dimerization difficult in these cell lines. The fact that

different cell lines can show different organization on membranes is the goal of a present study in our lab but has also been shown previously (Bag, Yap et al. 2014, Kraft and Klitzing 2014, Kreder, Pyrshev et al. 2015). The higher value of 10% for the negative control in CHO-K1 can be explained by spectral emission crosstalk of eGFP in the red detector channel. Besides the control experiments, the actual experiments have been evaluated to give insight into the EGFR-EGFR interactions in the absence of ligand. Three different individual experimental sets are displayed in Figure **4.2.2** and represent examples. In these selected FCCS plots, the positive control and the experiment revealed 43% and 37% complex fraction, respectively. In the case of the negative control, it did not form any complexes, leading to a *q* of 0%.

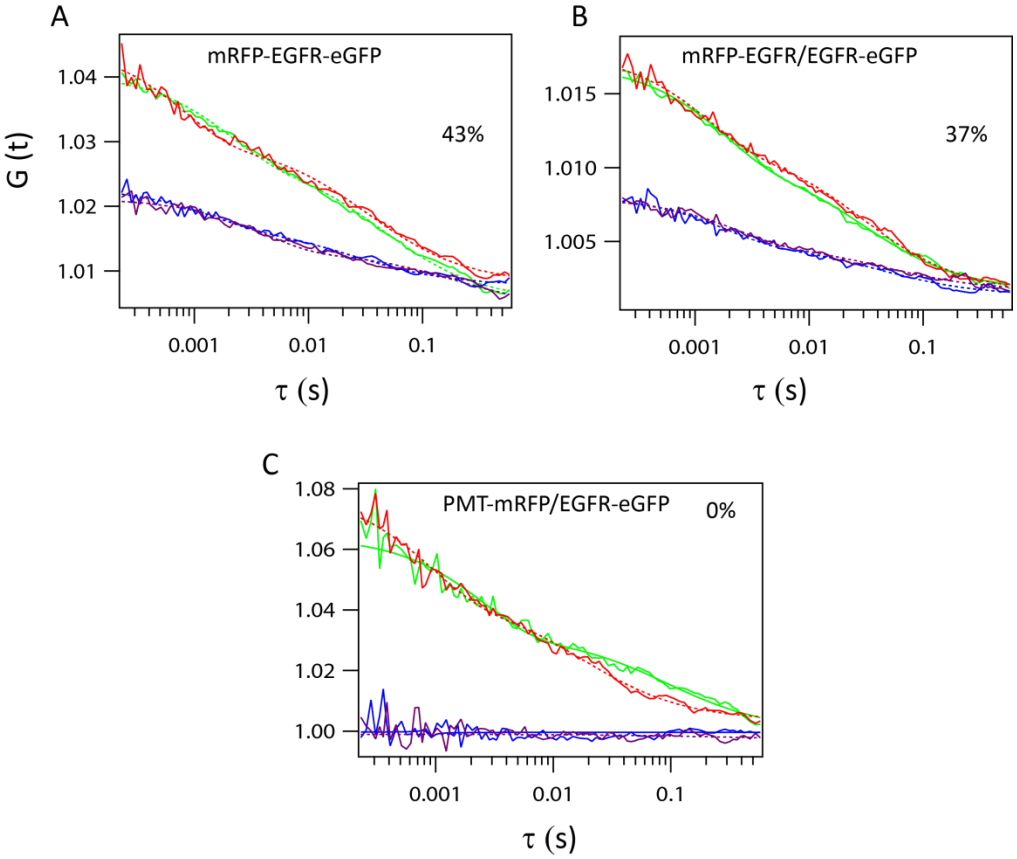

Figure 4.2.2 ACF and CCF samples of selected experimental targets in all cell lines. **(A)** Positive control mRFP-EGFR-eGFP **(B)** experiment mRFP-EGFR-eGFP and **(C)** negative control PMT-mRFP/EGFR-eGFP. Experiments were done in CHO-K1

The receptor interaction in the absence of ligand was extensively probed in CHO-K1 (epithelial cells) as it is known to not express endogenous EGFR. This cell line show apical and basal plasma membrane domains which is necessary to perform distinct cell processes. The density of the labeled receptors can be estimated by fitting the auto-correlation curves. It provides the number of particles *N* green and red in the defined confocal volume, which can be used to determine the density of the receptor in the entire cell. The surface of the CHO-K1 area was calculated as described in section **3.6.** The average surface from around 10 cells was ~691 μm^2, consistent with the literature value of~632 μm^2 (Kluba, Engelborghs et al. 2015). To probe whether the complex fraction is concentration-dependent, cells ranging from low to very high EGFR expression were examined. The number of receptors in the observation area was ranged between 3 to 462. These receptor amounts correspond approximately to cell surface receptor densities of 17 to 2222 per μm^2. Our results yielded an average apparent complex fraction of 32% ± 3% (n=47, 20 cells) on the basal (t-test, p=0.33) and 33% ± 5% (n=46, 19 cells) on the apical membrane (t-test, p=0.007) at room temperature (Figure **4.2.3**). At physiological temperature (37°C), the apparent complex fraction in the basal membrane is 28% ± 2% (n=47, 15 cells) which does not differ significantly (t-test, p=0.16) from the value at room temperature. A slight increase to 39% ± 4% (n=30, 17 cells) occurs in the apical membrane (t-test, p=0.16) (Figure **4.2.4**)**.** The data analyzed in the apical membrane at room temperature is consistent with previously reported values determined in our group (Liu, Sudhaharan et al. 2007) and given in the table **4.2.1.**

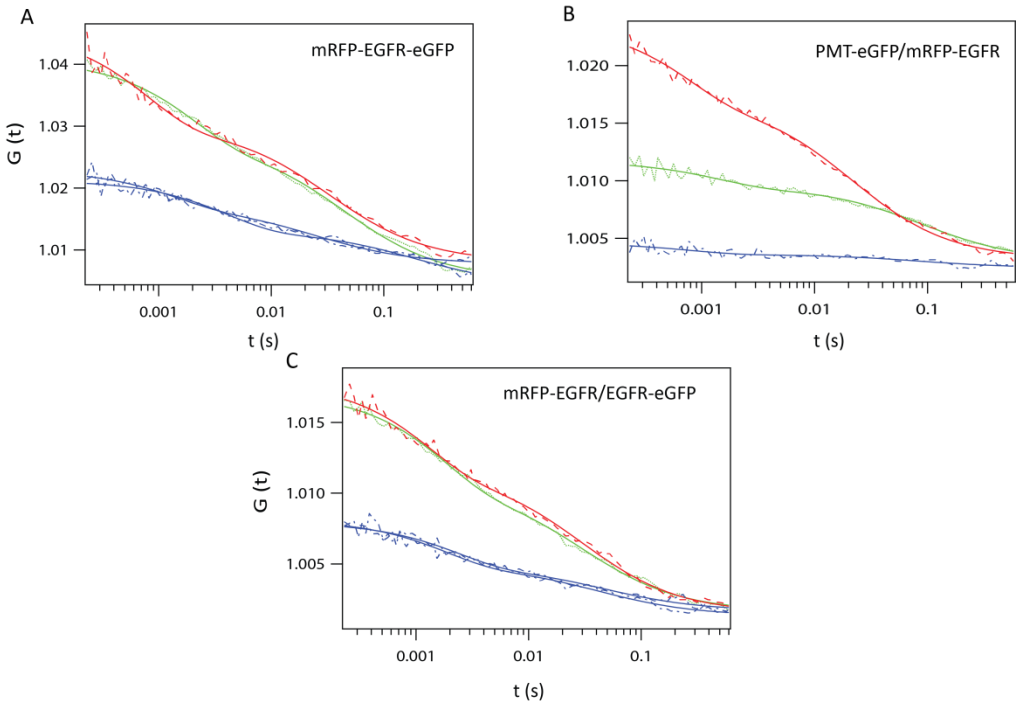

Figure 4.2.3 FCCS cuves obtained by SW-FCCS. **(A)** positive control mRFP-EGFR-eGFP **(B)** negative control PMT-eGFP/mRFP-EGFR and **(C)** mRFP-EGFR/EGFR-eGFP

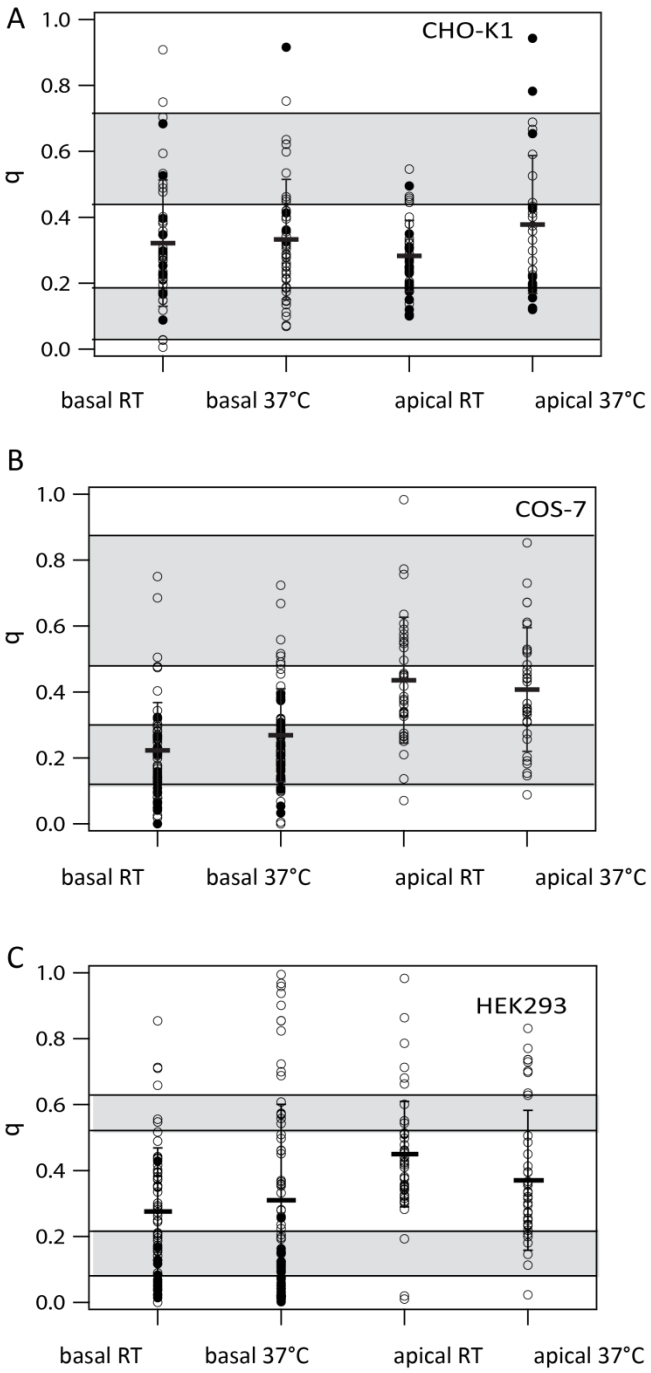

Figure 4.2.4 Complex fraction in distinct cell lines. **(A)** The cross-correlation amounts *q* in CHO-K1 cells expressing mRFP-EGFR/EGFR-eGFP with ≤ (●) or > (◌) 200 receptors per um^2 at different conditions (basal and apical membrane, physiological and room temperature) **(B)** An analogous plot for COS-7 cells expressing ≤ (●) or > (◌) 200 receptors per um^2 **(C)** *q* values for HEK293 cells expressing ≤ (●) or > (◌) 200 receptors per um^2. The upper and lower gray zones in **(A),** (**B)** and **(C)** represent the positive and negative controls with corresponding ± standard deviations (SD), respectively. The box represents the average *q* ± SD

A summary about the complex fraction of the receptors under different conditions is shown in table **4.2.1.** Assuming 100% dimerization in the positive control, we normalize these values by diving it by the average *q* of the positive control. The normalized values are an estimate of the actual dimer fraction and are represented in table **4.2.1**.

Protein in CHO-K1	Complex *q* (± SEM)	Normalized dimer	n (cell)
mRFP-EGFR/EGFR-eGFP at RT (Liu Ping)			
basal			
apical	0.50 ± 0.05	0.68 ± 0.08	- (18)
mRFP-EGFR/EGFR-eGFP at RT (Xiaoxiao Ma)			
basal	-		-
apical	0.33 ± 0.02	0.65 ± 0.04	- (71)
mRFP-EGFR/EGFR-eGFP at RT (this thesis)			
basal	0.32 ± 0.03	0.55 ± 0.05	47 (20)
apical	0.33 ± 0.03	0.57 ± 0.05	46 (19)
mRFP-EGFR/EGFR-eGFP 37°C (this thesis)			
basal	0.28 ± 0.02	0.53 ± 0.04	47 (15)
apical	0.39 ± 0.04	0.67 ± 0.07	30 (17)

Table 4.2.1 Comparison of EGFR-EGFR interaction amount with previous work and this present work measured at different conditions in CHO-K1. *the values were normalized to the average positive control 58% under different situations in this thesis

As seen in Figure **4.2.4**, the subpopulations of cells with receptor densities below and above 200 receptors per μm^2, respectively, do not differ in the apparent complex fractions. The independence of cross-correlation fraction on the expression level is even more evident from the plot of *q* versus the number of EGFR copies per detection area (Figure **4.2.5)**.

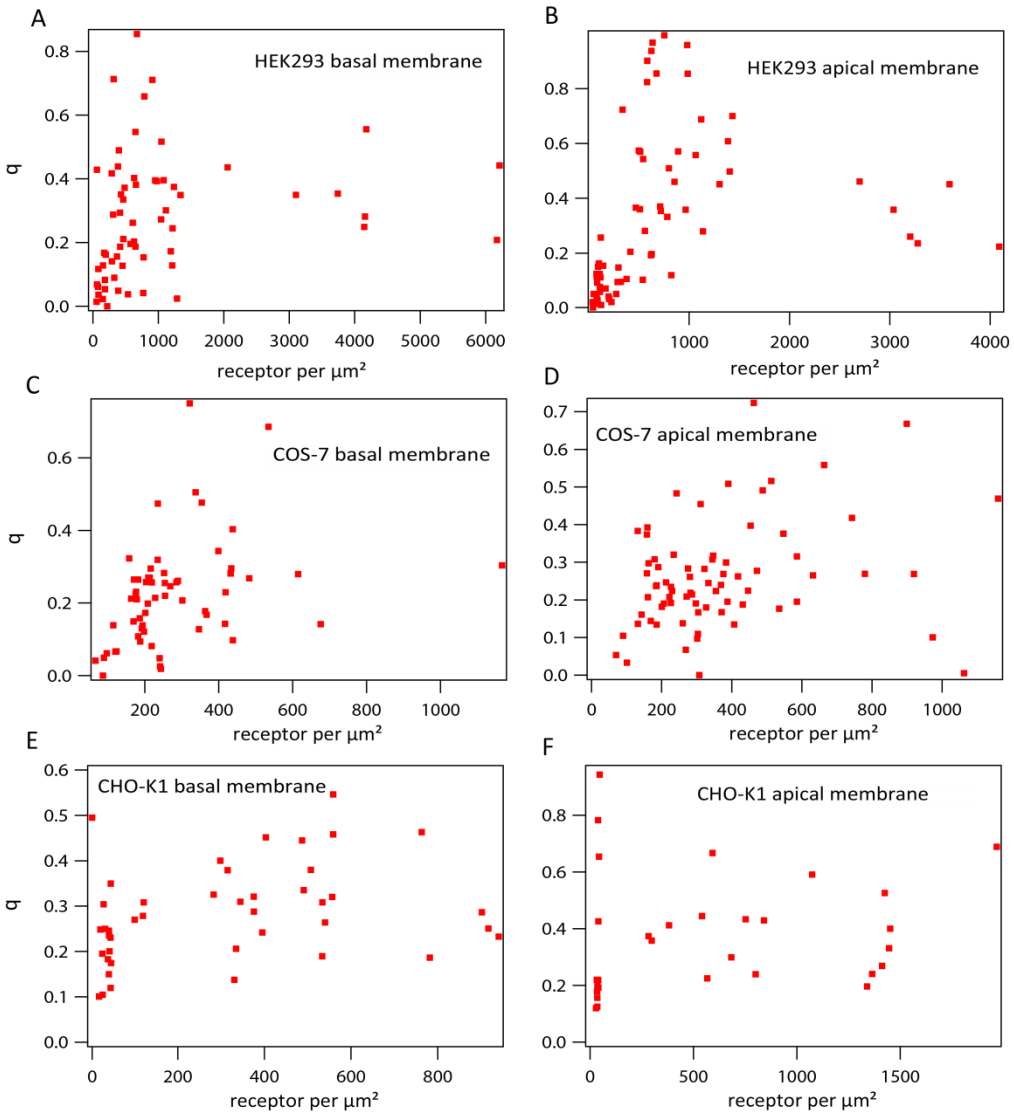

Figure 4.2.5 Scatter plots. **(A-D)** *q* for mRFP-EGFR/EGFR-eGFP in HEK293 and COS-7 plotted against cell surface density per µm². *q* increases with expression level (N_s) due to the presence of endogenous EGFR in these cell lines. Experiments were performed on the apical and the basal membranes in CHO-K1 at room temperature **(E-F)** *q* for mRFP-EGFR/EGFR-eGFP in CHO-K1 plotted against the receptor density per µm².

No dependence of *q* on receptor density was observed within the range of expression levels probed. Experiments were performed on the apical and the basal membranes at 37°C.

Furthermore, the investigation of EGFR complexation has been extended to the cell lines HEK293 and COS-7, which express endogenously approximately

20.000 and 100.000 EGFR copies per cell, respectively **(**Figure **4.2.4)**. The labeled receptor densities in HEK293 and in COS-7 cells were in the range of 34 to 6212 per µm^2 (N_s=7-1242) and 62 to 1543 per µm^2 (N_s=13-321), respectively (Figure **4.2.5**). In these cases, differences in *q* are observed between cells with labeled receptor densities below and above 200 per µm^2. In both cell lines HEK293 and COS-7, the dependence of the apparent *q* factor on the labeled EGFR expression level is apparent from Figure **4.2.5**.

In the presence of endogenous EGFR, the complex formation of labeled EGFR results in a decrease in cross-correlation amount *q* and, thus, in underestimation of the complex fraction, unless the number of endogenous receptors is made negligible by overexpressing of the labeled ones (Figure **4.2.5**). Figure **4.2.6** showst two different outcomes of cross-correlation amplitudes in HEK293 when using low to high expression levels. High receptor density with 427.420 receptors on the entire cell surface resulted in a complex formation of 35%. While at low receptor expression of 36.120 labeled receptors, the endogenously present receptor was noticeable and decreased the *q* value down to 10%, comparable with the negative control.

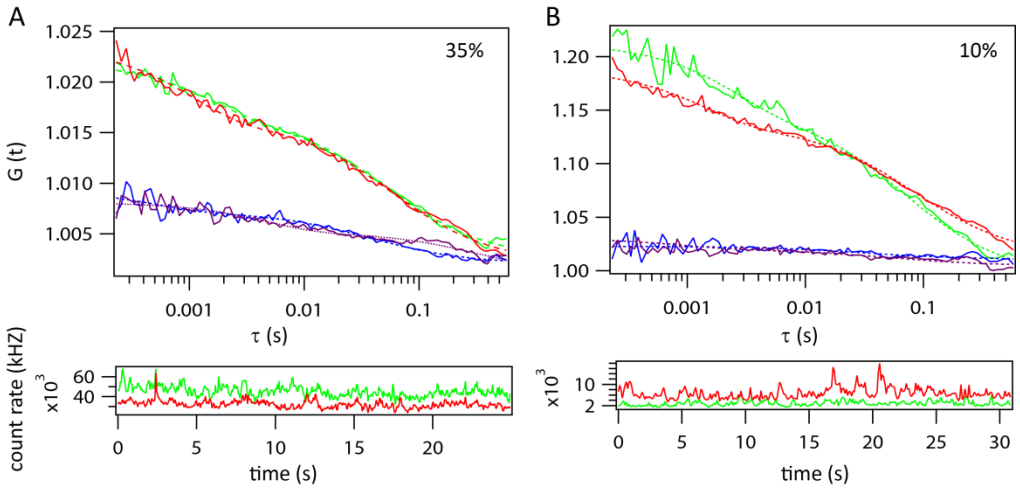

Figure 4.2.6 FCCS curves obtained from HEK293 cells expressing labeled EGFR **(A)** high expression level of labeled EGFR (427,420) compared to the presence of endogenous EGFR; leading to a *q* of 35%. (N_s=142) **(B)** In this case, low labeled receptor concentrations result in only 10% complex fraction (N_s=12) at 36.120 receptor densities

These results show that in the presence of endogenous receptor it is impossible to draw any definite conclusions on EGFR dimerization from FCCS measurements in cells that are not overexpressing the fluorescently labeled receptor.

4.3 Effect of Latrunculin A (LAT-A) treatment on EGFR dimerization

The movement of membrane proteins is assumed to be restricted by the cortical, membrane-associated F-actin, a component of the cytoskeleton (Chen and Resh 2002). It is supposed that the actin strands in the cytoskeleton network sterically interact with the cytoplasmic tail of the proteins, confining them into microdomains (Toral, Solano-Agama et al.

2007).To study the role of actin cytoskeleton on EGFR dimerization, we chose CHO-K1 cells as an endogenous EGFR free platform. The measurements were conducted at 37°C and focused on the upper and lower membrane. The cells were co-transfected with similar amounts of mRFP-EGFR/EGFR-eGFP, incubated overnight and serum-starved for a minimum of 4-5 h. Internalization inhibitors were added to keep the receptors on the cell surface and treated with a final concentration of 3 µM Latrunculin (LAT-A). This drug is commonly used to disrupt the cytoskeleton and is an indirect method to explore the association of EGFR dimers with the network of actin filaments. In this set of experiments, the glass dishes were fixed with a double-sided tape on the objective stage in order to detect the same cell before and after drug treatment. The non-treated cells were tested for the dimer fraction and the data of LAT-A treated cells were acquired after 15 min incubation at 37 °C. Three laser spots with maximal three data recording on each cell were evaluated.

LAT-A treated cells exhibit apparent complex fractions of 26% ± 2% (n=32, 4 cells) and 27% ± 3% (n=24, 4 cells) in the basal and the apical membrane, respectively. This agrees well with control cells having 23% ± 3% (n=27, 4 cells) and 27% ± 2% (n=28, 4 cells) complexes in the basal and the apical membrane, respectively.The results are displayed in Figure **4.3.1.**

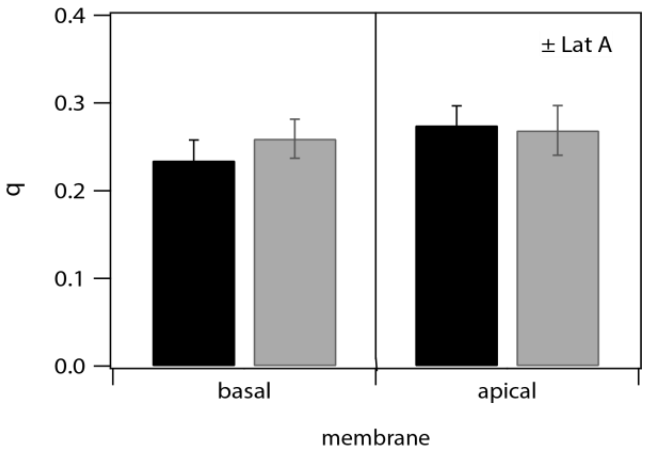

Figure 4.3.1 Disruption of the cytoskeleton in CHO-K1 cells. No changes are detected after LAT-A treatment compared with untreated cells. (t-test (one tail, type 1), p=0.28 (basal)and and p=0.45 (apical)).

Note that the average of *q* of untreated cells is slightly lower than the value that we stated in the previous section; this is most likely caused by the cell-to -cell variability and the limited size of the cells tested for cytoskeleton disruption.These results indicate that the EGFR complex formation in the plasma membrane does not depend on the actin cytoskeleton, which is consistent with the study of Ariotti et. al (Ariotti, Liang et al. 2010). In Table **4.3.1**, the mobility of EGFR is summarized and compared before and after the LAT-A treatment.

	Non-treated cells		LAT-A treated cells	
	basal	apical	basal	Apical
τ_DmRFP (ms ± SD)	53 ± 19	79 ± 38	84 ± 87	55 ± 24
τ_DeGFP (ms ± SD)	54 ± 37	69 ± 26	79 ± 12	48 ± 19
n (cells)	27 (4)	28 (4)	32 (4)	24 (4)

Table 4.3.1 The diffusion times of differently labeled EGFR. The diffusivity increases after cytoskeleton in the apical membrane. However, the diffusivity decreases after drug treatment in the basal surface

The diffusion times of eGFP- and mRFP-labeled receptors were 54 ± 37 ms and 53 ± 19 ms in the basal membrane, respectively, before the drug treatment. The LAT-A incubation reduced the diffusivity of the receptors to 79 ± 12 ms and 84 ± 87 ms in the lower surface, respectively. However, opposite effect was observed in the apical membrane. The data showed an overall increase in the motion of the green and red labeled protein. The average value of the diffusion time was for green and red receptors 69 ± 26 ms and 79 ± 38 ms before the treatment, respectively and changed to 48 ± 19 ms and 55 ± 24 ms for green and red EGFR, respectively, after the LAT-A treatment.

4.4 Influence of cholesterol depletion on EGFR complex fraction

In this work, the focus was to investigate the cause for inconsistent results of reported EGFR dimer amount. For this reason, dimerization of the receptor was tested at different experimental conditions and different techniques. It has been suggested that EGFR dimerization is dependent on the localization in the plasma membrane. A number of studies reported that the presence of EGFR in lipid rafts influences receptor dimerization (Nagy, Vereb et al. 2002, Ringerike, Blystad et al. 2002). Rafts on the cell membrane are tightly packed with cholesterol and glycosphingolipid. The studies of Kusumi et. al (2004) showed that ligand stimulation or receptor oligomerization lead to the fusion of small transient rafts into larger stable domains (Kusumi, Koyama-Honda et al. 2004). The function of these rafts is considered to serve as an intermediate platform in the signaling mechanism (Simons and Ikonen 1997, Simons and Ikonen 2000, Ikonen 2001). An indirect method to test the participation of lipid rafts in receptor dimerization and activation is the removal of cholesterol from the plasma membrane. A number of studies demonstrated that alteration of lipid rafts had a significant effect on signaling cascades (den Hartigh, van Bergen en Henegouwen et al. 1993, Chen and Resh 2002, Pike and Casey 2002, Roepstorff, Thomsen et al. 2002). Nevertheless, the underlying mechanism is not solved yet.

In this section, cholesterol was depleted to investigate the involvement of cholesterol-dependent domains in the receptor dimerization. The experiments were performed in cells expressing mRFP-EGFR/EGFR-eGFP in

CHO-K1. The effect of cholesterol disruption was tested in the apical and basal membrane with methyl-β-cyclodextrin (mβCD) that binds to cholesterol and induces depletion from the membrane. The final concentration was kept at 3mM. The same cell was analyzed before and after drug treatment. The receptor dynamics were monitored after 25 min mβCD incubation to maximize cholesterol depletion at room temperature (Bag, Huang et al. 2015). Independent cells were tested and the apparent dimer fraction in untreated cells was 26% ± 3% (n=25, 5 cells) in the basal and 33% ± 3% (n=36, 8 cells) in the apical membrane. On average, cholesterol depletion showed a trend to increase the complex forms up to 40% ± 4% (n=29, 5 cells) and 58% ± 5% (n=40, 8 cells) on basal and apical surface, respectively (Figure **4.4.1**). These values are higher than cross-correlation amounts measured in untreated cells, demonstrating that the EGFR complex formation is to some extent inhibited by partitioning of the receptor into cholesterol-dependent domains. The results are in agreement with a previously published study (Saffarian, Li et al. 2007) and are consistent with the findings that EGFR resides in cholesterol-dependent domains (Bag, Huang et al. 2015, Gao, Wang et al. 2015).

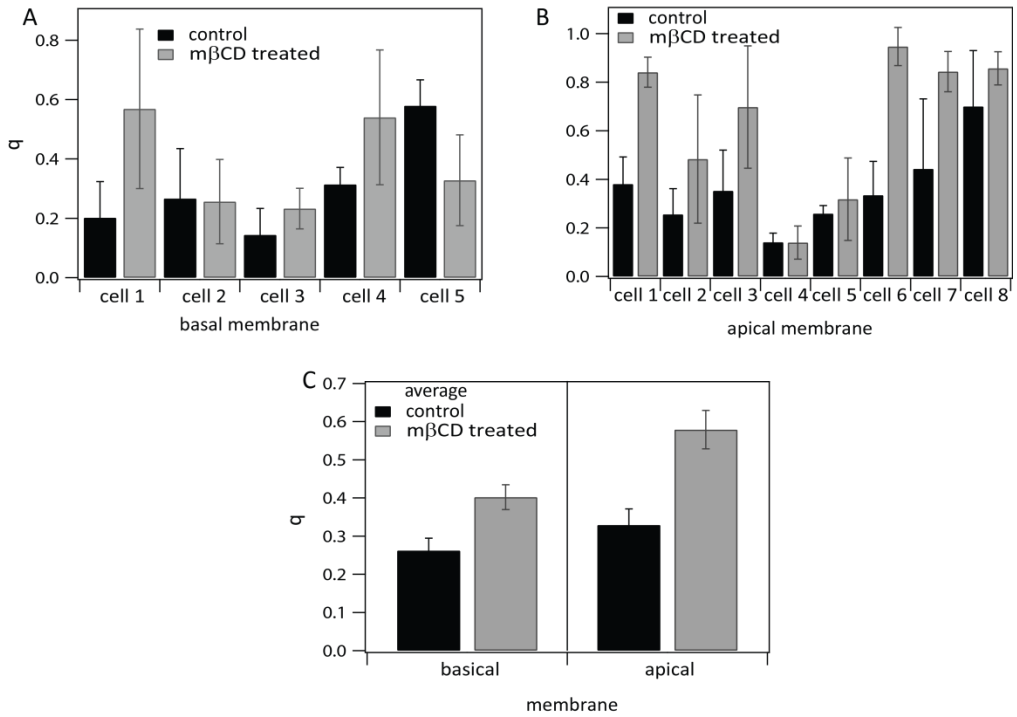

Figure 4.4.1 Influence of cholesterol removal on EGFR complex fraction **(A)** The cross-correlation amount of EGFR before and after cholesterol depletion in individual cells **(B)** In the apical membrane, the dimer amount increased mostly in all individual cells after drug treatment **(C)** average apparent complex fraction in mβCD treated cells in the lower (t-test (one tail, type 1): p=0.05 and the upper membrane p= 0.000057)

The mobility of EGFR before and after drug treatment is summarized in table **4.4.1.** Similar diffusion times of red and green labeled receptors were observed almost in all cases, only a slight increase in mobility in cholesterol depleted cells in the apical membrane is seen.

	Non-treated cells		mβCD treated cells	
	basal	apical	basal	apical
τ_DmRFP (ms ± SD)	91 ± 36	92 ± 40	104 ± 52	81 ± 85
τ_DeGFP (ms ± SD)	94 ± 55	80 ± 42	100± 78	118 ± 198
n (cells)	25 (5)	36 (8)	29 (5)	40 (8)

Table 4.4.1 Average lateral mobility of EGFR under different conditions

The impact of cholesterol disruption resulted in an overall increase in dimer fraction. However, it is important to show the difference in behavior in the case of a low dimer% before the drug treatment in a resting cell. As seen in Figure **4.4.2 A**, the complex fraction remained at the same level of 14% even after drug treatment. In all other cases, cholesterol removal had a significant effect on receptor dimerization. For instance, in a selected resting cell, the apparent dimer fraction was 38% which increased up to an amount 84% after depletion of cholesterol. Figure **4.4.2 B** displays FCCS analysis of EGFR after drug treatment.

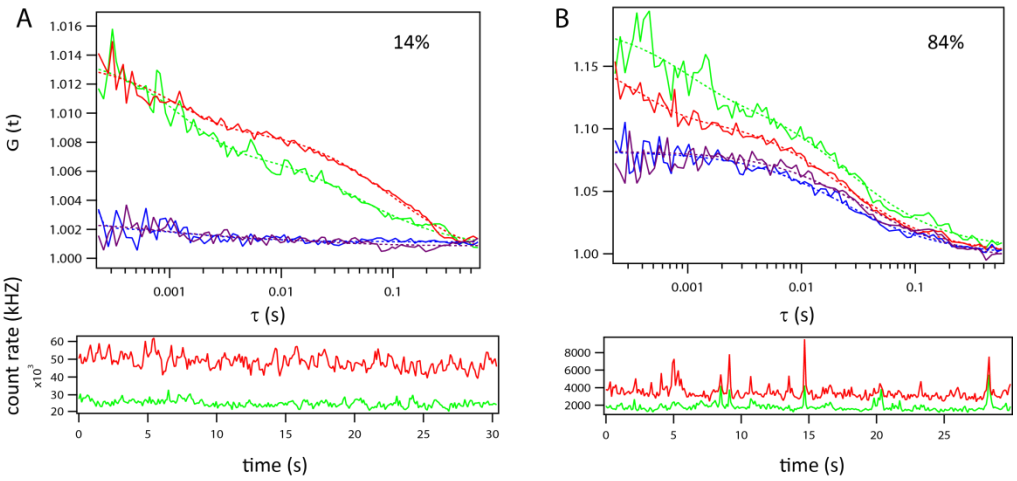

Figure 4.4.2 FCCS analysis of EGFR after drug treatment. **(A)** No changes on complex amount after cholesterol depletion when the initial cross-correlation amount was 14% **(B)** In the case of a complex fraction of 38%, the cross-correlation value increased up to 84% after drug treatment

4.5 Effect of unlabeled receptor molecules on apparent dimer fraction

When unlabeled EGFR molecules (such as the endogenous EGFR expressed by COS-7 and HEK293 cells) are present in the cell membrane, the dimer fraction derived from our FCCS data is underestimated because some of the labeled EGFR molecules dimerize with unlabeled ones and appear as apparent monomers in FCCS. To test the sensitivity of our method in the presence of unlabeled EGFR, we co-transfected CHO-K1 cells with labeled mRFP-EGFR, EGFR-eGFP and wild-type (wt) EGFR and performed SW-FCCS measurements at room temperature (Figure **4.5.1**). In the first experiment, EGFR-eGFP, mRFP-EGFR, and wild-type EGFR plasmids were transfected in the ratio 1:1.5:2 (EGFR-eGFP:mRFP-EGFR:wt EGFR). The apparent complex amounts were 19% ± 2% (n=25, 5 cells) in the basal and 22% ± 2% (n=34, 5 cells) in the

apical membrane. In the second experiment, the amount of transfected wild-type EGFR plasmid was reduced (1:1.5:1.3 ratio), and the results yield an increased apparent complex fractions of 23% ± 2% (n=16, 5 cells) and 34% ± 2% (n=20, 5 cells) in the basal and apical membrane, respectively.

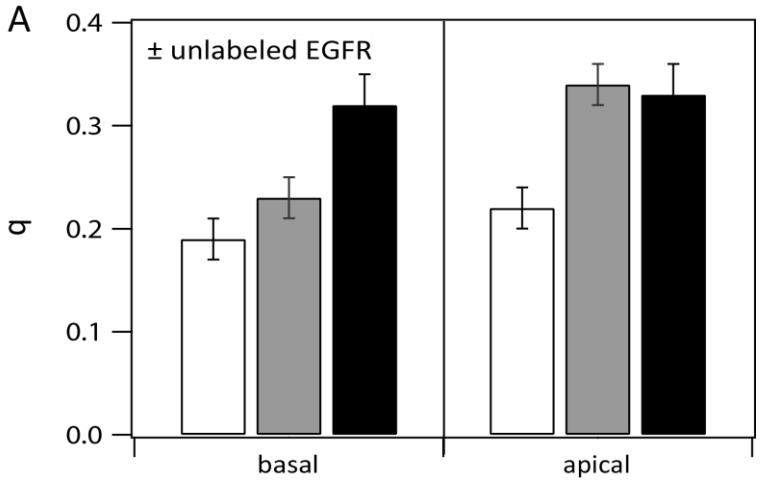

Figure 4.5.1 Decrease in *q* values in CHO-K1 cells co-transfected with fluorescent as well as wild-type EGFR. Cells transfected with mRFP-EGFR/EGFR-eGFP/wt-EGFR in the ratios of 1.5:1:2 (white bar) and 1.5:1:1.3 (gray bar) are compared to control cells (t-test (one tail, type 2)): p= 0.002 (white/black bar), p=0.04 (gray/black bar), p= 0.15 (white/gray bar) at basal; p= 0.0008 (white/black bar), p= 0.37 (gray/black bar), p= 0.0009 (white/gray bar) at apical) without unlabeled EGFR (black bar)

The *q* factor is therefore underestimated by artificially introduced wild-type EGFR and the values are given in the table **4.5.1**.

mRFP-EGFR/EGFR-eGFP/wt-EGFR	basal *q* (± SEM)	n (cell)	apical	n (cells)
1.5:1:2	0.19 ± 0.02	25 (5)	0.22 ± 0.02	34 (5)
1.5:1:1.3	0.23 ± 0.02	16 (5)	0.34 ± 0.02	20 (5)

Table 4.5.1 *q v*alues with different molar ratio of labeled and unlabeled EGFR

The expression level ofeGFP and mRFP labeled receptor varied between 99,663 and 3,375,269 on the entire 691 μm^2 CHO-K1 cell surface. It is not known how much unlabeled EGFR was expressed on the cell surface. Nevertheless, the effect of wild-type EGFR on dimer% can be seen in the results. The measurements with unlabeled EGFR demonstrate the sensitivity of our technique to changing complex fractions of the receptor; this is in line with our results in COS-7 and HEK293 cell lines where the competition between labeled and endogenous EGFR molecules causes an apparent dependence of the complex amount on the expression level.

4.6 Effect of internalization inhibitor on dimerization amount

In all the above described experiments, the cells were incubated for 30 min with internalization inhibitors (NaN_3, NaF and 2-deoxy-D-glucose) and the measurements were conducted in the presence of the inhibitors to avoid internalization and endocytosis of EGFR from the plasma membrane. To verify that the presence of inhibitors does not influence the measured

complex fraction of EGFR in the plasma membrane, we repeated the SW-FCCS experiments in CHO-K1 cells at room temperature in the absence of the inhibitors. The obtained apparent complex fractions of 23% ± 5% (n=21, 5 cells) on the basal and 33% ± 4% (n=25, 3 cells) on the apical membrane are in good agreement with the data acquired in the inhibitor-treated cells, confirming that the inhibitors do not interfere with EGFR complex formation. Additionally, no significant internalization of EGFR was observed within the time frame of the measurements (Figure **4.6.1**).

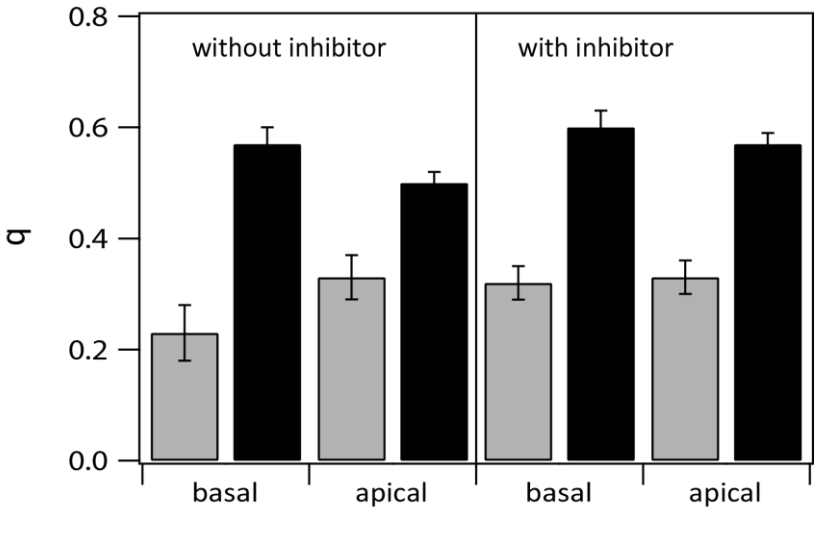

Figure 4.6.1 influence of inhibitors on the EGFR complex fraction**.** *q* values of the positive control mRFP-EGFR-EGFR (black bar, (p=0.41 for lower and 0.1 for upper membrane) and the experiment mRFP-EGFR/EGFR-eGFP (gray bar, p=0.04 for lower and 0.28 for upper membrane) without internalization inhibitors added in basal and apical membranes are compared to a control group treated with the inhibitors (p=0.41). No effect of internalization inhibitors on the *q* values is observed (t-test one tail, type 1).

However, the use of inhibitors ensures the compatibility of the present experiments with our previous study and with our future experiments in

which we intend to monitor the influence of EGFR activation upon its oligomerization. The results are summarized in table **4.6.1**.

Protein in CHO-K1	Complex *q* (± SEM) RT	n (cell)
mRFP-EGFR-eGFP (without inhibitor)		
basal	0.57 ± 0.03	27 (5)
apical	0.50 ± 0.02	30 (5)
mRFP-EGFR/EGFR-eGFP (without inhibitor)		
basal	0.23 ± 0.05	21 (5)
apical	0.33 ± 0.04	25 (3)
mRFP-EGFR-eGFP (with inhibitor)		
basal	0.60 ± 0.02	52 (18)
apical	0.57 ± 0.02	36 (14)
mRFP-EGFR/EGFR-eGFP (with inhibitor)		
basal	0.32 ± 0.03	47 (20)
apical	0.33 ± 0.03	46 (19)

Table 4.6.1 *q* factor of mRFP-EGFR/EGFR-eGFP and mRFP-EGFR-eGFP in the absence and presence of internalization inhibitors

4.7 EGFR complex fractions in CHO-K1 determined by DC-FCCS and quasi PIE-FCCS

The same sets of EGFR experiments in CHO-K1 cells at room temperature were also performed by DC-FCCS and quasi PIE-FCCS to test whether results

obtained by these FCCS modalities are consistent with our SW-FCCS findings. The correlation curves were analyzed as described in Materials and Methods. In the case of quasi PIE-FCCS, the cross-correlation amount q was calculated as $q = N_g/N_x$; N_g was preferred because the ACF in the green spectral channel was corrected for background and detector after-pulsing, unlike the ACF in the red channel (Padilla-Parra, Auduge et al. 2011).

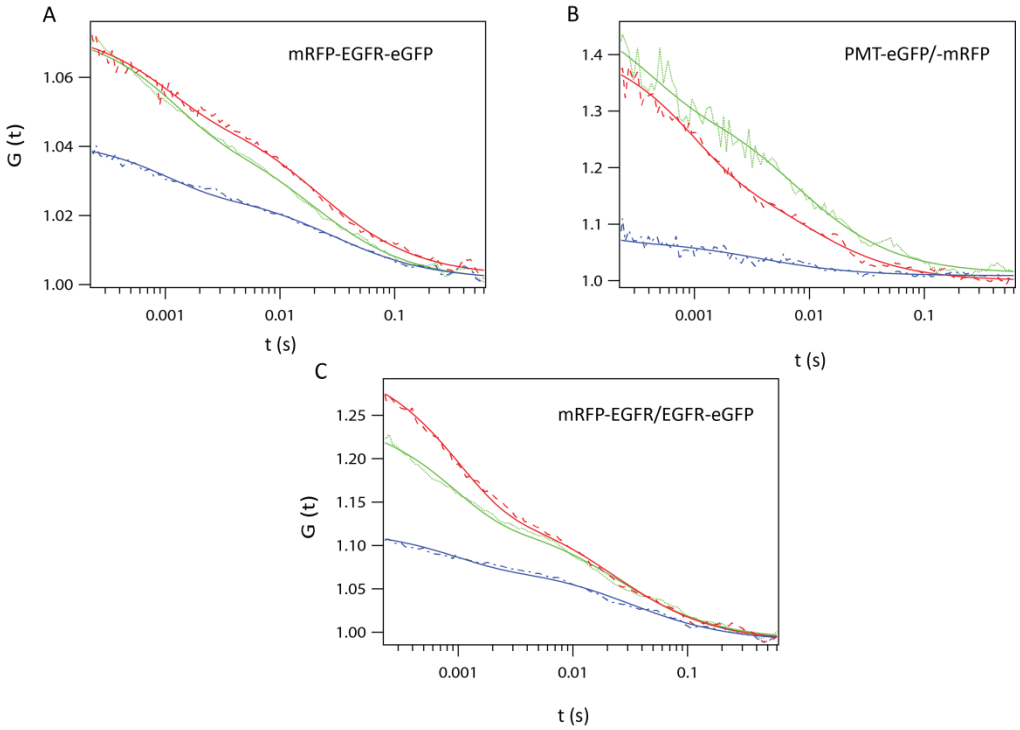

Figure 4.7.1 ACF curves for EGFR-eGFP (green) and mRFP-EGFR (red) and CCF curves (blue) recorded by DC-FCCS: **(A)** positive control mRFP-EGFR-eGFP, **(B)** negative controlPMT-eGFP/-mRFP and **(C)** mRFP-EGFR/EGFR-eGFP (the actual experiment)

The DC-FCCS curves are displayed in Figure **4.7.1.** It illustrates the correlation functions from distinct experimental sets and cross-correlation values are summarized in table **.7.1**.

	Quasi PIE-FCCS *q* (± SEM)	n	DC-FCCS *q* (± SEM)	N	SW-FCCS *q* (± SEM)	n
Positive control						
apical	0.51 ± 0.11	7 (5)	0.71 ± 0.06	28 (8)	0.57 ± 0.02	36 (14)
basal	-	-	0.60 ± 0.08	17 (7)	0.60 ± 0.02	52 (18)
EGFR-eGFP/mRFP-EGFR						
apical	0.33 ± 0.09	9 (7)	0.37 ± 0.04	19 (7)	0.33 ± 0.03	46 (19)
basal	-	-	0.44 ± 0.04	18 (9)	0.32 ± 0.03	47 (20)
Negative control						
apical	0	5 (2)	0.09 ±0.01	29 (5)	0.10 ± 0.02	16 (3)
basal	-	-	0.13 ± 0.02	22 (4)	0.10 ± 0.02	17 (4)

Table 4.7.1 The average cross-correlation amounts *q* from the different FCCS modalities. mRFP-EGFR-eGFP was used as a positive control. PMT-eGFP/PMT-mRFP was used as negative control for DC-FCCS and quasi PIE-FCCS whereas labeled PMT/EGFR used in the case of SW-FCCS

DC-FCCS measurements gave EGFR complex fractions of 44% ± 4% (n=18, 9 cells) at the basal and 37% ± 4% (n=19, 7 cells) at the apical membrane. The positive control mRFP-EGFR-eGFP yielded a cross-correlation amount of q = 60% ± 8% and 71% ± 6% at the apical and the basal membrane, respectively. The lower detection limit was determined by the negative control (PMT-eGFP/PMT-mRFP) to be 13% ± 2% and 9% ± 1% in the basal and the apical membrane, respectively (table **4.7.1**).

To obtain cross-talk free values of q, we repeated the measurements using quasi PIE-FCCS (Figure **4.7.2**). Negative control measurements in cells

expressing PMT-eGFR/PMT-mRFP give q = 0% ± 0%, thus, demonstrating the efficiency of spectral cross-talk elimination. For the positive control mRFP-EGFR-eGFP we found q = 51% ± 11%. The EGFR apparent dimer fraction in the apical membrane is 33% ± 9% (n=9, 7 cells). Collectively, all the FCCS modalities applied provided mutually consistent results, lending further support to the conclusions based on our SW-FCCS data.

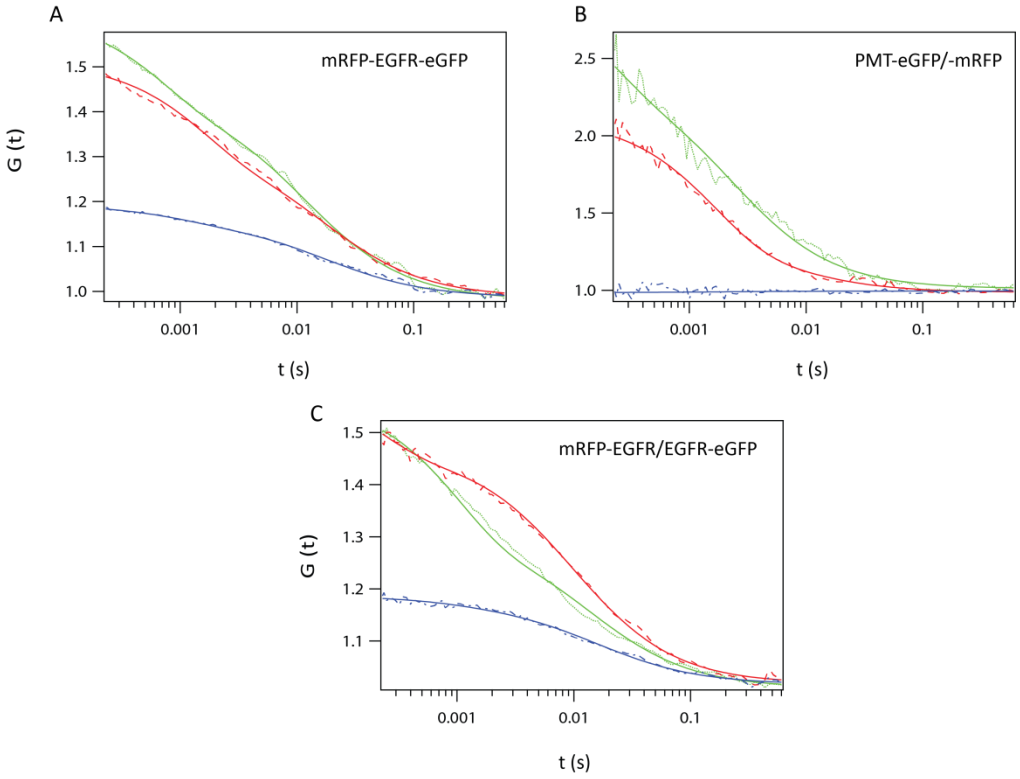

Figure 4.7.2 quasi PIE-FCCS curves **(A)** of the positive control mRFP-EGFR-eGFP **(B)** negative control PMT-eGFP/-mRFP and **(C)** mRFP-EGFR/EGFR-eGFP (the actual experiment)

4.8 Investigation of EGFR dimerization by using DC-ITIR-FCCS

The experiments on EGFR interaction were repeated with another FCCS modality DC-ITIR-FCCS to investigate the consistency of dimer amount and distribution of receptor state of monomers, dimers and oligomers.

Measurements were performed in the basal membranes of CHO-K1 cells at 37°C. Cells expressing PMT-eGFP and PMT-mRFP and cells expressing mRFP-EGFR-eGFP were used as the negative and the positive controls, respectively. The acquired image stacks were analyzed as described in the Materials and Methods chapter. An analyzed region of interest consisted typically of more than 1000 pixels, not all of which contained useful information. There were pixels corresponding to areas outside of cells or to regions within the cells where the membrane is too far from the glass surface to be efficiently excited by the evanescent field or, possibly, regions of cell membrane inaccessible to the fluorescent tracer. To exclude pixels outside of the cell from the calculation and fitting of correlation functions, an intensity threshold was set for each stack and only pixels having in the first frame larger than threshold intensity were processed. Most stacks contained some pixels, which, although having high intensity, gave very noisy ACFs, fitting of which was unreliable and likely to produce unrealistic values of parameters. In order to exclude such pixels from further analysis, upper and lower limits were set on D and G_{inf} obtained from ACFs fits. Only values from pixels for which the fitted D and G_{inf} in both of the autocorrelation channels lay between the respective lower and upper limits were included in the further evaluation. The limits for G_{inf} were $\pm 50\%$ of the correlation function amplitude $G(0)$ from the ideal asymptotic value, which in our definition of ACF was 1. The limits for D were set separately for EGFR and for PMT according to the actual distribution of the measured D values. Histograms of natural logarithms of measured D values were fitted with normal

distributions and the limits were set as the mean ± 3 times the standard deviation. For PMT they were D_{min} = 0.2 and D_{max} = 2.7 µm²/s and for EGFR D_{min} = 0.1 and D_{max} = 1.4 µm²/s.

There were some pixels in which both ACFs were fitted successfully and the fit parameters satisfied the above described criteria, yet the fit of the CCF did not give realistic parameter values. This was especially common in the case of the negative control, where the CCFs consist mainly of noise. The fits of such curves give sometimes extremely high value of *D* (e.g. on the order of 10^{16} µm²/s) or a very low value of *D* (e.g. on the order of 10^{-6} µm²/s) together with a very low G_{inf} (e.g. < 0). Both situations result in large overestimation of the amplitude (1/*N*, Figure **4.8.1**).

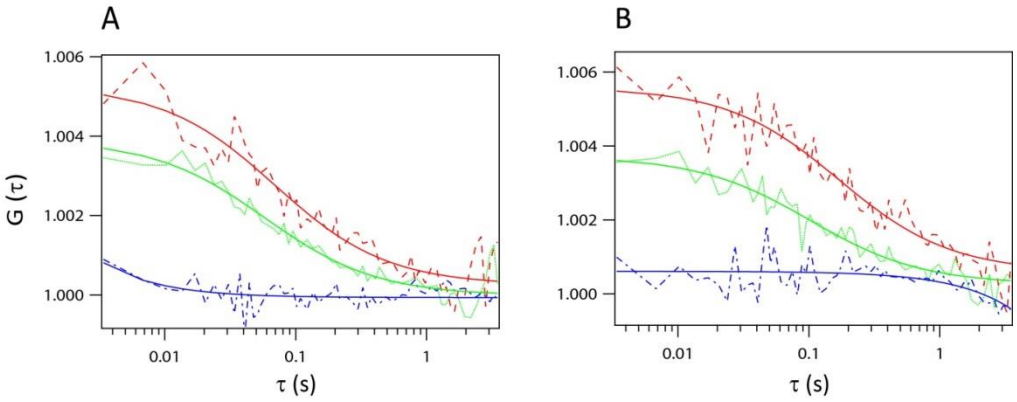

Figure 4.8.1 Illustration of artefacts in the fitting of CCFs with very low amplitudes. **(A)** shows an example of an erroneous fit with a very high value of D (on the order of 10^7 µm^{2}s^{-1}) resulting in q = 18,1429 **(B)** shows an example of an erroneous fit with a very low value of G_{inf} (-7.2) resulting in q = 2339. Both examples were taken from the fits of the negative control DC-ITIR-FCCS data

To avoid such unrealistic values, the amplitudes of CCFs were set to 0 if the fitted *D* and G_{inf} were not within certain limits. The limits for G_{inf} were the same as in the case of ACFs (± 50% of the amplitude from the ideal

asymptotic value) and the limits for *D*were broadened to $D_{min}/2$ and $2\,D_{max}$ where D_{min} and D_{max} are the respective limits for ACFs. In other words, $q = 0$ in such pixels. The CCF amplitude was set to 0 also in pixels where the CCF fit gave a negative value of *N*. *q* was, thus, set to 0 in almost 60% of pixels of the negative control, in 27% of pixels of the actual experiment and only in approximately 7% of pixels of the positive control.

The final values of *q*, thus obtained, were 10% ± 14% for the negative control, 53% ± 23% for the positive control and 34% ± 28% for the actual experiment. In Figure **4.8.2**, FCCS curves of distinct experimental data sets are presented. The values are given as mean ± standard deviation; the standard errors of the mean are negligible because of the large number of pixels evaluated.

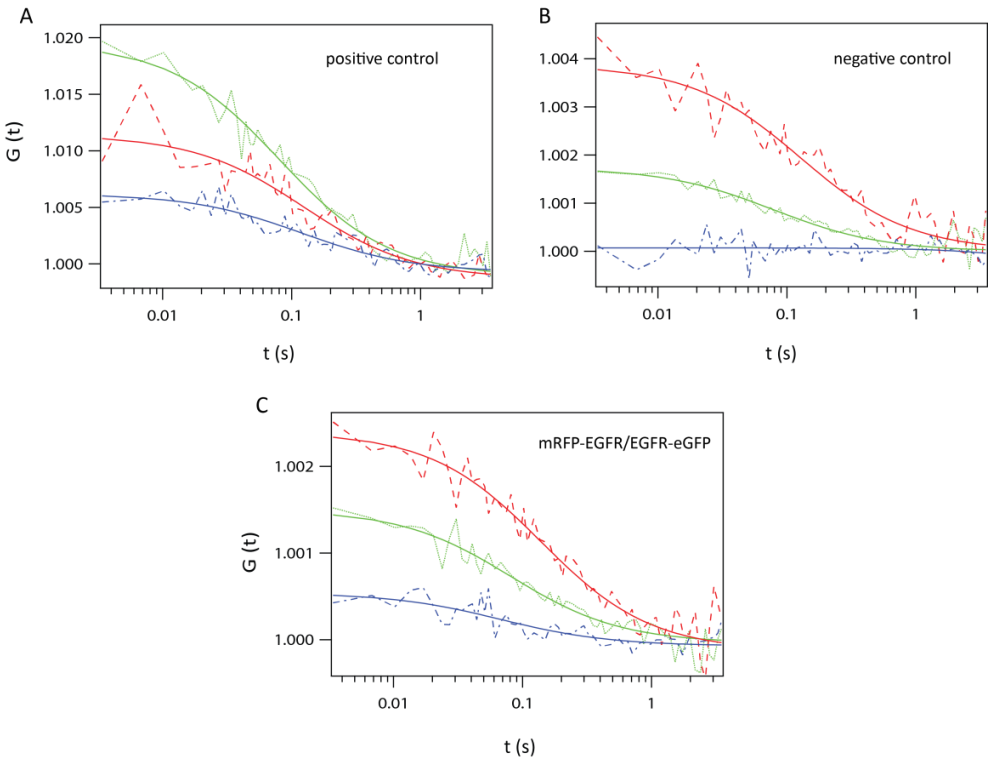

Figure 4.8.2 FCCS curves of distinct obtained experiment sets **(A)** positive control mRFP-EGFR-eGFP **(B)** negative control PMT-mRFP/-eGFP **(C)** actual experiment mRFP-EGFR/EGFR-eGFP.

It can be seen in Figure **4.8.3** that the distribution of *q* measured in the positive control has a shoulder around 80%. Out of the eight cells investigated, the shoulder around 80% was dominant in three cells while in the remaining cells the *q* distribution was mono-modal with a maximum around 45% (Figure **4.8.4**). The very high amount of cross-correlation observed in some pixels may be caused by elevated amounts of dimers of the EGFR tandem constructs or possibly even higher order EGFR oligomers. *Q* values obtained in the actual experiment show an even broader distribution.

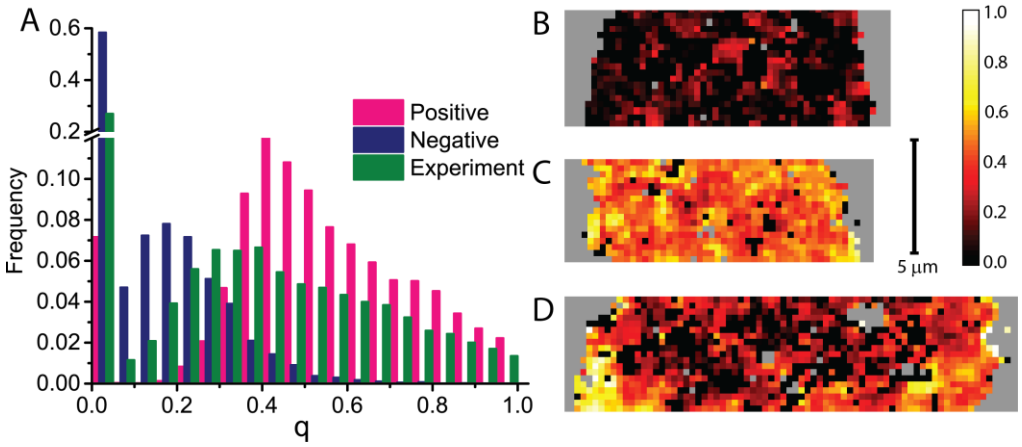

Figure 4.8.3 Histogram of pooled q values and examples of q maps obtained by DC-ITIR-FCCS. The q values obtained in all pixels of all investigated cells were pooled together for the three series of measurements: the negative control (10,053 pixels from 10 cells), the positive control (6,696 pixels from 8 cells) and the actual experiment with EGFR-eGFP and mRFP-EGFR (16,779 pixels from 16 cells). The frequencies plotted in the histogram (**A**) are numbers of pixels in each bin divided by the total number of pixels in the respective series. Examples of q maps are shown for a cell from the negative control (**B**) positive control (**C**) and the actual experiment (**D**) The colour-scale of q and a 10 µm scale-bar are shown next to the maps. Pixels shown in striped pattern were excluded from fitting (either because of having lower than threshold intensity or because the parameters obtained by fitting of the ACFs were not within the set limits)

In some cells, the average *q* was as low as 11% indicating negligible amounts of dimers, while in other cells the average *q* reached values as high as over

70% (Figure **4.8.4**). The cells with intermediate average values of *q* show regions of high and low *q*. The regions of high *q* values are typically located closer to the cell boundaries. It remains to be investigated further what is the nature of those regions and whether they contain only elevated amounts of dimers or whether they contain higher EGFR oligomers. To conclude, the DC-ITIR-FCCS data are in agreement with the results of the confocal FCCS modalities; moreover, they provide further insight into the distribution of dimer fraction values and how the cell-to-cell variations relate to variations in different regions of the membrane of each individual cell.

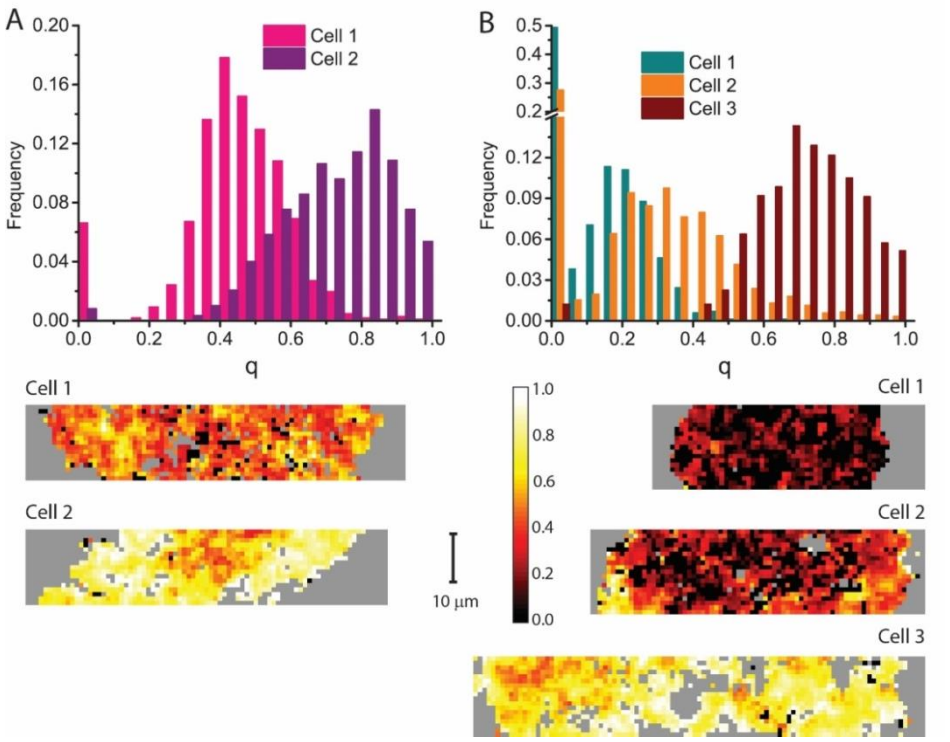

Figure 4.8.4 Illustration of cell-to-cell variability in the level of EGFR dimerization as measured by cross-correlation amount *q* obtained by DC-ITIR-FCCS. Data from two cells from the positive control **(A)** and from three cells from the actual experiment with EGFR-eGFP **(B)** are shown in the form of *q* maps and histograms of *q* values for each cell. The frequencies plotted in the histograms are numbers of pixels in each bin divided by the total number of pixels in the respective cell. The colour-scale of *q* and a 10 µm scale-bar are shown next to the maps. Pixels shown in gray were excluded from fitting (either because of having lower than threshold intensity or because the parameters obtained by fitting of the ACFs were not within the set limits).

4.9 PMT in different cell lines

As mention in the previous sections, the plasma membrane target (PMT), a small membrane protein, has been used as a negative control to set up the dynamic range in the FCCS system. In the studies of Liu et al. (2007), PMT labeled with eGFP and mRFP revealed a complex fraction of ~10-15% (Liu, Sudhaharan et al. 2007).This value is caused by spectral cross-talk from the green particles into the red detection channel. The membrane proteins PMT-eGFP/-mRFP, assumed to be monomeric and non-interacting, showed a considerably higher cross-correlation amount *q* in HEK293 and COS-7 than usually found in CHO-K1. To verify whether this high cross-correlation was caused by partitioning of the proteins into cholesterol-dependent domains, we depleted cholesterol from HEK293 cells at room temperature with mβCD (3 mM final concentration) and performed SW-FCCS measurements in the interval of 5-10 min after 25 min incubation. The results in Figure **4.9.1 B** show a *q* value of 23% ± 1% (n=46, 5 cells) in the basal membrane of untreated cells; mβCD treatment resulted in a value of 25% ± 2% (n=39, 4 cells). Similar results were obtained on the apical membrane; cholesterol depleted cells gave a cross-correlation amount of 28% ± 1% (n=40, 4 cells), which does not differ from untreated cells with an amount of 24% ± 2% (n=48, 6 cells). The results revealed that cholesterol removal did not affect the *q* value. We can therefore conclude that partitioning into cholesterol-dependent domains is not responsible for the elevated cross-correlation. Whether partitioning into cholesterol-independent domain or other interactions are the cause for the high cross-correlation remains to be

answered. However, this question is not relevant for the objectives of the present study.

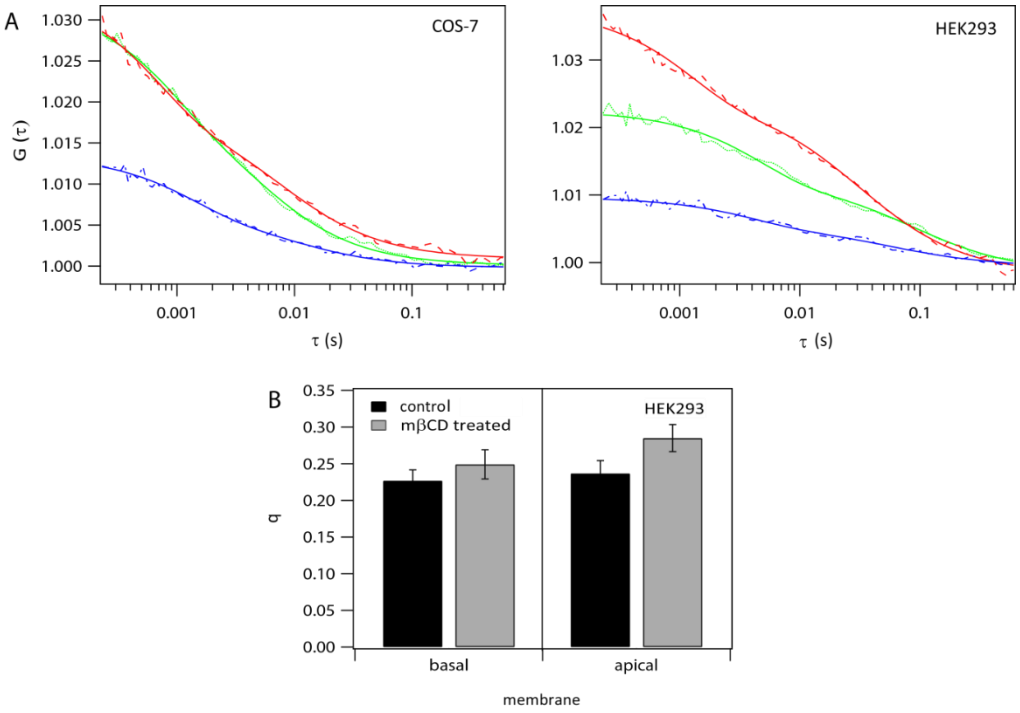

Figure 4.9.1 Co-localization of PMTs in domains in HEK293 and COS-7. **(A)** ACF curves of PMT-eGFP (green) and PMT-mRFP (red) and CCF (blue). In these cell lines, we get elevated CCF amplitudes **(B)** Depletion of cholesterol by mβCD did not induce significant differences in the *q* value on the membranes compared to the untreated cells. (t-test: one tail, type 1. p-values: 0.18 at basal and 0.03 at apical membrane)

4.10 Effect of (I706Q, V948R) Mutation on EGFR dimerization

The concept of EGFR dimerization is based on the stabilization of asymmetric dimers between the kinases. The C-terminus of one kinase and the N-terminus from the other kinase are responsible for the formation of an asymmetric dimer (Zhang, Berezov et al. 2007, Zhang, Pickin et al. 2007, Songtawee, Bevan et al. 2015). The studies of Tai Kiuchi et al. provided evidence that the double mutation (I706Q, V948R) leads to the destabilization of EGFR:ErBB4 dimers (Kiuchi, Ortiz-Zapater et al. 2014). These

mutations are located in N-terminal lobe (I706Q) and in C-terminal lobe (V948R). The combination of both of them impairs activator and receiver function and demonstrates that the N and C lobes have an impact in the formation of EGFR dimers. In this work, we have tested the influence of double mutated EGFR (I706Q, V948R) on the presence of preformed dimers by using SW-FCCS. This construct was transfected together with mRFP-EGFR into CHO-K1 cells and measured in the apical membrane at room temperature. Fitting of the correlation curves and data analysis (table **4.10.1,** Figure **4.10.1**) showed in the presence of EGFR (I706Q, V948R) a cross-correlation amount of 16% ± 2% (n=26, 5 cells).

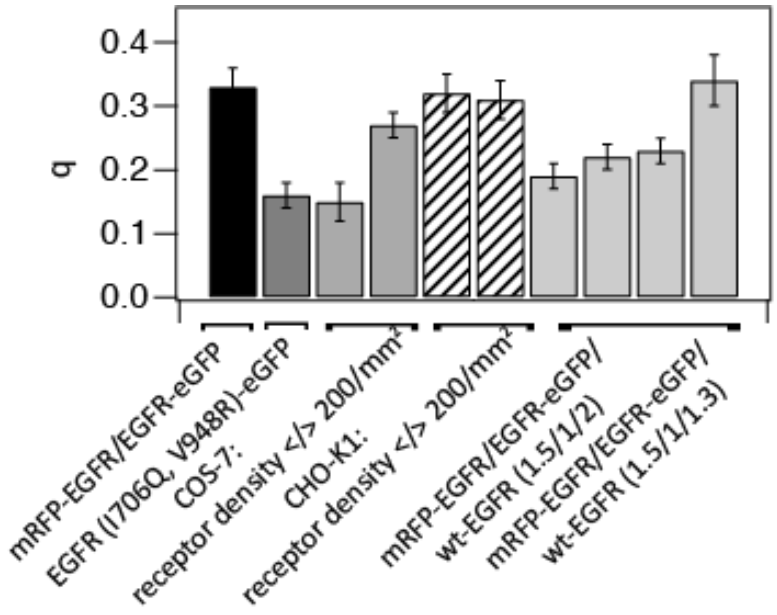

Figure 4.10.1 Factors effecting EGFR dimer fraction**.** Cross-correlation amount *q* of mRFP-EGFR/EGFR-eGFP (apical membrane, RT) compared with mRFP-EGFR/EGFR (I706Q, V948R)-eGFP (apical membrane, RT), EGFR interaction in COS-7 at receptor densities <200/µm² and >200/µm² (basal membrane, RT), EGFR dimerization in CHO-K1 at <200/µm² and >200/µm² (basal membrane, RT), mRFP-EGFR/EGFR/wt-EGFR (1.5:1:2) (basal and apical membrane, RT) and mRFP-EGFR/EGFR/wt-EGFR (1.5:1:1.3) basal and apical membrane, RT).The mean values and standard errors of the mean are shown.

Compared to the control measurement of mRF-EGFR/EGFR-eGFP, which exhibited ~33% cross-correlation amount, the dimerization of the mutated EGFR (I706Q, V948R) is significantly reduced (Figure **4.10.1**).

Figure **4.10.1** illustrates several factors leading to a decrease in the measured cross-correlation amount and, thus, to a decrease in the apparent dimer fraction. In the cell line CHO-K1 which lacks endogenous EGFR, the cross-correlation amount is independent of receptor density; the average complex fractions at densities <200 molecules/μm^2 and >200/μm^2 do not differ. However, the situation is different when using COS-7 cells expressing endogenously ~100.000 EGFR molecules per cell. At densities lower than 200 molecules/μm^2, the cross-correlation amount was only ~15% ± 3%, whereas, at densities higher than 200/μm^2, the average cross-correlation amount reached 27% ± 2%. A similar effect was obtained by co-expressing different concentrations of wt EGFR in CHO-K1 cells (Figure **4.10.1**). At ratios of (1.5/1/2) mRFP-eGFR/EGFR-eGFP/wt-EGFR, the cross-correlation was reduced to 19% ± 2% and 22% ± 2% in the basal and apical membrane, respectively. However, at ratios of (1.5/1/1.3) mRFP-eGFR/EGFR-eGFP/wt-EGFR, the cross-correlation amount was 22% ± 2% and 34% ± 2% in the basal and apical membrane, respectively. The unchanged cross-correlation amount of 34% in the presence of wt-EGFR might be caused by very low or lacking expression of the unlabeled protein.

apical membrane at room temperature	*q* (± SEM)	τ_DmRFP (ms ± SD)	τ_DeGFP (ms ± SD)	n (cells)
mRFP-EGFR/EGFR-eGFP	0.33 ± 0.03	54 ± 23	51 ± 22	46 (19)
mRFP-EGFR/EGFR-eGFP (I706Q, 948R)	0.16 ± 0.02	62 ± 24	29 ± 17	26 (5)

Table 4.10.1 *q* factor of the control experiment, EGFR mutation (I706Q, V948R) and the diffusion times

4.11 EGF stimulation of EGFR in CHO-K1

Analyzing EGFR interaction in different resting cells has shown the importance of the selection of cell lines. Cells expressing labeled EGFR were stimulated with the ligand EGF at low and high dose 10 ng/ml and 100ng/ml, respectively. At high EGF concentration, the cells have been tracked before stimulation and after 3 min, 10 min, 15 min and 20 min (Figure **4.11.1**)**.**

Before starting with the experiment, the glass dishes were fixed with double-sided tape on the objective stage to record the same cell before and after ligand activation. Some stimulated cells showed significant clusters, which were visible as spikes in the intensity traces or in the ACF and CCF curves itself. The data set chosen for analysis excludes this mentioned FCCS curves containing big oligomers. The measurements were focused on the apical membrane at room temperature.

Figure **4.11.1** displays the influence of the EGF ligand at high concentration 100 ng/ml on a selected cell captured at different time points after

stimulation. Before ligand activation, EGFR cross-correlation amount was 33%. After 3 min incubation with the ligand, the cross-correlation rose to 63%, which is around 50% increase in the complex fraction compared to the unstimulated one. Changes in the ACF and CCF shapes observed after 10 min of incubation with EGF demonstrate the formation of large EGFR oligomers. No evidence of the large oligomers remained 15 min after EGF addition; however, the cross-correlation did not decrease. This indicates loss of the large oligomers accompanied by an increase in the fraction of dimers and smaller oligomers (such as tetramers or hexamers), which do not affect the shape of the correlation functions. An overview of the average changes in cross-correlation amount is shown in table **4.11.1**.

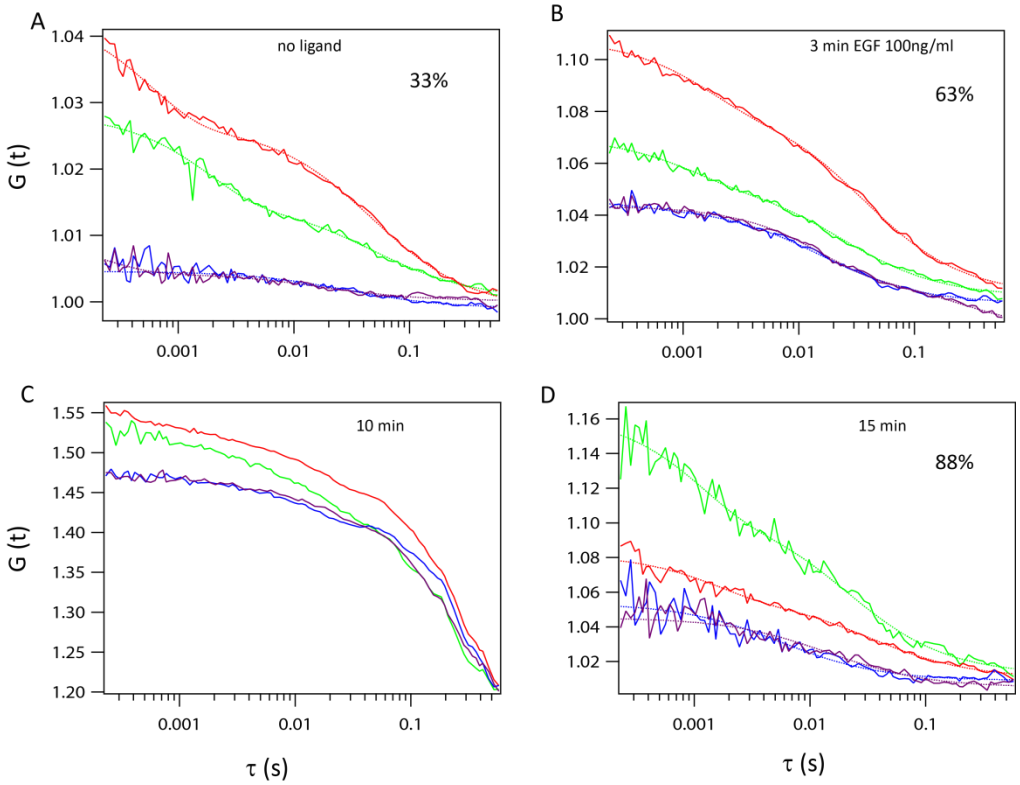

Figure 4.11.1 Analysis of EGFR-EGFR interaction in resting cells. **(A)** Around 33% of the receptors resided in a complex form **(B).** After 3 min EGF (100ng/ml) addition, the complex amount increased rapidly to ~63% **(C)** oligomerization of stimulated EGFR molecules **(D)** complex fraction of 88% at 15 min

In resting cells, the average value was 39% ± 3% (n=22, 4 cells), it increased slightly to 44% ± 5% (n=12, 4 cells) at 3 min and remained at 42% ± 6% (n=10, 4 cells) at 5 min and 44% ±6% (n=8, 4 cells) at 10 min. The cross-correlation then rose slightly to 52% ± 6% (n=9, 4 cells) at 15 min and remained at 53% ± 6% (n=8, 4 cells) at 20 min. The small average increase in cross-correlation and the lack of changes in cross-correlation in some of the cells do not contradict formation of large EGFR oligomers and clusters. Very large oligomers and clusters result in high spikes in intensity time-trace, which distort the correlation functions and were excluded from analysis. Furthermore, rapid endocytosis of those oligomers and clusters would deplete them from the plasma membrane.

A summary about the effect of EGF on the complex fraction is given in table **4.11.1.**The *q* factor increased in resting cells from 39% up to 53% after 20 min incubation.

EGF 100 ng/ml	τ_DmRFP (ms ± SD)	τ_DeGFP (ms ± SD)	EGFR-eGFP/mRFP-EGFR *q* (± SEM)	n (cell)
No EGF	58 ± 32	59 ±42	0.39 ± 0.03	22 (4)
3 min	69 ± 41	57 ± 30	0.44 ± 0.05	12 (4)
5 min	91 ± 55	81 ± 71	0.42 ± 0.06	10 (4)
10 min	72 ± 55	81 ± 73	0.44 ± 0.06	8 (4)
15 min	54 ± 32	62 ± 35	0.52 ± 0.06	9 (4)
20 min	62 ± 38	83 ± 73	0.53 ± 0.06	8 (4)

Table 4.11.1 Influence of EGF ligand (100 ng/ml) on the diffusion times of EGFR and changes in *q* value

Besides the changes in *q* value, the diffusion time was also monitored at different time points. As seen in table **4.11.1**, the diffusion time of mRFP labeled and eGFP labeled protein are in the same range in the absence of the ligand. Incubation with EGF increased slightly the diffusion times over the time. However, the standard deviation increased after 5min EGF incubation.

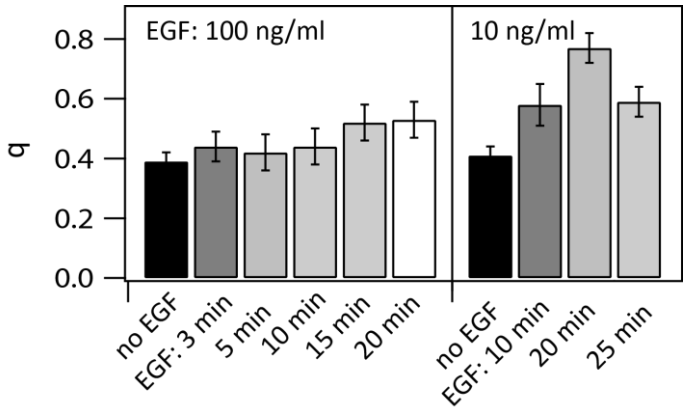

Figure 4.11.2 High dose (100 ng/ml) and low dose (10 ng/ml) EGF stimulation on mRFP-EGFR/EGFR-eGFP in CHO-K1

The same set of experiment was carried out at a lower EGF concentration of 10 ng/ml. In this case, the cells were monitored over a longer time period at 10 min, 20 min and 25 min after incubation with EGF as no strong internalization was expected at this concentration. As seen in Figure **4.11.3**, a stepwise increase in *q* factor was observed in the presence of EGF ligand.

Unstimulated cells showed an average cross-correlation of 41% ± 3% (n=13, 3 cells), which increased to 58% ± 7% (n=7, 3 cells) 10 min after stimulation. After 20 min of incubation with EGF, the cross-correlation reached its highest value of 77% ± 5% (n=4, 3 cells) and then decreased to 59% ± 8% at 25 min (n=7, 3 cells). The high cross-correlation of 77% ± 5% observed after 20 min of incubation with EGF is higher than the cross-correlation for the positive

control (positive control in average ~60%). This indicates that is most likely not caused by EGFR dimers only, but probably by higher oligomers (such as tetramers or hexamers) which are, however, not large enough to be manifested by the broadening of the correlation functions as observed after high dose EGF stimulation (Figure **4.11.2**).

The initial *q* amount of EGFR was around 32% before activation. However, after 10 min EGF influence, the cross-correlation curve rose up slightly, the *q* value was around 37%, very similar to the initial value of 32%. Even at 20 min EGF incubation, the *q* factor remained in the same range, with a calculated fraction of 32%. Nonetheless, an increase in *q* factor was observed which reached a value of 67% after 25 min. In average, a stepwise increase in *q* factor was observed in the presence of EGF ligand.

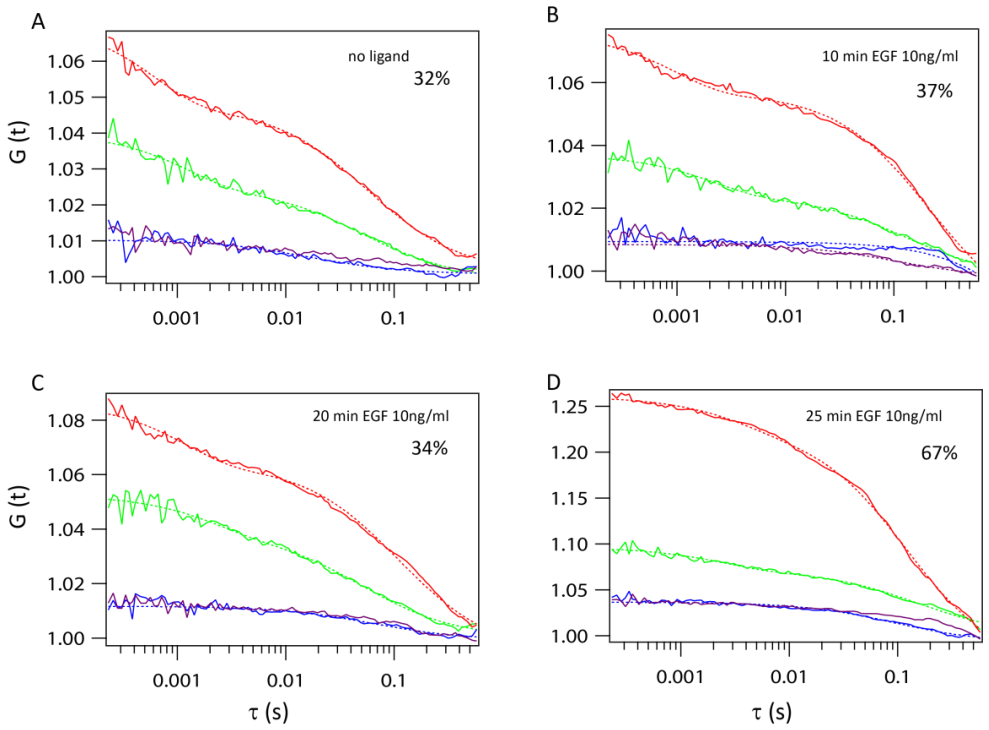

Figure 4.11.3 Impact of EGF ligand at a final concentration of 10ng/ml on a selected cell. **(A)** in the absence of the ligand, cross-correlation amount *q* was 32% **(B)** 10 min incubation of the cell with EGF, no changes in *q* observed **(C)** after 20 min incubation, the complex amount stayed at similar level at around 34% **(D)** up to 50**%** increase in *q* fraction at 25 min

The calculated value of EGFR interaction is summarized in the table **4.11.2**. A significant increase in EGFR complexation was recorded at 25 min ligand incubation.

EGF 10 ng/ml	EGFR-eGFP/mRFP-EGFR *q* (± SEM)
No EGF	0.41 ±0.03
10 min	0.58 ± 0.07
20 min	0.77 ± 0.05
25 min	0.59 ±0.08

Table 4.11.2 Effect of EGF ligand (10 ng/ml) on EGFR complex fraction. Three cells were measured. In average, the *q* factor is increasing by EGF incubation time

The diffusion time of red and green labeled receptors changed slightly during ligand treatment. These values are also similar with those measured at high EGF concentration of 100 ng/ml. The average values are summarized in table **4.11.3**.

EGF 10 ng/ml	No EGF	10 min EGF	20 min EGF	25 min EGF
τ_DmRFP (ms ± SD)	69 ± 39	67 ± 65	81 ± 21	52 ± 34
τ_DeGFP (ms ± SD)	69 ± 38	59 ± 37	64 ± 23	69 ± 47
n (cells)	13 (3)	7 (3)	4 (3)	7 (3)

Table 4.11.3 Diffusion times of EGFR complex in the absence and presence of EGF ligand (10 ng/ml). Three cells were measured. In average, the *q* factor is increasing by EGF incubation time

As previously mentioned, curves which showing oligomerization were excluded in the data. This phenomenon was visible on the shape of the ACF and CCF as well as the slow diffusion times. Some examples of the formation of clusters are shown in the following Figure **4.9.4**. Cells showed a different

response to the EGF at different concentrations. For instance, low EGF concentration (10 ng/ml) has induced clustering after 20 min. However, the same situation was recorded even at very short incubation time of 5 min at high dose EGF in Figure **4.9.4 B**. It has to be pointed out that not all cells respond with significant changes. Overall, EGF has induced receptor activation independent onEGF concentration differences but the impact of EGF was distinct.

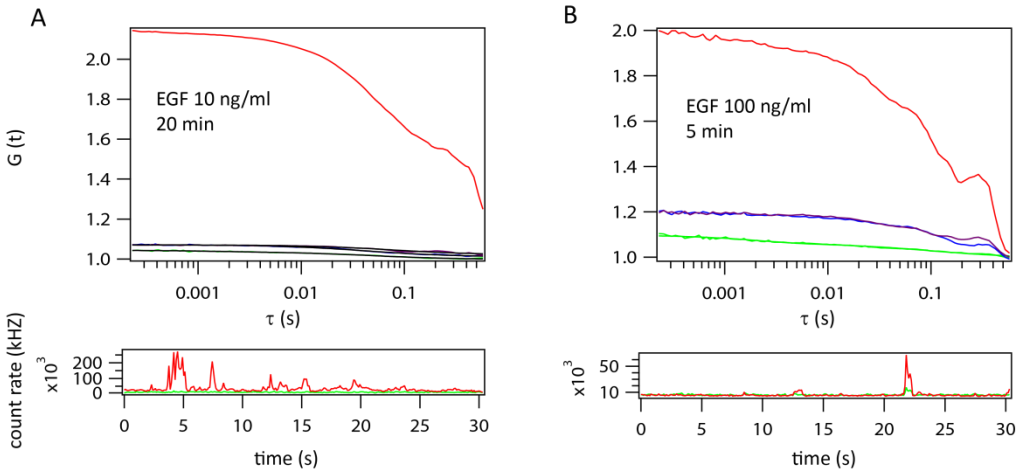

Figure 4.11.4 Impact of EGF ligand at distinct concentration of 10ng/ml and 100 ng/ml **(A)** 10 ng/ml EGF resulted in oligomerization after 20 min **(B)** 100ng/ml EGF induced oligomerization after 5 min

4.12 Discussion

In the present study, we have tested the influence of several experimental factors on the amount of EGFR complexes in resting cells as measured by SW-FCCS and other FCCS modalities. No significant differences were observed between the basal and the apical membranes in all cell lines. The lack of apical-basal polarity in fibroblasts might be the reason of seeing no differences in upper and lower membranes. Even performing experiments at differen temperature ranges (physiological (37°C) and room temperature

(22°C) did not play a crucial role in dimer estimation. The normalized complex fraction of around 57% obtained here is comparable with our previous study on EGFR (Liu, Sudhaharan et al. 2007 as well as the reported EGFR complex fractions of 30% (Saffarian, Li et al. 2007, Kluba, Engelborghs et al. 2015) or 40% (Hofman, Bader et al. 2010). On the other hand, we have observed significant cell-to-cell variability, which was especially obvious from the DC-ITIR-FCCS experiments. Approximately 1/3 of cells showed very low cross-correlation amounts indicating negligible complex fractions, while in approximately 1/3 of cells most EGFR molecules were in the form of complexes. The remaining cells, exhibiting on average intermediate cross-correlation, contained regions of very high as well as negligible complex fractions. This demonstrates the utility of DC-ITIR-FCCS (and imaging FCS modalities in general) for linking the cell-to-cell variability with the variability between regions within individual cells. The regions of high complex fractions were located predominantly at the cell periphery in agreement with previous reports (Chung, Akita et al. 2010, Bag, Huang et al. 2015). It remains to be investigated further what is the nature of those regions and whether they contain only elevated amounts of dimers or whether they contain higher EGFR oligomers. Interestingly, we have found recently that EGFR forms microscopic clusters upon activation in cholesterol-depleted cells, those clusters being in some cases more frequent at the cell periphery (Foo, Naredi-Rainer et al. 2012).

Our technique cannot easily discriminate between dimers and higher oligomers. The contribution to the cross-correlation in FCCS scales with the square of the brightness of the complexes; therefore, a very small fraction of large clusters can give rise to high CCF amplitudes. On the other hand, large clusters are expected to be manifested in the correlation functions by a component with slower diffusion, which we have not observed in resting cells. We, therefore, assume that the complexes observed in our study contain mostly small oligomers such as dimers or tetramers.

Besides the brightness, the lifetime of the complexes also determines their contribution to the CCF. The contribution increases with increasing lifetime of the complexes and saturates when the lifetime is longer than the characteristic residence time of the molecules in the effective observation area. The characteristic residence times are around 50 ms in our confocal measurements and close to 1s in the case of DC-ITIR-FCCS. The good agreement of the cross-correlation amount between confocal FCCS and DC-ITIR-FCCS indicates that the EGFR complexes are stable on timescales longer than the order of seconds. This is consistent for example with the single molecule study of Chung et al. reporting transient EGFR dimers in resting cells with lifetimes around 10 s (Chung, Akita et al. 2010).

Most of our measurements were done in CHO-K1 cells, which were selected because of their negligible endogenous EGFR expression. The presence of endogenous EGFR would interfere with the FCCS detection of complexes because dimers between an endogenous and a labeled receptor carry only a

single fluorescent label and contribute, therefore, to the monomer fraction. This is illustrated by the lower cross-correlation amount in the cells where wild-type EGFR was co-expressed alongside the labeled receptor. Another example of the influence of the endogenous EGFR on the apparent complex fraction is provided by the measurements in HEK293 and COS-7 cell lines, which express low to intermediate levels of endogenous EGFR (HEK-293 ~20,000 EGFR/cell (Carter and Sorkin 1998) and COS-7 ~100,000 EGFR/cell (Tong, Taylor et al. 2008). The cross-correlation amounts were low to negligible in cells expressing less than 200 labeled receptors per μm^2. Only at higher labeled receptor densities, which means at receptor densities much higher than those of the endogenous receptors (~30/μm^2 in HEK-293 and (~70/μm^2 in COS-7), the cross-correlation amounts are comparable to those obtained in CHO-K1 cells. Together, these results demonstrate the sensitivity of our FCCS approach to the changes in the EGFR complex fraction. Even more importantly, they prove that the observed complex formation is not an artifact of the artificially introduced labeled receptor, but that the same phenomenon involves also the EGFR in cells where it is endogenously expressed. Contrary to the situation in HEK293 and COS-7 cells, no dependence of the cross-correlation amount on the EGFR expression level was observed in CHO-K1 cells. The measurements were performed in cells expressing from ~10.000 to 1.600.000 EGFR copies, values ranging from very low expression to over-expression (Carpenter and Cohen 1979). We can therefore conclude that the complex formation is not an artifact induced by high receptor densities.

The involvement of cholesterol-dependent lipid rafts in EGFR activation and signaling has been reported earlier (Nagy, Vereb et al. 2002, Ringerike, Blystad et al. 2002). A line of evidence shows that the activation of EGF receptors which reside in these domains are prevented (Chen and Resh 2002, Roepstorff, Thomsen et al. 2002). At the other hand, other reports suggest that lipid rafts enhance EGFR activation and signaling (Zhuang, Lin et al. 2002, Peres, Yart et al. 2003). Studies with cholesterol depletion have demonstrated that EGFR signaling is totally disrupted (Orr, Hu et al. 2005). Our recent results show that EGFR partitions into cholesterol-dependent as well as cholesterol-independent domains and that its diffusion is affected by the actin cytoskeleton (Bag, Huang et al. 2015). Our data revealed that cholesterol depletion by mßCD leads to an increase in the EGFR complex fraction. This increase is more pronounced in the apical membrane, which is possibly related to differences in lipid or lipid domain distribution between the two cell surfaces. The result proves that the observed cross-correlation does not stem from co-localization of multiple receptors into small plasma membrane domains, but that it is rather a result of the formation of EGFR complexes held together by receptor-receptor interactions. At the same time, we may speculate that the complexes are of a transient nature; the transient trapping of receptor molecules into small cholesterol-dependent domains prevents them from diffusing freely and, thus, reduces the frequency of their encounters with other receptors, which lead to the formation of the transient complexes. At the same time, there is no obvious reason why the fraction of long-lived stable dimers should be affected in any

way by their membrane domain partitioning. Consistently with our results, Saffarian et. al (2007) reported an increase of oligomeric EGFR fraction after cholesterol depletion (Saffarian, Li et al. 2007). Other studies have reported decreased EGFR clustering upon cholesterol depletion (Ariotti, Liang et al. 2010, Gao, Wang et al. 2015); however, the EGFR clusters described in those studies are much larger and most likely of a different nature than the mobile complexes investigated here. In addition, the disruption of the actin cytoskeleton by LAT-A treatment had no effect on the EGFR complex fraction. Similarly, Low-Nam et al. (2011) reported that actin disruption did not change the EGFR dimer stability (Low-Nam, Lidke et al. 2011).

Our results showed that the usage of internalization inhibitors did not affect the cross-correlation amount. By adding of unlabeled EGFR, a decrease incross-correlation amount q was observed which is due to dimerization of the labeled one with the unlabeled and therefore underestimation of the apparent fraction.

Activation of EGFR by its ligand EGF has been usually reported to enhance formation of receptor complexes, either dimers or higher oligomers (Ariotti, Liang et al. 2010, de Heus, Kagie et al. 2013, Yamashita, Yano et al. 2015). Our results agree with that. At 10 ng/ml EGF induced a considerable increase in the EGFR complex fraction. Stimulation by EGF also triggers increased complex formation. The high values of cross-correlation (comparable to the positive control) suggest that the increase is not only caused by elevated dimerization, but probably also by higher oligomers (such as tetramers or

hexamers) which are, however, not large enough to be manifested by the broadening of the correlation functions. Different effects were observed after stimulation with a higher dose of EGF (100 ng/ml). The average increase in the cross-correlation amount was smaller in this case; on the other hand, broadening of correlation curves indicated the presence of large EGFR complexes or clusters, which diffuse slower than the monomers and small oligomers. While oligomers of increasing size contribute more prominently to the CCF (the contribution scales with the square of brightness), very large oligomers and clusters by FCCS is problematic. Due to their decreasing mobility, their passages through the observation area are increasingly rare and the measured ensemble of resulting intensity bursts is not statistically significant enough to be suitable for correlation analysis. Besides, our recent findings show that such large complexes and clusters undergo rapid endocytosis which depletes them from the plasma membrane (Bag, Huang et al. 2015).

In conclusion, we have demonstrated the experimental factors investigated (basal versus apical plasma membrane and physiological versus room temperature) have no systematic influence on EGFR complex formation in resting cells; we have observed EGFR complexes in all cases. Nevertheless, there is a considerable cell-to-cell variability with approximately 1/3 of cells showing negligible complex fractions. We believe this large variability existing even within the same culture dish is a potential explanation of the discrepancies between different studies. The fraction of receptors in complexes increases upon cholesterol depletion and is insensitive to actin

cytoskeleton disruption. Stimulation by EGF increases EGFR complex fraction in a dose dependant manner. We assume the EGFR complexes to be transient with lifetimes longer than the order of seconds. The complexes potentially represent the population of EGFR with high affinity towards EGF, which is believed to facilitate faster signaling. Future studies - taking into account receptor transport to the membrane and internalization will have to elucidate how the receptor dimerization and its domain clustering are dynamically regulated and how an equilibrium is reached.

5 Evaluation of alternative genetic tags and improved fluorescent protein

In our previous sections, receptors labeled with red (mRFP) and green (eGFP) fluorescent proteins (FPs) were tracked at different conditions and different FCCS modalities to quantify receptor dimerization in living cells. However, protein maturation issue of mRFP posed constraints in dynamic measurements. Studies by Foo et. al (2012) showed that only ~30% mRFP is fluorescent (Foo, Naredi-Rainer et al. 2012). Therefore, results obtained with mRFP will lead to the underestimation of the percentage of dimers. In this chapter, an advanced red FP, mApple, had been fused to the N-terminus of EGFR. This improved red FP had been tested for its biological functionality and applied to FCCS experiments. Here, we also constructed a range of other new o genetic tags such as SNAP- and CLIP-tag on EGFR and investigated their suitability in dynamics measurements.

5.1 Improved version of red fluorescent protein: mApple

Fluorescent proteins (FP) (~25 kD) have a large application in live cell imaging. FP are genetically fused on the target molecule and have the advantage that they do not require further labeling with exogenous molecules or other procedures such as fixation or permeabilization such as in the case of immunofluorescence. However, many FP versions suffer from low photostability and brightness. The variants of red FPs show a high occurrence of protein misfolding which limits its usage for tracking in live cells.

The first developed monomeric red fluorescent protein (mRFP) showed acceptable brightness, however, it has a drawback of fast photobleaching. To resolve this issue, Shaner et al. (2008) designed improved versions of the available red fluorescent protein, namely mApple and TagRFP-T (Shaner, Lin et al. 2008). mApple possesses higher photostability and brightness than mRFP and mCherry. Brightness is defined as the average fluorescence intensity divided by the particle number in the observation volume. Therefore, mApple was cloned into EGFR to study the dimerization percentage in resting live cells. The cloning was conducted under my supervision by LiuYanting (FYP student, NUS, 2015). The new clone, mApple-EGFR, was transfected into CHO-K1 cells to determine the fluorescence properties in order to compare it with mRFP labeled EGFR protein. Overall, mApple displays higher brightness compared to mRFP. mApple has a brightness of ~500 counts per second (cps). A similar value was obtained for mRFP. When multiplying the brightness with the extinction coefficients of mApple (75,000 $M^{-1}cm^{-1}$) and mRFP (50,000 $M^{-1}cm^{-1}$), mApple (37,500,000) gave a higher brightness as compared to mRFP (25,000,000).

To test the performance of mApple fused EGFR in receptor dynamics studies, this protein and EGFR-eGFP were co-transfected. In FCCS measurements, the cross-correlation amount was 44% in the basal surface, whereas a cross-correlation amount of 51% was determined in the apical surface. The results are summarized in table **5.1.1**. Experiments conducted with mApple receptors revealed higher complex fraction than those of mRFP-based

experiments that can be explained by improved fluorescence properties of this protein.

Protein in CHO-K1	basal *q* (± SEM)	n (cell)	apical *q* (± SEM)	n (cell)
mApple-EGFR/EGFR-eGFP	0.44 ± 0.02	26 (4)	0.51 ± 0.05	27 (4)

Table 5.1.1 *q* factor measured with mApple-EGFR/EGFR-eGFP combination in CHO-K1 at room temperature

In addition, the diffusion times were estimated and are consistent with the times of mRFP and EGFP labeled receptors. On average, it was 70 ± 41 ms and 51 ± 27 ms in the basal and apical membrane, respectively (table **5.1.2**).

	basal	apical
τ_DmApple (ms ± SD)	70 ± 41	51 ± 27
τ_DeGFP (ms ± SD)	86 ± 29	65 ± 44
n (cells)	26 (4)	27 (4)

Table 5.1.2 Diffusion times of mApple and eGFP labeled receptor in resting CHO-K1 cells

5.1.1 Biological Functionality test of chimeric receptor: mApple-EGFR

After determining the dimer amount of EGFR in resting cells, the biological functionality of the new construct was investigated by SDS and Western blot analysis. For that purpose, approximately 5 µg of mApple-EGFR were transfected into 4-5 x10^6 cells and incubated overnight. Afterward, the

medium was replaced with serum-free medium and kept for a minimum of 4-5 h in the incubator. In the next step, transfected cells were activated with EGF at a final concentration of 100 ng/ml for 30 min at 4 °C. The incubation was conducted at a lower temperature as it was necessary to avoid receptor internalization (Oksvold, Skarpen et al. 2000). Degradation of activated EGFR from the membrane will result in multiple bands in the western blot. Reactions at lower temperature prolong dynamics, which allows stimulating the cells for up to 60 min or longer (Defize, Boonstra et al. 1989). The reaction was stopped by washing the cells with 1xPBS buffer and subsequently lysing with RIPA buffer supplemented with phosphatase and protease inhibitor cocktail. This supplement is important to keep the phosphorylated protein and protect it from denaturation. It was mixed with Lamelli buffer and heated up for 10 min at 95 °C. A 7% SDS-gel was prepared to separate the proteins and the gel was transferred to a Hybond-P PVDF membrane. The incubation time of the first antibody anti-pTyr (PY20) was around 4-5 h, while the second antibody sheep anti-mouse IgG remained in the membrane solution for 1-2 h. As a positive control, the endogenous EGFR in COS-7 cells were phosphorylated by EGF and blotted on the membrane. This experiment was repeated three times independently. The western blot analysis in Figure **5.1.1.1** displayed one band between 150-200kD which corresponds to the size of tyrosine phosphorylated ~170 kD EGFR. This protein band verified the full biological functionality of the mApple labeled receptor.

Figure 5.1.1.1 Western Blotting of COS-7 cells and mApple-EGFR in CHO-K1. The band present in this plot confirmed the biological activity as the second antibody specifically binds to phosphorylated tyrosine residues

5.2 Evaluation of the genetic tag Acyl Carrier Protein (ACP)-EGFR

FPs have shortcomings as their photophysical properties and color palette are limited. Besides FPs, another class of protein-based tags is available for live cell imaging. The principle of these tags is based on the process of self-labeling with organic dyes or fluorophores. The self-labeling procedure shows advantages over the commonly used FPs. For instance, labeling can be conducted sequentially tagged protein is fluorescent only after its labeling and tagged protein can change its substrates which are available in a wide color range of different organic dyes and fluorophores. Another expected advantage of this new tagging system is the increase of signal to noise ratio enabled by using bright organic dyes. The company New England Biolabs (NEB) developed different tagging systems such as ACP-tag, SNAP- and CLIP-tag that uses different labeling strategies and substrates.

Acyl carrier protein (ACP)-tag is a small protein of ~8 kDa (77aa) and the labeling process requires an ACP-synthase for the covalent binding of CoA

derivates. The labeling mechanisms of ACP-tagged proteins is shown in Figure **5.2.1**. In the presence of ACP-synthase, CoA-substrate will be covalently attached to the ACP-tag protein.

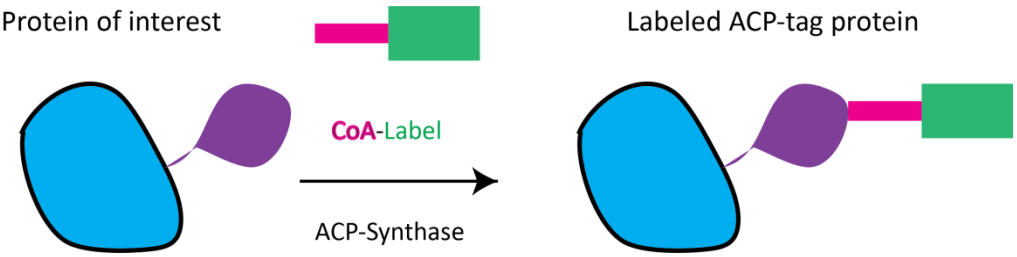

Figure 5.2.1 Labeling system of ACP-tagged proteins with a CoA-derivate

However, ACP substrates do not penetrate through the plasma membrane and are limited in their application. In this work, the ACP-tagged EGFR was analyzed in order to test for its eligibility in FCS measurements and to apply it in interaction measurements. For that purpose, ACP-EGFR was transiently transfected into CHO-K1 cells. Labeling was carried out with 1 µM CoA-label (CoA-Atto488, CoA-OregonGreen or CoA-Cy3) in the presence of 10 mM $MgCl_2$and 1 µM ACP Synthase in phenol-red and serum free DMEM supplemented with 1% bovine serum albumin (BSA) for 30-40 min. The cells were detected in the presence of internalization inhibitors.

Protein	τ_D (ms ± SD)	n (cell)
EGFR-eGFP	59 ±42	22 (4)
ACP-EGFR (CoA-OregonGreen488)	576 ± 278	9 (4)
ACP-EGFR (CoA-Cy3)	315 ± 328	6 (2)
ACP-EGFR (CoA-Atto488)	281 ± 167	30 (4)

Table 5.2.1 Diffusion times of different genetic tags on EGFR measured in CHO-K1

As shown in table **5.2.1**, the calculated diffusion times of labeled ACP-EGFR with distinct CoA derivates are all much higher than those of the fluorescent protein labeled EGFR-eGFP. The slowest diffusion time was obtained by labeling with CoA-OregonGreen488 which gave an average value of 576 ms, followed by CoA-Cy3 with a value of 315 ms and CoA-Atto488 with 281 ms. This illustrates that the ACP-tag has modified the kinetics of EGFR which makes it improper to investigate the mechanisms of EGFR in FCS. The large diffusion time of ACP-EGFR might be due to cluster formation by ACP-tag itself. Another reason for the altered mobility can be caused by unspecific labeling of the ACP-substrates to endogenous proteins or other biomolecules or transport to certain organelles into the cell. In addition, a large fraction of CoA-Cy3 dye showed photobleaching and therefore many data was excluded from data evaluation

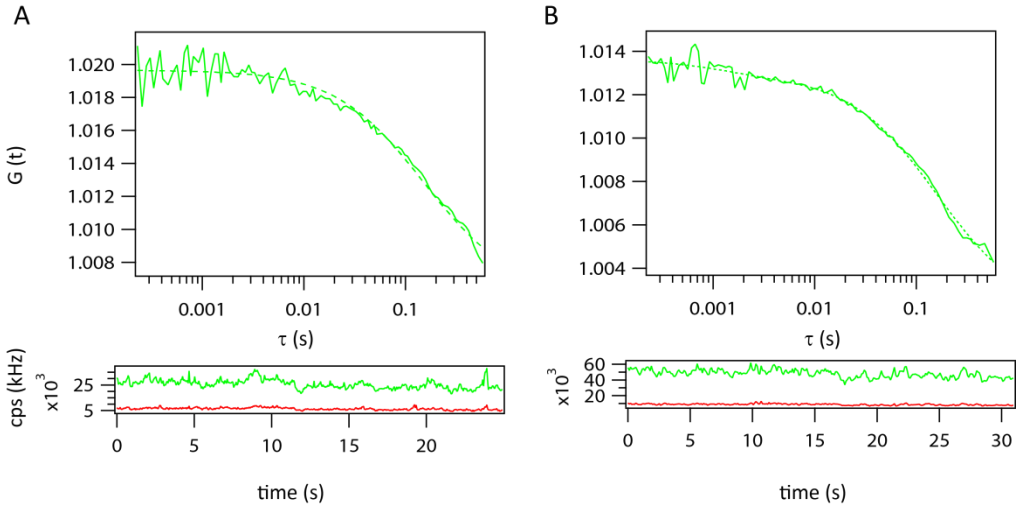

Figure 5.2.2 ACF of ACP-EGFR **(A)** labeled (τ_D = 150 ms) with CoA-Cy3 and **(B)** CoA-Atto488 (τ_D = 158 ms) in CHO-K1

Figure **5.2.2** represents some selected ACF curves of ACP-EGFR labeled with CoA-Cy3 and CoA-Atto488. The red fluorescent fluctuations in the intensity trace in Figure **5.2.2** are caused by crosstalk of CoA-Atto488 into the red channel. The crosstalk amount was on average ~15-20% which is higher than eGFP`s (~10%).

5.3 Cloning and evaluation of new genetic tags: SNAP-EGFR, CLIP-EGFR and SNAP-EGFR-CLIP

SNAP-tag, with a size of 20 kDa, is evolved from the DNA repair protein O^6-alkylguanine-DNA alkyltransferase (AGT) (Juillerat, Gronemeyer et al. 2003, Keppler, Gendreizig et al. 2003). The reaction is based on specifical binding of benzylguanine (BG) derivatives to the cysteine residues of the protein that leads to irreversible covalent labeling. The O^6-alkylguanine is degraded afterward to inhibit toxic effect to the cell. Cells expressing SNAP-tag fused proteins can be labeled specifically with various organic dyes and fluorophores. Another similar variant is the CLIP-tag, a derivate of SNAP-tag, which specifically reacts with O_2-benzylcytosine (BC) derivatives (Gautier, Juillerat et al. 2008). CLIP-tag is commonly used together with SNAP-tag to conduct dual-labeling with two distinct substrates. The reaction mechanism is presented in Figure **5.3.1**.

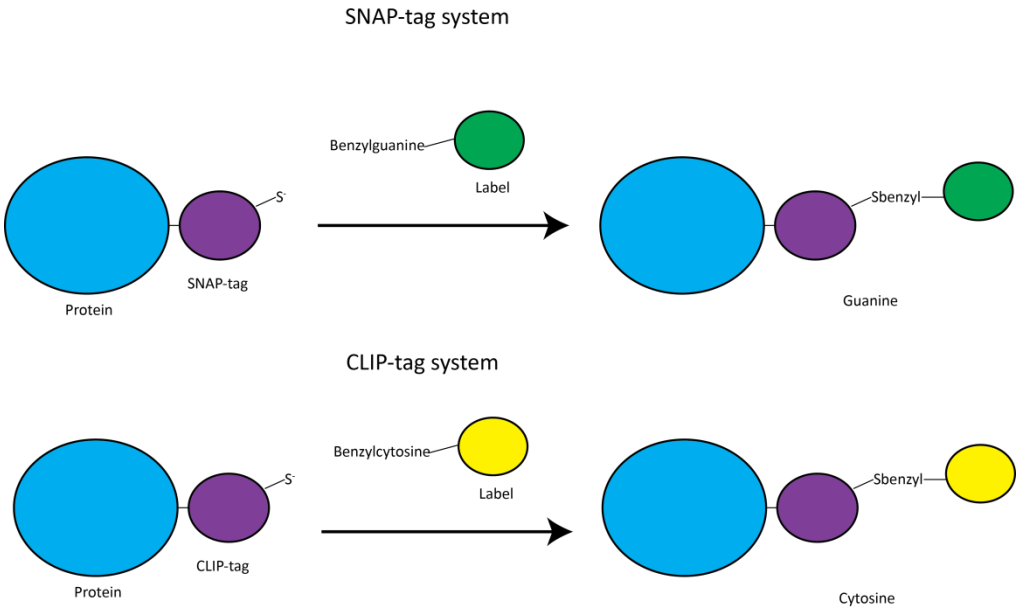

Figure 5.3.1 Principles of SNAP- and CLIP-tag labeling with appropriate substrates

The fusion of SNAP and CLIP-tag to EGFR was prepared in our lab. For that purpose, EGFR was amplified by PCR and inserted into the CLIP vectorbone purchased by NEB and SNAP was amplified and replaced mRFP in the EGFR vectorbone as described in Materials and Methods. The expression and labeling efficiency of SNAP and CLIP-receptors were probed in CHO-K1 at RT. In this set of experiments, cells were incubated with SNAP-Surface® 488 or CLIP-Cell™ TMR-Star for SNAP- and CLIP-tag EGFR, respectively. The diffusivity of these tags are compared with EGFR-eGFPand displayed in table **5.3.1**

Protein	τ_D (ms ± SD)	n (cell)
EGFR-eGFP	59 ±42	22 (4)
SNAP-EGFR (SNAP-Surface® 488)	62 ± 47	15 (5)
EGFR-CLIP (CLIP-Cell™ TMR-Star)	31 ± 10	9 (9)

Table 5.3.1 Lateral mobility of the receptors measured at RT in CHO-K1

SNAP-EGFR and EGFR-eGFP revealed similar diffusion times of around 60 ms. The diffusion time of the construct EGFR-CLIP (31 ms) was a bit faster than the others. However, EGFR-CLIP showed another set of fast moving molecules ranging from 1-10 ms which had been excluded. This might be explained by unreacted CLIP substrates that remain in the cell even after extensive washing and incubation for a certain time in serum- and phenolred-free DMEM which allowed them to diffuse out of the intracellular part. Another possible reason for the fast diffusion time could be due to nonspecific staining of CLIP substrates to the cells or nonspecific binding to other biomolecules/proteins. The specific binding of SNAP substrates to SNAP-tag proteins made it eligible for further investigations of receptor dimerization. However, it should be noted that high specific labeling efficiency of SNAP-Surface® 488 was not detected and the results did not show high signal to noise ratios. Figure **5.3.2** displays the ACF curves of labeled SNAP-and CLIP-EGFR.

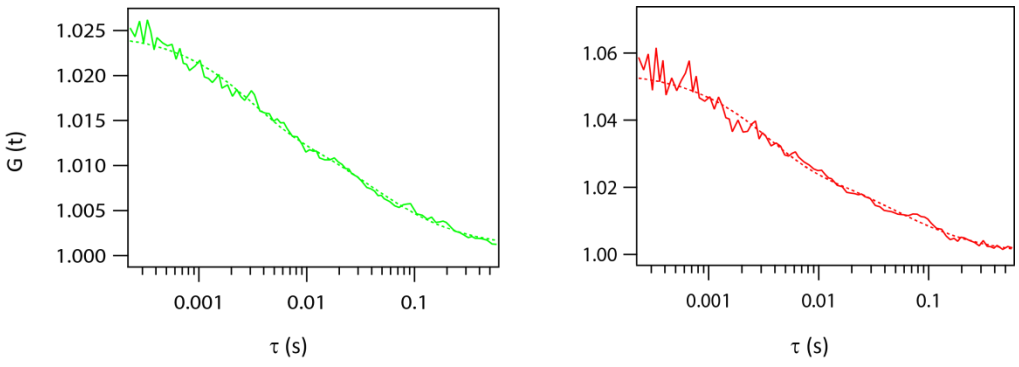

Figure 5.3.2 ACF curves of SNAP-EGFR covalently labeled with SNAP-Surface® 488 (left) and EGFR-CLIP with CLIP-Cell™ TMR-Star (right) obtained by SW-FCCS

After testing and comparing the lateral mobility of these tags, the next step was to investigate its biological functionality. SNAP-EGFR, CLIP-EGFR and SNAP-EGFR-CLIP were transfected separately into CHO-K1 cells and serum starved cells were activated by EGF at a final concentration of 100 ng/ml for 30 min. After cell lysis, ~25 µl lysate were mixed with SDS containing mercaptaethanol and heated at 95 °C for 10 min. The proteins were separated in a 7% SDS gel that was running for 1.20 h, blotted onto the membrane, and visualized. However, the constructs showed no bands in the western blotting. This trial was repeated five times (Figure **5.3.3**). These results indicate that these protein tags are not biologically functional. To confirm this, internalization assay was used to further test its biological activity.

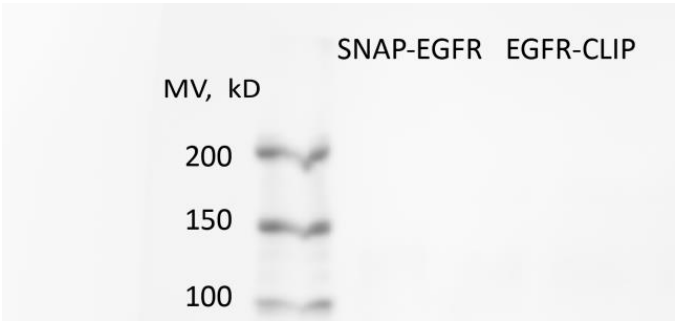

Figure 5.3.3 Western Blot analysis of SNAP-EGFR and EGFR-CLIP to detect phosphorylated tyrosine residues. No band is visible in the range of 170 KD

Cells expressing SNAP-fused EGFR were first labeled with 5 µM SNAP-Surface®488 and washed several times to remove unreacted substrates. However, nonspecific binding of substrates was observed in Figure **5.3.4** at the stage before ligand stimulation. This substrate is known to be cell impermeable (NEB website) but even in the absence of EGF, some substrates are visible inside the cell and in the background. A recent study reported

suitability of certain SNAP-substrates and demonstrated unspecific labeling and high background caused by certain ligands (Bosch, Correa et al. 2014).

In addition, the substrate concentrations of 5 µM lie in the range of the recommended labeling concentration between 1 and 5 µM. However, high labeling efficiency was still not achieved as visible in the images.

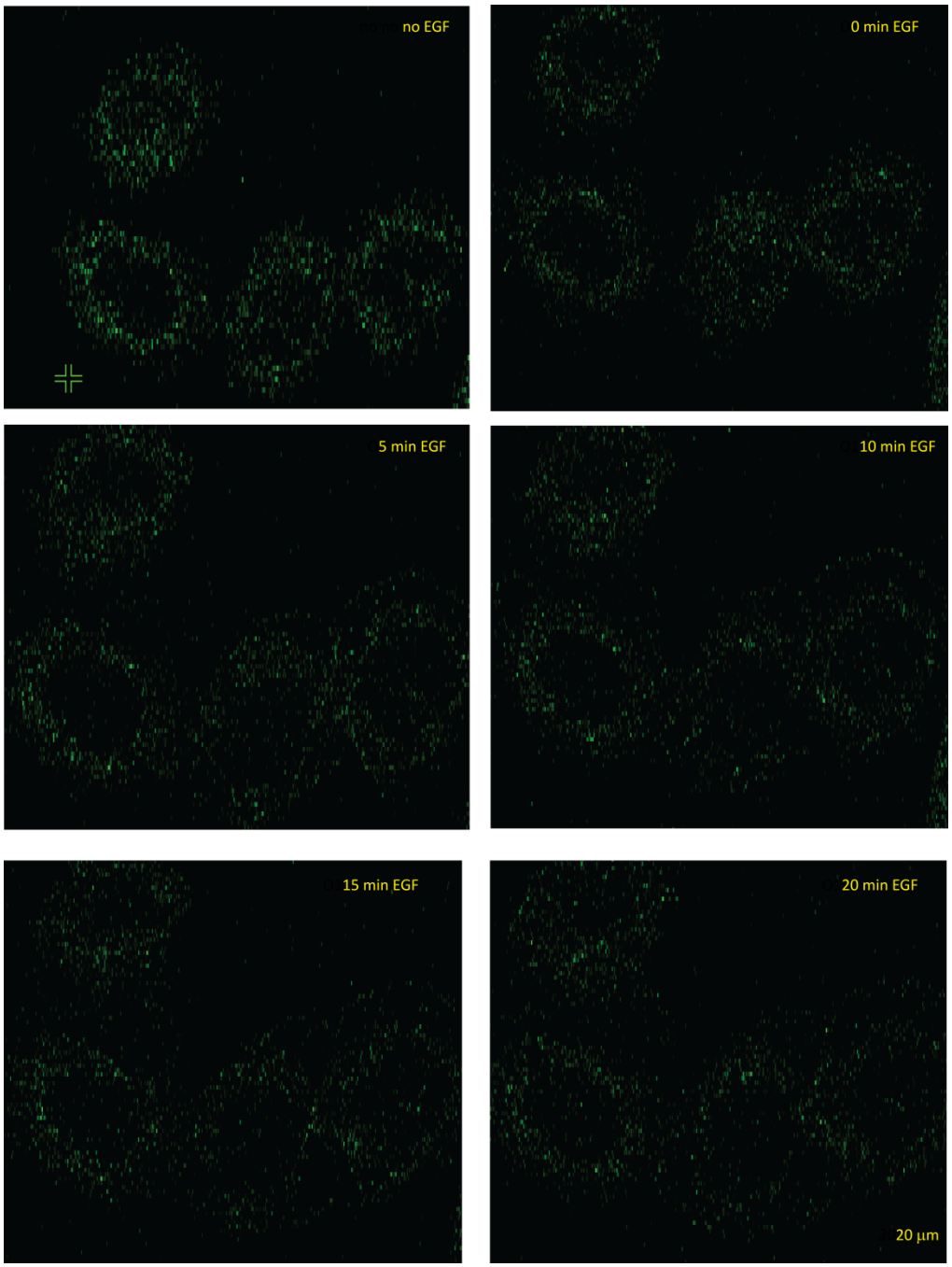

Figure 5.3.4 Internalization assay of SNAP-EGFR. Receptors were stimulated by EGF at a final concentration of 100 ng/ml

Confocal images of cells were recorded before and after 100 ng/ml EGF stimulation. As can be seen in Figure **5.3.4**, receptor dynamics were recorded every five minutes. The membrane fluorescence did not change before and even after 20 min EGF addition for the four cells. The internalization assay of SNAP-EGFR provides further evidence for the non-biological functionality of this receptor. In addition, dead cells showed more nonspecific binding and higher background than live cells. As this protein did not show any biological activity, it was not applied in the estimation of interaction amount in resting cells.

5.4 Dual labeling of SNAP-EGFR-CLIP

The construct SNAP-EGFR-CLIP was prepared in order to investigate its function as an alternative positive control to the existing fluorescently double-labeled mRFP-EGFR-eGFP. As shown previously, the upper limit of the dynamic range by using mRFP-EGFR-eGFP reached, on average, ~60% in different cell lines. The value of less than 100% is caused by the restricted photophysical properties of the FPs. By labeling of SNAP-EGFR-eGFP with bright and photostable organic dyes, an improvement in the complex level is expected. For that purpose, cells expressing this tandem receptor were labeled with 7 µM SNAP-Surface® 488 and 1.8 µM CLIP-Cell™ TMR-Star sequentially, according to NEB recommendations. Labeled receptors were excited by 488 nm and 543 nm lasers. The measurement revealed a 62% complex fraction of this positive control (n=10, 4 cells) and did not reach the

expected value close to 100%. This might be due to several reasons (Figure **5.4.1**). The labeling of SNAP-substrate was not very efficient. A count rate of approximately 9000 cps was detected even after labeling with high substrate concentration. The cells were very dimly labeled and high background signal was recorded. Our data showed that labeling of SNAP-tag was not very specific with this substrate and some tags may not have been labeled successfully. This might explain the lower value of the positive control. 1:1 labeling was not achieved. This low labeling efficiency led to the underestimation of protein interaction.

However, the substrate CLIP-Cell™ TMR-Star bound very specifically to CLIP-tag and with high affinity. Therefore, the labeling of SNAP-EGFR-CLIP was repeated few times to adjust the intensity rate to similar values. Due to the low labeling efficiency of the SNAP-tag, the concentration of CLIP-substrate was lowered significantly. In addition, the diffusion times of EGFR were in the range of cytosolic proteins and far away from transmembrane receptors, likely caused by unbound substrates in the cell.

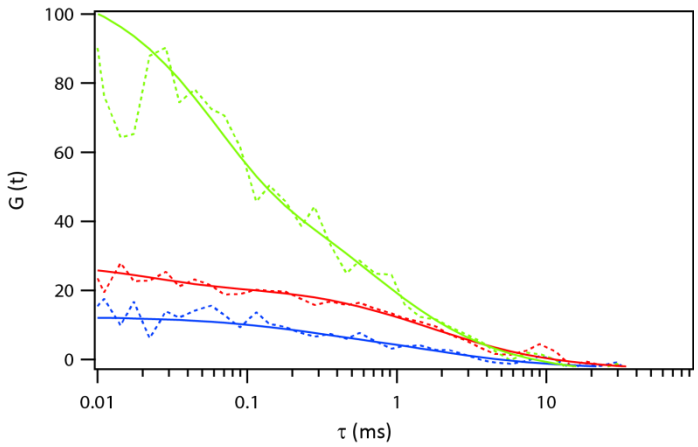

Figure 5.4.1 FCCS curve of dual labeled SNAP-EGFR-CLIP

However, testing of different SNAP-substrates could help to increase the dynamic range. There are different kinds of green color substrates from different companies available.

5.5 Discussion

Available red fluorescent proteins exhibit deficiencies in brightness and photostability. Unfortunately, the performance of these proteins does not match with the one of eGFP. Therefore, alternative constructs with improved red fluorescent protein and different genetic tags on the receptor have been cloned in order to test their performance and eligibility in FCS measurements. An improved red version of mRFP, known as mApple, shows improved photophysical properties over currently available red variants. Accordingly, mApple on the N-terminus of EGFR was constructed and the expression and biological activity were investigated in living CHO-K1 cells. Biochemical methods such as SDS page and Western plot assay proved the biological functionality of the construct mApple-EGFR. The addition of EGF led to the phosphorylation of EGFR that was evident in the Western plot assay. Maturation time and subsequent brightness of FPs depend on many local factors, such as oxygen level, cell type, temperature and linker protein. To obtain a parameter about the properties of this construct, the cell expression and brightness of mApple-labeled protein was evaluated. mApple-tagged protein revealed improved brightness compared to mRFP with an excitation laser wavelength of 514 nm. This result is in agreement with previously

reported studies (Shaner, Lin et al. 2008). Therefore, mApple labeled EGFR was used for FCCS measurements to determine the cross-correlation amount of EGFR. Our data revealed a cross-correlation amount of 44% in the basal membrane and cross-correlation amount of 51% in the apical membrane. Compared to the measurements with mRFP, the *q* amount was ~30% in the basal and apical membrane using different FCCS modalities. The results demonstrate that using improved red fluorescent proteins, which in contrast to mRFP showed a larger fluorescent fraction, increased the detected cross-correlation amount in living cells.

The cloning of the new constructs SNAP-EGFR, EGFP-CLIP and SNAP-EGFR-CLIP was successful and they were tested for their performance. The diffusivity of SNAP-EGFR was in a similar range as EGFR-EGFP, whereas EGFR-CLIP showed a fraction with fast moving molecules. This is possibly caused by unreacted CLIP substrates in the cells. However, western blot assay could not detect any bands of the phosphorylated receptor with these new constructs after their stimulation with EGF. In addition, the alternative positive control SNAP-EGFR-CLIP was labeled with distinct substrates and revealed a cross-correlation amount of 62%. This value is close to the value obtained by the positive control labeled with fluorescent proteins. The expected value of 100% is not reached, which is due to non-specific and weak labeling of SNAP-Atto488. However, the cross- correlation amount of this construct can be improved by testing further substrates with improved labeling efficiency.

6 Conclusion and Outlook

6.1 Conclusion

The goal of this work was to investigate EGFR dimerization by SW-FCCS (Hwang and Wohland 2004, Liu, Sudhaharan et al. 2007) with the aim to understand the potential role of selected experimental factors in the discrepancies in reported levels of EGFR dimerization in resting cells. Intense research has contributed to the quantification of the level of receptor dimers in the absence of a ligand in the past. However, the results vary extremely from study to study. Reported values range over almost all possible values from 0 to 100%. The discrepancies arose in the estimation of dimerization amount required an explanation, and investigation of the source of these differences was needed. The inconsistency of EGFR results can originate from using different techniques and conditions, handling in cell culture, measurements on different membrane locations and using different temperature ranges. Besides using SW-FCCS, other advanced FCCS modalities including dual-color FCCS, quasi-PIE-FCCS and DC-ITIR-FCCS were utilized to analyze the dimer fraction of EGFR and test whether we obtain consistent results by measuring with different techniques. The important finding is that we found evidence for the existence of EGFR complexes under all experimental conditions probed. Our results show that temperature has little effect and the dimer fraction is consistent between measurements at room temperature and physiological temperature. Also membrane location on the apical and basal membranes does not show strong differences. In contrast to

these parameters, the cell line plays a strong role in the results. Cell lines that express endogenous EGFR (COS-7, HEK293) show low apparent dimerization at low expression of the labeled EGFR as the endogenous receptor will interfere and mainly dimers between endogenous and transiently expressed, labeled receptors will be observed. The apparent dimer fraction in these cases will increase with the expression level of labeled EGFR due to competition between labeled and endogenous EGFR molecules. The presence of endogenous EGFR suppressed the actual apparent complex fraction when the labeled EGFR was at low to middle expression level. For cells that do not possess any endogenous EGFR (CHO-K1), the dimer fraction is always high, independent of the expression level of labeled EGFR. The normalized dimerization amount of 57% tested in CHO-K1 cells is comparable and in agreement with our previous studies (Liu, Sudhaharan et al. 2007, Ma, Ahmed et al. 2011). Our findings also provid evidence for the complex concept of ligand-independent activation in which EGFR exists as a mixture of monomeric, dimerc and oligomeric fraction in the plasma membrane. A body of data also indicates the presence of preformed dimers in the absence of ligand (Maruyama 2014, Valley, Lidke et al. 2014). EGFR dimerization plays an important role also in *C.elegans*; it was found in dimeric state in unliganded environment (Freed, Alvarado et al. 2015). Recent reports propose that EGFR resides in oligomeric form in the plasma membrane in the absence of ligand (Needham, Zanetti-Domingues et al. 2015, Needham, Roberts et al. 2016). Current studies together with our results implicate the complexity of this membrane receptor in signal activation. Our results indicate a complex model

in which signaling is drived by dimeric and oligomeric organization of EGFR in the absence of ligand.

All FCCS modalities used in this work (SW-FCCS, DCFCCS, quasi PIE-FCCS, and imaging FCCS) show the same high dimer fraction but provide different advantages. SW-FCCS is the simplest in terms of setup but even the negative control will have some cross-correlation due to spectral cross-talk. Quasi PIE-FCCS is cross-talk free and provides perfect negative controls that should increase the sensitivity of the technique when low cross-correlation need to be quantified. Imaging FCCS has a lower time resolution but is well suited for membrane measurements. Its main advantage is the multiplexing of measurements and its spatial resolution. Here we were able to show that dimer fractions tend to be higher at the border compared to the center of the cell in agreement with previous reports (Chung, Akita et al. 2010, Bag, Huang et al. 2015). This would not have been easily possible with single-point FCS measurements. Overall, our results indicate that the largest factors in the variability of dimer measurements are cell line and cell-to cell variability, and to some extent the location of the measurement while temperature plays a minor role.

Further investigations of EGF dimers by drug treatments by LAT-A revealed no changes in EGFR complex fraction after the depletion of the actin cytoskeleton compared to the control cells. However, the situation was different when cholesterol was removed from the plasma membrane by the drug mβCD. The complex fraction rose up significantly in the apical as well as in the basal membrane when cholesterol was removed consistent with

previous reports (Saffarian, Li et al. 2007). This finding is also in agreement with our recent publication (Bag, Huang et al. 2015) in which its indicating that EGFR resides in cholesterol and cholesterol-independent domains. The increase in complex fraction after drug treatment indicates that EGFR complexes are held together by receptor-receptor interactions. EGFR at least co-exists as monomers dimers and possibly higher oligomers. However, by using FCCS, it is not possible to distinguish between dimers and higher-oder oligomers. EGFR is domain dependent and insensitive to cytoskeleton disruption. An early study demonstrated that EGFR dynamics is influenced in some extent by cholesterol level. The localization of EGFR in lipid domains affects EGFR activation. Cholesterol depletion induced release of EGFR from lipid rafts, which caused suppression of EGFR activation (Pike and Casey 2002). This data is in agreement with our findings as we observed an increase in the EGFR complex fraction after cholesterol removal. The transient trapping of receptor molecules into small cholesterol-dependent domains prevents them from diffusing freely and, thus, reduces the frequency of their encounters with other receptors, which lead to formation of the transient complexes. Furthermore, the binding of EGF on EGFR has shown to change receptor organization and to promote oligomerization (McLaughlin, Smith et al. 2005). This property of EGF binding to EGFR is comparable with our results; EGF enhanced the formation of complexes.

The last research topic involved the cloning and evaluation of alternative tags to FP`s labeled receptors. The purpose of this project was to evaluate the influence of fluorescent properties of alternative tags on the quantification of

EGFR complexes. An improved version of mRFP, named mApple was successfully cloned to EGFR and the biological activity confirmed by Western blot assay. The application of mApple labeled receptors in the interaction measurements with eGFP-labeled EGFR showed an increase in the average apparent complex fraction. This was enabled by the improved fluorescence properties of the red FP mApple.

6.2 Outlook

The findings illustrated in this work provide insight into factors, which need to be considered, for the quantification of EGFR dimers in live cells. We showed that EGFR exists as preformed dimers under resting conditions, while EGF ligand causes increase in dimerization amount and oligomerization. The biological meaning of predimerization of EGFR relies on speeding up the signaling cascades.

An important factor is cell-to-cell variability, which is considerable. In confocal FCS measurements, this is difficult to quantify as one has only a limited number of measurements per cell. Imaging FCS allowed us to quantify with good statistical significance the dimer fraction over a large part of the cell membrane. This showed that we have about a third of all cells that have a high dimer fraction, a third that has low dimer fraction and a third in between. This alone can lead to large variability when averaging measurements over different cells and is possibly one of the factors leading to a variety of results. It will be interesting to investigate whether this

variability in 2D cell cultures is an artefact or whether it also exists in 3D cell cultures, tissues and live organisms. Other possible approaches are to create a CRISPR/CAS9 transgenic lines in cells with endogenous level of EGFR which allows measuring of receptor interaction in a stable expressing cell line. The performance of measurements in synchronized cells would provide useful information about EGFR dynamics at each single cell cycle.

Another outstanding future work is a detailed investigation of the nature of the receptor complex regions in resting cells can be performed, by using DC-ITIR-FCCS, in order to understand if these complex regions contain only elevated amounts of dimers or also contains higher EGFR oligomers.

A possible future direction is the clinical study on biopsies in lung cancer patients. Available drugs from the class TKIs (gefinitib and erlotinib) requires further investigation on lung cancer patients as many of them develop a second mutation during the drug treatment. Biopysies are ideal samples from patients before and after drug treatment to monitor tumor dynamics and to understand the relationship between drug and receptor interaction by using FCCS.

7. Bibliogrpahy

Alvarado, D., D. E. Klein and M. A. Lemmon (2010). "Structural Basis for Negative Cooperativity in Growth Factor Binding to an EGF Receptor." Cell **142**(4): 568-579.

Alvarado, D., D. E. Klein and M. A. Lemmon (2010). "Structural basis for negative cooperativity in growth factor binding to an EGF receptor." Cell **142**(4): 568-579.

Anikovsky, M., L. Dale, S. Ferguson and N. Petersen (2008). "Resonance energy transfer in cells: a new look at fixation effect and receptor aggregation on cell membrane." Biophys J **95**(3): 1349-1359.

Ariotti, N., H. Liang, Y. Xu, Y. Zhang, Y. Yonekubo, K. Inder, G. Du, R. G. Parton, J. F. Hancock and S. J. Plowman (2010). "Epidermal growth factor receptor activation remodels the plasma membrane lipid environment to induce nanocluster formation." Molecular and Cellular Biology **30**(15): 3795-3804.

Arkhipov, A., Y. B. Shan, R. Das, N. F. Endres, M. P. Eastwood, D. E. Wemmer, J. Kuriyan and D. E. Shaw (2013). "Architecture and Membrane Interactions of the EGF Receptor." Cell **152**(3): 557-569.

Ashdown, G., E. Pandzic, A. Cope, P. Wiseman and D. Owen (2015). "Cortical Actin Flow in T Cells Quantified by Spatio-temporal Image Correlation Spectroscopy of Structured Illumination Microscopy Data." J Vis Exp(106): e53749.

Axelrod, D. (1981). "Cell-substrate contacts illuminated by total internal reflection fluorescence." J Cell Biol **89**(1): 141-145.

Axelrod, D., N. L. Thompson and T. P. Burghardt (1983). "Total internal inflection fluorescent microscopy." J Microsc **129**(Pt 1): 19-28.

Bag, N., S. Huang and T. Wohland (2015). "Plasma Membrane Organization of Epidermal Growth Factor Receptor in Resting and Ligand-Bound States." Biophysical Journal **109**(9): 1925-1936.

Bag, N., S. Huang and T. Wohland (2015). "Plasma Membrane Organization of Epidermal Growth Factor Receptor in Resting and Ligand-Bound States." Biophys J **109**(9): 1925-1936.

Bag, N., J. Sankaran, A. Paul, R. S. Kraut and T. Wohland (2012). "Calibration and limits of camera-based fluorescence correlation spectroscopy: a supported lipid bilayer study." Chemphyschem **13**(11): 2784-2794.

Bag, N., D. H. Yap and T. Wohland (2014). "Temperature dependence of diffusion in model and live cell membranes characterized by imaging fluorescence correlation spectroscopy." Biochim Biophys Acta **1838**(3): 802-813.

Barriere, H., C. Nemes, K. Du and G. L. Lukacs (2007). "Plasticity of polyubiquitin recognition as lysosomal targeting signals by the endosomal sorting machinery." Mol Biol Cell **18**(10): 3952-3965.

Baselga, J. (2002). "Why the epidermal growth factor receptor? The rationale for cancer therapy." Oncologist **7 Suppl 4**: 2-8.

Baumdick, M., Y. Bruggemann, M. Schmick, G. Xouri, O. Sabet, L. Davis, J. W. Chin and P. I. Bastiaens (2015). "EGF-dependent re-routing of vesicular recycling switches spontaneous phosphorylation suppression to EGFR signaling." Elife **4**.

Berland, K. and G. Shen (2003). "Excitation saturation in two-photon fluorescence correlation spectroscopy." Applied optics **42**(27): 5566-5576.

Bi, H., Y. Yin, B. Pan, G. Li and X. S. Zhao (2016). "Scanning Single-Molecule Fluorescence Correlation Spectroscopy Enables Kinetics Study of DNA Hairpin Folding with a Time Window from Microseconds to Seconds." J Phys Chem Lett **7**(10): 1865-1871.

Böhmer, M., M. Wahl, H.-J. Rahn, R. Erdmann and J. Enderlein (2002). "Time-resolved fluorescence correlation spectroscopy." Chemical Physics Letters **353**(5–6): 439-445.

Bosch, P. J., I. R. Correa, Jr., M. H. Sonntag, J. Ibach, L. Brunsveld, J. S. Kanger and V. Subramaniam (2014). "Evaluation of fluorophores to label SNAP-tag fused proteins for multicolor single-molecule tracking microscopy in live cells." Biophys J **107**(4): 803-814.

Bosch, P. J., I. R. Correa, Jr., M. H. Sonntag, J. Ibach, L. Brunsveld, J. S. Kanger and V. Subramaniam (2014). "Evaluation of Fluorophores to Label SNAP-Tag Fused Proteins for Multicolor Single-Molecule Tracking Microscopy in Live Cells." Biophysical Journal **107**(4): 803-814.

Brand, T. M., M. Iida, C. Li and D. L. Wheeler (2011). "The Nuclear Epidermal Growth Factor Receptor Signaling Network and its Role in Cancer." Discovery Medicine **12**(66): 419-432.

Brandao, H. B., H. Sangji, E. Pandzic, S. Bechstedt, G. J. Brouhard and P. W. Wiseman (2014). "Measuring ligand-receptor binding kinetics and dynamics using k-space image correlation spectroscopy." Methods **66**(2): 273-282.

Brasitus, T. A. and D. Schachter (1980). "Lipid dynamics and lipid-protein interactions in rat enterocyte basolateral and microvillus membranes." Biochemistry **19**(12): 2763-2769.

Brown, M. S. and J. L. Goldstein (1992). "Koch's postulates for cholesterol." Cell **71**(2): 187-188.

Buccione, R., J. D. Orth and M. A. McNiven (2004). "Foot and mouth: podosomes, invadopodia and circular dorsal ruffles." Nat Rev Mol Cell Biol **5**(8): 647-657.

Campbell, R. E., O. Tour, A. E. Palmer, P. A. Steinbach, G. S. Baird, D. A. Zacharias and R. Y. Tsien (2002). "A monomeric red fluorescent protein." Proc Natl Acad Sci U S A **99**(12): 7877-7882.

Carpenter, G. (1987). "Receptors for epidermal growth factor and other polypeptide mitogens." Annu Rev Biochem **56**: 881-914.

Carpenter, G. and S. Cohen (1979). "Epidermal growth factor." Annu Rev Biochem **48**: 193-216.

Carpenter, G., L. King, Jr. and S. Cohen (1978). "Epidermal growth factor stimulates phosphorylation in membrane preparations in vitro." Nature **276**(5686): 409-410.

Carter, R. E. and A. Sorkin (1998). "Endocytosis of functional epidermal growth factor receptor-green fluorescent protein chimera." J Biol Chem **273**(52): 35000-35007.

Chapple, J. P., A. J. Hardcastle, C. Grayson, K. R. Willison and M. E. Cheetham (2002). "Delineation of the plasma membrane targeting domain of the X-linked retinitis pigmentosa protein RP2." Invest Ophthalmol Vis Sci **43**(6): 2015-2020.

Chen, J. and J. Irudayaraj (2010). "Fluorescence lifetime cross correlation spectroscopy resolves EGFR and antagonist interaction in live cells." Anal Chem **82**(15): 6415-6421.

Chen, X. and M. D. Resh (2002). "Cholesterol depletion from the plasma membrane triggers ligand-independent activation of the epidermal growth factor receptor." J Biol Chem **277**(51): 49631-49637.

Chen, Y., J. D. Muller, P. T. So and E. Gratton (1999). "The photon counting histogram in fluorescence fluctuation spectroscopy." Biophys J **77**(1): 553-567.

Chung, I., R. Akita, R. Vandlen, D. Toomre, J. Schlessinger and I. Mellman (2010). "Spatial control of EGF receptor activation by reversible dimerization on living cells." Nature **464**(7289): 783-787.

Ciardiello , F. and G. Tortora (2008). "EGFR Antagonists in Cancer Treatment." New England Journal of Medicine **358**(11): 1160-1174.

Citri, A., K. B. Skaria and Y. Yarden (2003). The deaf and the dumb: The biology of ErbB-2 and ErbB-3. The EGF Receptor Family. G. Carpenter. Burlington, Academic Press**:** 57-68.

Clayton, A. H., S. G. Orchard, E. C. Nice, R. G. Posner and A. W. Burgess (2008). "Predominance of activated EGFR higher-order oligomers on the cell surface." Growth Factors **26**(6): 316-324.

Clayton, A. H., F. Walker, S. G. Orchard, C. Henderson, D. Fuchs, J. Rothacker, E. C. Nice and A. W. Burgess (2005). "Ligand-induced dimer-tetramer transition during the activation of the cell surface epidermal growth factor receptor-A multidimensional microscopy analysis." J Biol Chem **280**(34): 30392-30399.

Cochet, C., O. Kashles, E. M. Chambaz, I. Borrello, C. R. King and J. Schlessinger (1988). "Demonstration of epidermal growth factor-induced receptor dimerization in living cells using a chemical covalent cross-linking agent." J Biol Chem **263**(7): 3290-3295.

Cohen, S. (1962). "Isolation of a mouse submaxillary gland protein accelerating incisor eruption and eyelid opening in the new-born animal." J Biol Chem **237**: 1555-1562.

Cutler, P. J., M. D. Malik, S. Liu, J. M. Byars, D. S. Lidke and K. A. Lidke (2013). "Multi-color quantum dot tracking using a high-speed hyperspectral line-scanning microscope." PLoS One **8**(5): e64320.

Dassonville, O., A. Bozec, J. L. Fischel and G. Milano (2007). "EGFR targeting therapies: monoclonal antibodies versus tyrosine kinase inhibitors. Similarities and differences." Crit Rev Oncol Hematol **62**(1): 53-61.

Daub, H., F. U. Weiss, C. Wallasch and A. Ullrich (1996). "Role of transactivation of the EGF receptor in signalling by G-protein-coupled receptors." Nature **379**(6565): 557-560.

Day, R. N. and M. W. Davidson (2009). "The fluorescent protein palette: tools for cellular imaging." Chem Soc Rev **38**(10): 2887-2921.

de Heus, C., N. Kagie, R. Heukers, P. M. van Bergen en Henegouwen and H. C. Gerritsen (2013). "Analysis of EGF receptor oligomerization by homo-FRET." Methods Cell Biol **117**: 305-321.

Defize, L. H., J. Boonstra, J. Meisenhelder, W. Kruijer, L. G. Tertoolen, B. C. Tilly, T. Hunter, P. M. van Bergen en Henegouwen, W. H. Moolenaar and S. W. de Laat (1989). "Signal transduction by epidermal growth factor occurs through the subclass of high affinity receptors." J Cell Biol **109**(5): 2495-2507.

den Hartigh, J. C., P. M. van Bergen en Henegouwen, J. Boonstra and A. J. Verkleij (1993). "Cholesterol and phosphoinositides increase affinity of the epidermal growth factor receptor." Biochim Biophys Acta **1148**(2): 249-256.

den Hartigh, J. C., P. M. van Bergen en Henegouwen, A. J. Verkleij and J. Boonstra (1992). "The EGF receptor is an actin-binding protein." J Cell Biol **119**(2): 349-355.

Di Rienzo, C., V. Piazza, E. Gratton, F. Beltram and F. Cardarelli (2014). "Probing short-range protein Brownian motion in the cytoplasm of living cells." Nature Communications **5**: 5891.

Dittrich, P. and P. Schwille (2001). "Photobleaching and stabilization of. fluorophores used for single-molecule analysis. with one-and two-photon excitation." Applied Physics B **73**(8): 829-837.

Edelstein, A. D., M. A. Tsuchida, N. Amodaj, H. Pinkard, R. D. Vale and N. Stuurman (2014). "Advanced methods of microscope control using muManager software." J Biol Methods **1**(2).

Eigen, M. and R. Rigler (1994). "Sorting single molecules: application to diagnostics and evolutionary biotechnology." Proc Natl Acad Sci U S A **91**(13): 5740-5747.

El-Shaheny, R. N. (2014). "Evaluation of agomelatine stability under different stress conditions using an HPLC method with fluorescence detection: application to the analysis of tablets and human plasma." Luminescence **29**(7): 920-928.

Endres, Nicholas F., R. Das, Adam W. Smith, A. Arkhipov, E. Kovacs, Y. Huang, Jeffrey G. Pelton, Y. Shan, David E. Shaw, David E. Wemmer, Jay T. Groves and J. Kuriyan (2013). "Conformational Coupling across the Plasma Membrane in Activation of the EGF Receptor." Cell **152**(3): 543-556.

Foo, Y. H., N. Naredi-Rainer, D. C. Lamb, S. Ahmed and T. Wohland (2012). "Factors affecting the quantification of biomolecular interactions by fluorescence cross-correlation spectroscopy." Biophys J **102**(5): 1174-1183.

Franovic, A., L. Gunaratnam, K. Smith, I. Robert, D. Patten and S. Lee (2007). "Translational up-regulation of the EGFR by tumor hypoxia provides a nonmutational explanation for its overexpression in human cancer." Proc Natl Acad Sci U S A **104**(32): 13092-13097.

Freed, D. M., D. Alvarado and M. A. Lemmon (2015). "Ligand regulation of a constitutively dimeric EGF receptor." Nat Commun **6**: 7380.

Gadella Jr, T. W. J. and T. M. Jovin (1995). "Oligomerization of epidermal growth factor receptors on A431 cells studied by time-resolved fluorescence imaging microscopy. A stereochemical model for tyrosine kinase receptor activation." Journal of Cell Biology **129**(6): 1543-1558.

Gajiwala, K. S. (2013). "EGFR: tale of the C-terminal tail." Protein Sci **22**(7): 995-999.

Gan, H. K., A. N. Cvrljevic and T. G. Johns (2013). "The epidermal growth factor receptor variant III (EGFRvIII): where wild things are altered." Febs j **280**(21): 5350-5370.

Gao, J., Y. Wang, M. Cai, Y. Pan, H. Xu, J. Jiang, H. Ji and H. Wang (2015). "Mechanistic insights into EGFR membrane clustering revealed by super-resolution imaging." Nanoscale **7**(6): 2511-2519.

Garrett, T. P. J., N. M. McKern, M. Lou, T. C. Elleman, T. E. Adams, G. O. Lovrecz, M. Kofler, R. N. Jorissen, E. C. Nice, A. W. Burgess and C. W. Ward (2003). "The Crystal

Structure of a Truncated ErbB2 Ectodomain Reveals an Active Conformation, Poised to Interact with Other ErbB Receptors." Molecular Cell **11**(2): 495-505.

Garrett, T. P. J., N. M. McKern, M. Lou, T. C. Elleman, T. E. Adams, G. O. Lovrecz, H.-J. Zhu, F. Walker, M. J. Frenkel, P. A. Hoyne, R. N. Jorissen, E. C. Nice, A. W. Burgess and C. W. Ward (2002). "Crystal Structure of a Truncated Epidermal Growth Factor Receptor Extracellular Domain Bound to Transforming Growth Factor α." Cell **110**(6): 763-773.

Gautier, A., A. Juillerat, C. Heinis, I. R. Correa, Jr., M. Kindermann, F. Beaufils and K. Johnsson (2008). "An engineered protein tag for multiprotein labeling in living cells." Chem Biol **15**(2): 128-136.

Goh, L. K., F. Huang, W. Kim, S. Gygi and A. Sorkin (2010). "Multiple mechanisms collectively regulate clathrin-mediated endocytosis of the epidermal growth factor receptor." J Cell Biol **189**(5): 871-883.

Goh, L. K. and A. Sorkin (2013). "Endocytosis of Receptor Tyrosine Kinases." Cold Spring Harbor Perspectives in Biology **5**(5).

Gosch, M., H. Blom, J. Holm, T. Heino and R. Rigler (2000). "Hydrodynamic flow profiling in microchannel structures by single molecule fluorescence correlation spectroscopy." Anal Chem **72**(14): 3260-3265.

Greulich, H., T. H. Chen, W. Feng, P. A. Janne, J. V. Alvarez, M. Zappaterra, S. E. Bulmer, D. A. Frank, W. C. Hahn, W. R. Sellers and M. Meyerson (2005). "Oncogenic transformation by inhibitor-sensitive and -resistant EGFR mutants." PLoS Med **2**(11): e313.

Gummadi, S. N. and K. S. Kumar (2005). "The mystery of phospholipid flip-flop in biogenic membranes." Cell Mol Biol Lett **10**(1): 101-121.

Harris, R. C., E. Chung and R. J. Coffey (2003). "EGF receptor ligands." Exp Cell Res **284**(1): 2-13.

Hess, S. T. and W. W. Webb (2002). "Focal volume optics and experimental artifacts in confocal fluorescence correlation spectroscopy." Biophys J **83**(4): 2300-2317.

Hillesheim, L. N., Y. Chen and J. D. Müller (2006). "Dual-Color Photon Counting Histogram Analysis of mRFP1 and EGFP in Living Cells." Biophysical Journal **91**(11): 4273-4284.

Hinrichsen, L., J. Harborth, L. Andrees, K. Weber and E. J. Ungewickell (2003). "Effect of clathrin heavy chain- and alpha-adaptin-specific small inhibitory RNAs on endocytic accessory proteins and receptor trafficking in HeLa cells." J Biol Chem **278**(46): 45160-45170.

Hiroshima, M., Y. Saeki, M. Okada-Hatakeyama and Y. Sako (2012). "Dynamically varying interactions between heregulin and ErbB proteins detected by single-molecule analysis in living cells." Proc Natl Acad Sci U S A **109**(35): 13984-13989.

Hofman, E. G., A. N. Bader, J. Voortman, D. J. Van Den Heuvel, S. Sigismund, A. J. Verkleij, H. C. Gerritsen and P. M. P. Van Bergen en Henegouwen (2010). "Ligand-induced EGF receptor oligomerization is kinase-dependent and enhances internalization." Journal of Biological Chemistry **285**(50): 39481-39489.

Hoon, J.-L., W.-K. Wong and C.-G. Koh (2012). "Functions and regulation of circular dorsal ruffles." Molecular and cellular biology **32**(21): 4246-4257.

Huang, F., A. Khvorova, W. Marshall and A. Sorkin (2004). "Analysis of clathrin-mediated endocytosis of epidermal growth factor receptor by RNA interference." J Biol Chem **279**(16): 16657-16661.

Huang, Y., S. Bharill, D. Karandur, S. M. Peterson, M. Marita, X. Shi, M. J. Kaliszewski, A. W. Smith, E. Y. Isacoff and J. Kuriyan (2016). "Molecular basis for multimerization in the activation of the epidermal growth factor receptor." Elife **5**.

Hubbard, S. R. (2009). "The juxtamembrane region of EGFR takes center stage." Cell **137**(7): 1181-1183.

Hwang, L. C. and T. Wohland (2004). "Dual-Color Fluorescence Cross-Correlation Spectroscopy Using Single Laser Wavelength Excitation." Chemphyschem **5**(4): 549-551.

Hwang, L. C. and T. Wohland (2005). "Single wavelength excitation fluorescence cross-correlation spectroscopy with spectrally similar fluorophores: resolution for binding studies." J Chem Phys **122**(11): 114708.

Hynes, N. E. and H. A. Lane (2005). "ERBB receptors and cancer: the complexity of targeted inhibitors." Nat Rev Cancer **5**(5): 341-354.

Ikonen, E. (2001). "Roles of lipid rafts in membrane transport." Curr Opin Cell Biol **13**(4): 470-477.

Jiang, X. and A. Sorkin (2003). "Epidermal growth factor receptor internalization through clathrin-coated pits requires Cbl RING finger and proline-rich domains but not receptor polyubiquitylation." Traffic **4**(8): 529-543.

Jones, J. T., R. W. Akita and M. X. Sliwkowski (1999). "Binding specificities and affinities of egf domains for ErbB receptors." FEBS Lett **447**(2-3): 227-231.

Jovin, Thomas M. (2014). "Pinning Down the EGF Receptor." Biophysical Journal **107**(11): 2486-2488.

Juillerat, A., T. Gronemeyer, A. Keppler, S. Gendreizig, H. Pick, H. Vogel and K. Johnsson (2003). "Directed Evolution of O6-Alkylguanine-DNA Alkyltransferase for Efficient Labeling of Fusion Proteins with Small Molecules In Vivo." Chemistry & Biology **10**(4): 313-317.

Jura, N., N. F. Endres, K. Engel, S. Deindl, R. Das, M. H. Lamers, D. E. Wemmer, X. W. Zhang and J. Kuriyan (2009). "Mechanism for Activation of the EGF Receptor Catalytic Domain by the Juxtamembrane Segment." Cell **137**(7): 1293-1307.

Kannan, B., L. Guo, T. Sudhaharan, S. Ahmed, I. Maruyama and T. Wohland (2007). "Spatially resolved total internal reflection fluorescence correlation microscopy using an electron multiplying charge-coupled device camera." Anal Chem **79**(12): 4463-4470.

Kannan, B., J. Y. Har, P. Liu, I. Maruyama, J. L. Ding and T. Wohland (2006). "Electron multiplying charge-coupled device camera based fluorescence correlation spectroscopy." Anal Chem **78**(10): 3444-3451.

Kanno, D. M. and M. Levitus (2014). "Protein oligomerization equilibria and kinetics investigated by fluorescence correlation spectroscopy: a mathematical treatment." J Phys Chem B **118**(43): 12404-12415.

Kapanidis, A. N., N. K. Lee, T. A. Laurence, S. Doose, E. Margeat and S. Weiss (2004). "Fluorescence-aided molecule sorting: analysis of structure and interactions by alternating-laser excitation of single molecules." Proc Natl Acad Sci U S A **101**(24): 8936-8941.

Kapusta, P., M. Wahl, A. Benda, M. Hof and J. Enderlein (2007). "Fluorescence lifetime correlation spectroscopy." J Fluoresc **17**(1): 43-48.

Kask, P., K. Palo, N. Fay, L. Brand, U. Mets, D. Ullmann, J. Jungmann, J. Pschorr and K. Gall (2000). "Two-dimensional fluorescence intensity distribution analysis: theory and applications." Biophysical Journal **78**(4): 1703-1713.

Keppler, A., S. Gendreizig, T. Gronemeyer, H. Pick, H. Vogel and K. Johnsson (2003). "A general method for the covalent labeling of fusion proteins with small molecules in vivo." Nat Biotechnol **21**(1): 86-89.

King, A. C. and P. Cuatrecasas (1982). "Resolution of high and low affinity epidermal growth factor receptors. Inhibition of high affinity component by low temperature, cycloheximide, and phorbol esters." J Biol Chem **257**(6): 3053-3060.

Kiuchi, T., E. Ortiz-Zapater, J. Monypenny, D. R. Matthews, L. K. Nguyen, J. Barbeau, O. Coban, K. Lawler, B. Burford, D. J. Rolfe, E. de Rinaldis, D. Dafou, M. A. Simpson, N. Woodman, S. Pinder, C. E. Gillett, V. Devauges, S. P. Poland, G. Fruhwirth, P. Marra, Y. L. Boersma, A. Pluckthun, W. J. Gullick, Y. Yarden, G. Santis, M. Winn, B. N. Kholodenko, M. L. Martin-Fernandez, P. Parker, A. Tutt, S. M. Ameer-Beg and T. Ng (2014). "The ErbB4 CYT2 variant protects EGFR from ligand-induced degradation to enhance cancer cell motility." Sci Signal **7**(339): ra78.

Klapper, L. N., M. H. Kirschbaum, M. Sela and Y. Yarden (2000). "Biochemical and clinical implications of the ErbB/HER signaling network of growth factor receptors." Advances in Cancer Research, Vol 77 **77**: 25-79.

Klein, P., D. Mattoon, M. A. Lemmon and J. Schlessinger (2004). "A structure-based model for ligand binding and dimerization of EGF receptors." Proceedings of the National Academy of Sciences of the United States of America **101**(4): 929-934.

Kluba, M., Y. Engelborghs, J. Hofkens and H. Mizuno (2015). "Inhibition of Receptor Dimerization as a Novel Negative Feedback Mechanism of EGFR Signaling." PLoS ONE **10**(10): e0139971.

Kobayashi, S., T. J. Boggon, T. Dayaram, P. A. Janne, O. Kocher, M. Meyerson, B. E. Johnson, M. J. Eck, D. G. Tenen and B. Halmos (2005). "EGFR mutation and resistance of non-small-cell lung cancer to gefitinib." N Engl J Med **352**(8): 786-792.

Kohl, T., E. Haustein and P. Schwille (2005). "Determining protease activity in vivo by fluorescence cross-correlation analysis." Biophysical Journal **89**(4): 2770-2782.

Koppel, D. E. (1974). "Statistical accuracy in fluorescence correlation spectroscopy." Physical Review A **10**(6): 1938-1945.

Kraft, M. L. and H. A. Klitzing (2014). "Imaging lipids with secondary ion mass spectrometry." Biochimica et Biophysica Acta (BBA) - Molecular and Cell Biology of Lipids **1841**(8): 1108-1119.

Krall, J. A., E. M. Beyer and G. MacBeath (2011). "High- and low-affinity epidermal growth factor receptor-ligand interactions activate distinct signaling pathways." PLoS One **6**(1): e15945.

Kreder, R., K. A. Pyrshev, Z. Darwich, O. A. Kucherak, Y. Mely and A. S. Klymchenko (2015). "Solvatochromic Nile Red probes with FRET quencher reveal lipid order heterogeneity in living and apoptotic cells." ACS Chem Biol **10**(6): 1435-1442.

Kremers, G. J., S. G. Gilbert, P. J. Cranfill, M. W. Davidson and D. W. Piston (2011). "Fluorescent proteins at a glance." J Cell Sci **124**(Pt 2): 157-160.

Kusumi, A., I. Koyama-Honda and K. Suzuki (2004). "Molecular dynamics and interactions for creation of stimulation-induced stabilized rafts from small unstable steady-state rafts." Traffic **5**(4): 213-230.

Kusumi, A. and K. Suzuki (2005). "Toward understanding the dynamics of membrane-raft-based molecular interactions." Biochimica et Biophysica Acta (BBA) - Molecular Cell Research **1746**(3): 234-251.

Lajoie, P., E. A. Partridge, G. Guay, J. G. Goetz, J. Pawling, A. Lagana, B. Joshi, J. W. Dennis and I. R. Nabi (2007). "Plasma membrane domain organization regulates EGFR signaling in tumor cells." J Cell Biol **179**(2): 341-356.

Lange, Y. (1991). "Disposition of intracellular cholesterol in human fibroblasts." J Lipid Res **32**(2): 329-339.

Lee, N. K., A. N. Kapanidis, Y. Wang, X. Michalet, J. Mukhopadhyay, R. H. Ebright and S. Weiss (2005). "Accurate FRET measurements within single diffusing biomolecules using alternating-laser excitation." Biophys J **88**(4): 2939-2953.

Lemmon, M. A. and J. Schlessinger (2010). "Cell signaling by receptor tyrosine kinases." Cell **141**(7): 1117-1134.

Levi-Montalcini, R. and S. Cohen (1960). "Effects of the extract of the mouse submaxillary salivary glands on the sympathetic system of mammals." Ann N Y Acad Sci **85**: 324-341.

Li, Y., J. Macdonald-Obermann, C. Westfall, D. Piwnica-Worms and L. J. Pike (2012). "Quantitation of the Effect of ErbB2 on Epidermal Growth Factor Receptor Binding and Dimerization." The Journal of Biological Chemistry **287**(37): 31116-31125.

Lidke, D. S., P. Nagy, B. G. Barisas, R. Heintzmann, J. N. Post, K. A. Lidke, A. H. Clayton, D. J. Arndt-Jovin and T. M. Jovin (2003). "Imaging molecular interactions in cells by dynamic and static fluorescence anisotropy (rFLIM and emFRET)." Biochem Soc Trans **31**(Pt 5): 1020-1027.

Lin, S. Y., K. Makino, W. Xia, A. Matin, Y. Wen, K. Y. Kwong, L. Bourguignon and M. C. Hung (2001). "Nuclear localization of EGF receptor and its potential new role as a transcription factor." Nat Cell Biol **3**(9): 802-808.

Liu, P., T. Sudhaharan, R. M. Koh, L. C. Hwang, S. Ahmed, I. N. Maruyama and T. Wohland (2007). "Investigation of the dimerization of proteins from the epidermal growth factor receptor family by single wavelength fluorescence cross-correlation spectroscopy." Biophys J **93**(2): 684-698.

Liu, P., T. Sudhaharan, R. M. L. Koh, L. C. Hwang, S. Ahmed, I. N. Maruyama and T. Wohland (2007). "Investigation of the Dimerization of Proteins from the Epidermal Growth Factor Receptor Family by Single Wavelength Fluorescence Cross-Correlation Spectroscopy." Biophysical Journal **93**(2): 684-698.

London, E. and D. A. Brown (2000). "Insolubility of lipids in triton X-100: physical origin and relationship to sphingolipid/cholesterol membrane domains (rafts)." Biochim Biophys Acta **1508**(1-2): 182-195.

Low-Nam, S. T., K. A. Lidke, P. J. Cutler, R. C. Roovers, P. M. P. Van Bergen En Henegouwen, B. S. Wilson and D. S. Lidke (2011). "ErbB1 dimerization is promoted

by domain co-confinement and stabilized by ligand binding." Nature Structural and Molecular Biology **18**(11): 1244-1249.

Ma, X., S. Ahmed and T. Wohland (2011). "EGFR activation monitored by SW-FCCS in live cells." Front Biosci (Elite Ed) **3**: 22-32.

Macdonald-Obermann, J. L. and L. J. Pike (2009). "The intracellular juxtamembrane domain of the epidermal growth factor (EGF) receptor is responsible for the allosteric regulation of EGF binding." J Biol Chem **284**(20): 13570-13576.

Macdonald, J. L. and L. J. Pike (2008). "Heterogeneity in EGF-binding affinities arises from negative cooperativity in an aggregating system." Proc Natl Acad Sci U S A **105**(1): 112-117.

Machan, R., P. Kapusta and M. Hof (2014). "Statistical filtering in fluorescence microscopy and fluorescence correlation spectroscopy." Anal Bioanal Chem **406**(20): 4797-4813.

Magde, D., E. Elson and W. W. Webb (1972). "Thermodynamic fluctuations in a reacting system—measurement by fluorescence correlation spectroscopy." Physical Review Letters **29**(11): 705.

Magde, D., W. W. Webb and E. L. Elson (1978). "Fluorescence correlation spectroscopy. III. Uniform translation and laminar flow." Biopolymers **17**(2): 361-376.

Margolis, B. and E. Y. Skolnik (1994). "Activation of Ras by receptor tyrosine kinases." J Am Soc Nephrol **5**(6): 1288-1299.

Martin-Fernandez, M., D. T. Clarke, M. J. Tobin, S. V. Jones and G. R. Jones (2002). "Preformed Oligomeric Epidermal Growth Factor Receptors Undergo an Ectodomain Structure Change during Signaling." Biophysical Journal **82**(5): 2415-2427.

Maruyama, I. N. (2014). "Mechanisms of Activation of Receptor Tyrosine Kinases: Monomers or Dimers." Cells **3**(2): 304-330.

Masui, H., L. Castro and J. Mendelsohn (1993). "Consumption of EGF by A431 cells: evidence for receptor recycling." J Cell Biol **120**(1): 85-93.

Mattoon, D., P. Klein, M. A. Lemmon, I. Lax and J. Schlessinger (2004). "The tethered configuration of the EGF receptor extracellular domain exerts only a limited control of receptor function." Proceedings of the National Academy of Sciences of the United States of America **101**(4): 923-928.

Mayawala, K., D. G. Vlachos and J. S. Edwards (2005). "Heterogeneities in EGF receptor density at the cell surface can lead to concave up scatchard plot of EGF binding." FEBS Letters **579**(14): 3043-3047.

McIntosh, D. P., X. Y. Tan, P. Oh and J. E. Schnitzer (2002). "Targeting endothelium and its dynamic caveolae for tissue-specific transcytosis in vivo: a pathway to overcome cell barriers to drug and gene delivery." Proc Natl Acad Sci U S A **99**(4): 1996-2001.

McLaughlin, S., S. O. Smith, M. J. Hayman and D. Murray (2005). "An electrostatic engine model for autoinhibition and activation of the epidermal growth factor receptor (EGFR/ErbB) family." J Gen Physiol **126**(1): 41-53.

Meseth, U., T. Wohland, R. Rigler and H. Vogel (1999). "Resolution of fluorescence correlation measurements." Biophysical Journal **76**(3): 1619-1631.

Mets, Ü. and R. Rigler (1994). "Submillisecond detection of single rhodamine molecules in water." Journal of Fluorescence **4**(3): 259-264.

Metzler, R., J. H. Jeon and A. G. Cherstvy (2016). "Non-Brownian diffusion in lipid membranes: Experiments and simulations." Biochimica et Biophysica Acta (BBA) - Biomembranes **1858**(10): 2451-2467.

Moriki, T., H. Maruyama and I. N. Maruyama (2001). "Activation of preformed EGF receptor dimers by ligand-induced rotation of the transmembrane domain." Journal of Molecular Biology **311**(5): 1011-1026.

Motley, A., N. A. Bright, M. N. Seaman and M. S. Robinson (2003). "Clathrin-mediated endocytosis in AP-2-depleted cells." J Cell Biol **162**(5): 909-918.

Müller, B. K., E. Zaychikov, C. Bräuchle and D. C. Lamb (2005). "Pulsed Interleaved Excitation." Biophysical Journal **89**(5): 3508-3522.

Müller, J. D., Y. Chen and E. Gratton (2000). "Resolving heterogeneity on the single molecular level with the photon-counting histogram." Biophysical Journal **78**(1): 474-486.

Murata, M., J. Peranen, R. Schreiner, F. Wieland, T. V. Kurzchalia and K. Simons (1995). "VIP21/caveolin is a cholesterol-binding protein." Proc Natl Acad Sci U S A **92**(22): 10339-10343.

Nagy, P., J. Claus, T. M. Jovin and D. J. Arndt-Jovin (2010). "Distribution of resting and ligand-bound ErbB1 and ErbB2 receptor tyrosine kinases in living cells using number and brightness analysis." Proceedings of the National Academy of Sciences of the United States of America **107**(38): 16524-16529.

Nagy, P., G. Vereb, Z. Sebestyen, G. Horvath, S. J. Lockett, S. Damjanovich, J. W. Park, T. M. Jovin and J. Szollosi (2002). "Lipid rafts and the local density of ErbB proteins influence the biological role of homo- and heteroassociations of ErbB2." J Cell Sci **115**(Pt 22): 4251-4262.

Nair, P. (2005). "Epidermal growth factor receptor family and its role in cancer progression." Current Science **88**(6): 890-898.

Needham, S. R., M. Hirsch, D. J. Rolfe, D. T. Clarke, L. C. Zanetti-Domingues, R. Wareham and M. L. Martin-Fernandez (2013). "Measuring EGFR separations on cells

with ~10 nm resolution via fluorophore localization imaging with photobleaching." PLoS One **8**(5): e62331.

Needham, S. R., S. K. Roberts, A. Arkhipov, V. P. Mysore, C. J. Tynan, L. C. Zanetti-Domingues, E. T. Kim, V. Losasso, D. Korovesis, M. Hirsch, D. J. Rolfe, D. T. Clarke, M. D. Winn, A. Lajevardipour, A. H. Clayton, L. J. Pike, M. Perani, P. J. Parker, Y. Shan, D. E. Shaw and M. L. Martin-Fernandez (2016). "EGFR oligomerization organizes kinase-active dimers into competent signalling platforms." Nat Commun **7**: 13307.

Needham, S. R., L. C. Zanetti-Domingues, M. Hirsch, D. J. Rolfe, C. J. Tynan, S. K. Roberts, M. L. Martin-Fernandez and D. T. Clarke (2014). "Structure-function relationships and supramolecular organization of the EGFR (epidermal growth factor receptor) on the cell surface." Biochem Soc Trans **42**(1): 114-119.

Needham, S. R., L. C. Zanetti-Domingues, K. M. Scherer, M. Hirsch, D. J. Rolfe, S. K. Roberts, M. L. Martin-Fernandez, D. T. Clarke and C. J. Tynan (2015). "Determining the geometry of oligomers of the human epidermal growth factor family on cells with <10 nm resolution." Biochem Soc Trans **43**(3): 309-314.

Nishijo, J., S. Moriyama and S. Shiota (2003). "Interactions of cholesterol with cyclodextrins in aqueous solution." Chem Pharm Bull (Tokyo) **51**(11): 1253-1257.

Ogiso, H., R. Ishitani, O. Nureki, S. Fukai, M. Yamanaka, J.-H. Kim, K. Saito, A. Sakamoto, M. Inoue, M. Shirouzu and S. Yokoyama (2002). "Crystal Structure of the Complex of Human Epidermal Growth Factor and Receptor Extracellular Domains." Cell **110**(6): 775-787.

Okabe, T., I. Okamoto, K. Tamura, M. Terashima, T. Yoshida, T. Satoh, M. Takada, M. Fukuoka and K. Nakagawa (2007). "Differential constitutive activation of the epidermal growth factor receptor in non-small cell lung cancer cells bearing EGFR gene mutation and amplification." Cancer Res **67**(5): 2046-2053.

Oksvold, M. P., E. Skarpen, B. Lindeman, N. Roos and H. S. Huitfeldt (2000). "Immunocytochemical localization of Shc and activated EGF receptor in early endosomes after EGF stimulation of HeLa cells." J Histochem Cytochem **48**(1): 21-33.

Olson, E., R. Torres and M. J. Levene (2013). "Integrated fluorescence correlation spectroscopy device for point-of-care clinical applications." Biomedical Optics Express **4**(7): 1074-1082.

Orr, G., D. Hu, S. Özçelik, L. K. Opresko, H. Steven Wiley and S. D. Colson (2005). "Cholesterol Dictates the Freedom of EGF Receptors and HER2 in the Plane of the Membrane." Biophysical Journal **89**(2): 1362-1373.

Orr, G., D. Hu, S. Özçelik, L. K. Opresko, H. S. Wiley and S. D. Colson (2005). "Cholesterol Dictates the Freedom of EGF Receptors and HER2 in the Plane of the Membrane." Biophysical Journal **89**(2): 1362-1373.

Orth, J. D., E. W. Krueger, S. G. Weller and M. A. McNiven (2006). "A novel endocytic mechanism of epidermal growth factor receptor sequestration and internalization." Cancer Res **66**(7): 3603-3610.

Orth, J. D. and M. A. McNiven (2006). "Get off my back! Rapid receptor internalization through circular dorsal ruffles." Cancer research **66**(23): 11094-11096.

Oura, M., J. Yamamoto, H. Ishikawa, S. Mikuni, R. Fukushima and M. Kinjo (2016). "Polarization-dependent fluorescence correlation spectroscopy for studying structural properties of proteins in living cell." Scientific Reports **6**: 31091.

Padfield, E., H. P. Ellis and K. M. Kurian (2015). "Current Therapeutic Advances Targeting EGFR and EGFRvIII in Glioblastoma." Front Oncol **5**: 5.

Padilla-Parra, S., N. Auduge, M. Coppey-Moisan and M. Tramier (2011). "Dual-color fluorescence lifetime correlation spectroscopy to quantify protein-protein interactions in live cell." Microsc Res Tech **74**(8): 788-793.

Palo, K., L. Brand, C. Eggeling, S. Jäger, P. Kask and K. Gall (2002). "Fluorescence intensity and lifetime distribution analysis: toward higher accuracy in fluorescence fluctuation spectroscopy." Biophysical Journal **83**(2): 605-618.

Pan, X., W. Foo, W. Lim, M. H. Fok, P. Liu, H. Yu, I. Maruyama and T. Wohland (2007). "Multifunctional fluorescence correlation microscope for intracellular and microfluidic measurements." Rev Sci Instrum **78**(5): 053711.

Pao, W., V. A. Miller, K. A. Politi, G. J. Riely, R. Somwar, M. F. Zakowski, M. G. Kris and H. Varmus (2005). "Acquired resistance of lung adenocarcinomas to gefitinib or erlotinib is associated with a second mutation in the EGFR kinase domain." PLoS Med **2**(3): e73.

Peres, C., A. Yart, B. Perret, J. P. Salles and P. Raynal (2003). "Modulation of phosphoinositide 3-kinase activation by cholesterol level suggests a novel positive role for lipid rafts in lysophosphatidic acid signalling." FEBS Lett **534**(1-3): 164-168.

Pike, L. J. (2003). "Lipid rafts: bringing order to chaos." J Lipid Res **44**(4): 655-667.

Pike, L. J. (2005). "Growth factor receptors, lipid rafts and caveolae: an evolving story." Biochim Biophys Acta **1746**(3): 260-273.

Pike, L. J. and L. Casey (2002). "Cholesterol levels modulate EGF receptor-mediated signaling by altering receptor function and trafficking." Biochemistry **41**(32): 10315-10322.

Pike, L. J., X. Han and R. W. Gross (2005). "Epidermal growth factor receptors are localized to lipid rafts that contain a balance of inner and outer leaflet lipids: a shotgun lipidomics study." J Biol Chem **280**(29): 26796-26804.

Pike, L. J. and J. M. Miller (1998). "Cholesterol depletion delocalizes phosphatidylinositol bisphosphate and inhibits hormone-stimulated phosphatidylinositol turnover." J Biol Chem **273**(35): 22298-22304.

Pillay, V., L. Allaf, A. L. Wilding, J. F. Donoghue, N. W. Court, S. A. Greenall, A. M. Scott and T. G. Johns (2009). "The plasticity of oncogene addiction: implications for targeted therapies directed to receptor tyrosine kinases." Neoplasia **11**(5): 448-458, 442 p following 458.

Polozov, I. V. and K. Gawrisch (2006). "Characterization of the liquid-ordered state by proton MAS NMR." Biophys J **90**(6): 2051-2061.

Pralle, A., P. Keller, E. L. Florin, K. Simons and J. K. Horber (2000). "Sphingolipid-cholesterol rafts diffuse as small entities in the plasma membrane of mammalian cells." J Cell Biol **148**(5): 997-1008.

Predescu, S. A., D. N. Predescu and A. B. Malik (2007). "Molecular determinants of endothelial transcytosis and their role in endothelial permeability." Am J Physiol Lung Cell Mol Physiol **293**(4): L823-842.

Prenzel, N., E. Zwick, H. Daub, M. Leserer, R. Abraham, C. Wallasch and A. Ullrich (1999). "EGF receptor transactivation by G-protein-coupled receptors requires metalloproteinase cleavage of proHB-EGF." Nature **402**(6764): 884-888.

Qian, X., C. M. LeVea, J. K. Freeman, W. C. Dougall and M. I. Greene (1994). "Heterodimerization of epidermal growth factor receptor and wild-type or kinase-deficient Neu: a mechanism of interreceptor kinase activation and transphosphorylation." Proc Natl Acad Sci U S A **91**(4): 1500-1504.

Red Brewer, M., S. H. Choi, D. Alvarado, K. Moravcevic, A. Pozzi, M. A. Lemmon and G. Carpenter (2009). "The juxtamembrane region of the EGF receptor functions as an activation domain." Mol Cell **34**(6): 641-651.

Rees, A. R., M. Gregoriou, P. Johnson and P. B. Garland (1984). "High affinity epidermal growth factor receptors on the surface of A431 cells have restricted lateral diffusion." Embo j **3**(8): 1843-1847.

Reiter, J. L., D. W. Threadgill, G. D. Eley, K. E. Strunk, A. J. Danielsen, C. S. Sinclair, R. S. Pearsall, P. J. Green, D. Yee, A. L. Lampland, S. Balasubramaniam, T. D. Crossley, T. R. Magnuson, C. D. James and N. J. Maihle (2001). "Comparative genomic sequence analysis and isolation of human and mouse alternative EGFR transcripts encoding truncated receptor isoforms." Genomics **71**(1): 1-20.

Resat, H., J. A. Ewald, D. A. Dixon and H. S. Wiley (2003). "An Integrated Model of Epidermal Growth Factor Receptor Trafficking and Signal Transduction." Biophysical Journal **85**(2): 730-743.

Ries, J., S. Chiantia and P. Schwille (2009). "Accurate Determination of Membrane Dynamics with Line-Scan FCS." Biophysical Journal **96**(5): 1999-2008.

Rigby, A. C., C. W. Grant and G. S. Shaw (1998). "Solution and solid state conformation of the human EGF receptor transmembrane region." Biochim Biophys Acta **1371**(2): 241-253.

Rigler, R., Ü. Mets, J. Widengren and P. Kask (1993). "Fluorescence correlation spectroscopy with high count rate and low background: analysis of translational diffusion." European Biophysics Journal **22**(3): 169-175.

Ringerike, T., F. D. Blystad, F. O. Levy, I. H. Madshus and E. Stang (2002). "Cholesterol is important in control of EGF receptor kinase activity but EGF receptors are not concentrated in caveolae." J Cell Sci **115**(Pt 6): 1331-1340.

Roepstorff, K., L. Grøvdal, M. Grandal, M. Lerdrup and B. van Deurs (2008). "Endocytic downregulation of ErbB receptors: mechanisms and relevance in cancer." Histochemistry and Cell Biology **129**(5): 563-578.

Roepstorff, K., P. Thomsen, K. Sandvig and B. van Deurs (2002). "Sequestration of epidermal growth factor receptors in non-caveolar lipid rafts inhibits ligand binding." J Biol Chem **277**(21): 18954-18960.

Saffarian, S., Y. Li, E. L. Elson and L. J. Pike (2007). "Oligomerization of the EGF Receptor Investigated by Live Cell Fluorescence Intensity Distribution Analysis." Biophysical Journal **93**(3): 1021-1031.

Saffarian, S., Y. Li, E. L. Elson and L. J. Pike (2007). "Oligomerization of the EGF receptor investigated by live cell fluorescence intensity distribution analysis." Biophys J **93**(3): 1021-1031.

Saito, T., S. Okada, K. Ohshima, E. Yamada, M. Sato, Y. Uehara, H. Shimizu, J. E. Pessin and M. Mori (2004). "Differential activation of epidermal growth factor (EGF) receptor downstream signaling pathways by betacellulin and EGF." Endocrinology **145**(9): 4232-4243.

Sako, Y., S. Minoghchi and T. Yanagida (2000). "Single-molecule imaging of EGFR signalling on the surface of living cells." Nat Cell Biol **2**(3): 168-172.

Sankaran, J., N. Bag, R. S. Kraut and T. Wohland (2013). "Accuracy and precision in camera-based fluorescence correlation spectroscopy measurements." Anal Chem **85**(8): 3948-3954.

Sankaran, J., M. Manna, L. Guo, R. Kraut and T. Wohland (2009). "Diffusion, transport, and cell membrane organization investigated by imaging fluorescence cross-correlation spectroscopy." Biophys J **97**(9): 2630-2639.

Sankaran, J., X. Shi, L. Y. Ho, E. H. Stelzer and T. Wohland (2010). "ImFCS: a software for imaging FCS data analysis and visualization." Opt Express **18**(25): 25468-25481.

Sarabipour, S. and K. Hristova (2015). "FGFR3 Unliganded Dimer Stabilization by the Juxtamembrane Domain." Journal of Molecular Biology **427**(8): 1705-1714.

Sasaki, T., K. Hiroki and Y. Yamashita (2013). "The role of epidermal growth factor receptor in cancer metastasis and microenvironment." Biomed Res Int **2013**: 546318.

Schindelin, J., I. Arganda-Carreras, E. Frise, V. Kaynig, M. Longair, T. Pietzsch, S. Preibisch, C. Rueden, S. Saalfeld, B. Schmid, J.-Y. Tinevez, D. J. White, V. Hartenstein, K. Eliceiri, P. Tomancak and A. Cardona (2012). "Fiji: an open-source platform for biological-image analysis." Nat Meth **9**(7): 676-682.

Schlessinger, J. (2002). "Ligand-Induced, Receptor-Mediated Dimerization and Activation of EGF Receptor." Cell **110**(6): 669-672.

Schneider, M. R. and E. Wolf (2009). "The epidermal growth factor receptor ligands at a glance." J Cell Physiol **218**(3): 460-466.

Schulze, W. X., L. Deng and M. Mann (2005). "Phosphotyrosine interactome of the ErbB-receptor kinase family." Molecular Systems Biology **1**: 2005.0008-2005.0008.

Schwille, P., F. J. Meyer-Almes and R. Rigler (1997). "Dual-color fluorescence cross-correlation spectroscopy for multicomponent diffusional analysis in solution." Biophysical Journal **72**(4): 1878-1886.

Sequist, L. V., B. A. Waltman, D. Dias-Santagata, S. Digumarthy, A. B. Turke, P. Fidias, K. Bergethon, A. T. Shaw, S. Gettinger, A. K. Cosper, S. Akhavanfard, R. S. Heist, J. Temel, J. G. Christensen, J. C. Wain, T. J. Lynch, K. Vernovsky, E. J. Mark, M. Lanuti, A. J. Iafrate, M. Mino-Kenudson and J. A. Engelman (2011). "Genotypic and histological evolution of lung cancers acquiring resistance to EGFR inhibitors." Sci Transl Med **3**(75): 75ra26.

Seshacharyulu, P., M. P. Ponnusamy, D. Haridas, M. Jain, A. K. Ganti and S. K. Batra (2012). "Targeting the EGFR signaling pathway in cancer therapy." Expert Opin Ther Targets **16**(1): 15-31.

Shaner, N. C., M. Z. Lin, M. R. McKeown, P. A. Steinbach, K. L. Hazelwood, M. W. Davidson and R. Y. Tsien (2008). "Improving the photostability of bright monomeric orange and red fluorescent proteins." Nat Methods **5**(6): 545-551.

Shi, F., S. E. Telesco, Y. Liu, R. Radhakrishnan and M. A. Lemmon (2010). "ErbB3/HER3 intracellular domain is competent to bind ATP and catalyze autophosphorylation." Proceedings of the National Academy of Sciences of the United States of America **107**(17): 7692-7697.

Siegelin, M. D. and A. C. Borczuk (2014). "Epidermal growth factor receptor mutations in lung adenocarcinoma." Lab Invest **94**(2): 129-137.

Sigismund, S., E. Argenzio, D. Tosoni, E. Cavallaro, S. Polo and P. P. Di Fiore (2008). "Clathrin-mediated internalization is essential for sustained EGFR signaling but dispensable for degradation." Dev Cell **15**(2): 209-219.

Sigismund, S., T. Woelk, C. Puri, E. Maspero, C. Tacchetti, P. Transidico, P. P. Di Fiore and S. Polo (2005). "Clathrin-independent endocytosis of ubiquitinated cargos." Proc Natl Acad Sci U S A **102**(8): 2760-2765.

Silvius, J. R., D. del Giudice and M. Lafleur (1996). "Cholesterol at different bilayer concentrations can promote or antagonize lateral segregation of phospholipids of differing acyl chain length." Biochemistry **35**(48): 15198-15208.

Simons, K. and E. Ikonen (1997). "Functional rafts in cell membranes." Nature **387**(6633): 569-572.

Simons, K. and E. Ikonen (2000). "How cells handle cholesterol." Science **290**(5497): 1721-1726.

Simons, K. and G. van Meer (1988). "Lipid sorting in epithelial cells." Biochemistry **27**(17): 6197-6202.

Singer, S. J. and G. L. Nicolson (1972). "The fluid mosaic model of the structure of cell membranes." Science **175**(4023): 720-731.

Singh, A. P., J. W. Krieger, J. Buchholz, E. Charbon, J. Langowski and T. Wohland (2013). "The performance of 2D array detectors for light sheet based fluorescence correlation spectroscopy." Opt Express **21**(7): 8652-8668.

Sizeland, A. M. and A. W. Burgess (1992). "Anti-sense transforming growth factor alpha oligonucleotides inhibit autocrine stimulated proliferation of a colon carcinoma cell line." Mol Biol Cell **3**(11): 1235-1243.

Slieker, L. J., T. M. Martensen and M. D. Lane (1986). "Synthesis of epidermal growth factor receptor in human A431 cells. Glycosylation-dependent acquisition of ligand binding activity occurs post-translationally in the endoplasmic reticulum." J Biol Chem **261**(32): 15233-15241.

Songtawee, N., D. R. Bevan and K. Choowongkomon (2015). "Molecular dynamics of the asymmetric dimers of EGFR: simulations on the active and inactive conformations of the kinase domain." J Mol Graph Model **58**: 16-29.

Sorkin, A., S. Krolenko, N. Kudrjavtceva, J. Lazebnik, L. Teslenko, A. M. Soderquist and N. Nikolsky (1991). "Recycling of epidermal growth factor-receptor complexes in A431 cells: identification of dual pathways." J Cell Biol **112**(1): 55-63.

Sorokin, A., M. A. Lemmon, A. Ullrich and J. Schlessinger (1994). "Stabilization of an active dimeric form of the epidermal growth factor receptor by introduction of an inter-receptor disulfide bond." J Biol Chem **269**(13): 9752-9759.

Sun, G., M. Guo, C. Teh, V. Korzh, M. Bathe and T. Wohland (2015). "Bayesian Model Selection Applied to the Analysis of Fluorescence Correlation Spectroscopy Data of Fluorescent Proteins in Vitro and in Vivo." Analytical chemistry **87**(8): 4326-4333.

Swift, J. L., M. C. Burger, D. Massotte, T. E. Dahms and D. T. Cramb (2007). "Two-photon excitation fluorescence cross-correlation assay for ligand-receptor binding: cell membrane nanopatches containing the human micro-opioid receptor." Anal Chem **79**(17): 6783-6791.

Swift, J. L., A. G. Godin, K. Dore, L. Freland, N. Bouchard, C. Nimmo, M. Sergeev, Y. De Koninck, P. W. Wiseman and J. M. Beaulieu (2011). "Quantification of receptor tyrosine kinase transactivation through direct dimerization and surface density measurements in single cells." Proc Natl Acad Sci U S A **108**(17): 7016-7021.

Szabo, A., G. Horvath, J. Szollosi and P. Nagy (2008). "Quantitative characterization of the large-scale association of ErbB1 and ErbB2 by flow cytometric homo-FRET measurements." Biophys J **95**(4): 2086-2096.

Tanos, B. and E. Rodriguez-Boulan (2008). "The epithelial polarity program: machineries involved and their hijacking by cancer." Oncogene **27**(55): 6939-6957.

Tao, R. H. and I. N. Maruyama (2008). "All EGF(ErbB) receptors have preformed homo- and heterodimeric structures in living cells." Journal of Cell Science **121**(19): 3207-3217.

Thiel, K. W. and G. Carpenter (2007). "Epidermal growth factor receptor juxtamembrane region regulates allosteric tyrosine kinase activation." Proc Natl Acad Sci U S A **104**(49): 19238-19243.

Tong, J., P. Taylor, E. Jovceva, J. R. St-Germain, L. L. Jin, A. Nikolic, X. Gu, Z. H. Li, S. Trudel and M. F. Moran (2008). "Tandem immunoprecipitation of phosphotyrosine-mass spectrometry (TIPY-MS) indicates C19ORF19 becomes tyrosine-phosphorylated and associated with activated epidermal growth factor receptor." J Proteome Res **7**(3): 1067-1077.

Toral, C., C. Solano-Agama, B. Reyes-Marquez, M. Sabanero, P. Talamas, M. Gonzalez del Pliego and M. E. Mendoza-Garrido (2007). "Role of extracellular matrix-cell interaction and epidermal growth factor (EGF) on EGF-receptors and actin cytoskeleton arrangement in infantile pituitary cells." Cell Tissue Res **327**(1): 143-153.

Torres, R., J. R. Genzen and M. J. Levene (2012). "Clinical measurement of von Willebrand factor by fluorescence correlation spectroscopy." Clin Chem **58**(6): 1010-1018.

Tsuda, T., Y. Ikeda and N. Taniguchi (2000). "The Asn-420-linked sugar chain in human epidermal growth factor receptor suppresses ligand-independent spontaneous oligomerization. Possible role of a specific sugar chain in controllable receptor activation." J Biol Chem **275**(29): 21988-21994.

Ullrich, A. and J. Schlessinger (1990). "Signal transduction by receptors with tyrosine kinase activity." Cell **61**(2): 203-212.

Unruh, J. R. and E. Gratton (2008). "Analysis of molecular concentration and brightness from fluorescence fluctuation data with an electron multiplied CCD camera." Biophys J **95**(11): 5385-5398.

Valley, C. C., K. A. Lidke and D. S. Lidke (2014). "The spatiotemporal organization of ErbB receptors: insights from microscopy." Cold Spring Harb Perspect Biol **6**(2).

Valley, C. C., K. A. Lidke and D. S. Lidke (2014). "The spatiotemporal organization of ErbB receptors: Insights from microscopy." Cold Spring Harbor Perspectives in Biology **6**(2).

van Meer, G. (2005). "Cellular lipidomics." Embo j **24**(18): 3159-3165.

van Meer, G. (2011). "Dynamic transbilayer lipid asymmetry." Cold Spring Harb Perspect Biol **3**(5).

van Meer, G., D. R. Voelker and G. W. Feigenson (2008). "Membrane lipids: where they are and how they behave." Nat Rev Mol Cell Biol **9**(2): 112-124.

Varma, R. and S. Mayor (1998). "GPI-anchored proteins are organized in submicron domains at the cell surface." Nature **394**(6695): 798-801.

Verkleij, A. J., R. F. Zwaal, B. Roelofsen, P. Comfurius, D. Kastelijn and L. L. van Deenen (1973). "The asymmetric distribution of phospholipids in the human red cell membrane. A combined study using phospholipases and freeze-etch electron microscopy." Biochim Biophys Acta **323**(2): 178-193.

Wada, T., X. L. Qian and M. I. Greene (1990). "Intermolecular association of the p185neu protein and EGF receptor modulates EGF receptor function." Cell **61**(7): 1339-1347.

Walker, F., S. G. Orchard, R. N. Jorissen, N. E. Hall, H. H. Zhang, P. A. Hoyne, T. E. Adams, T. G. Johns, C. Ward, T. P. Garrett, H. J. Zhu, M. Nerrie, A. M. Scott, E. C. Nice and A. W. Burgess (2004). "CR1/CR2 interactions modulate the functions of the cell surface epidermal growth factor receptor." J Biol Chem **279**(21): 22387-22398.

Wang, Z., P. A. Longo, M. K. Tarrant, K. Kim, S. Head, D. J. Leahy and P. A. Cole (2011). "Mechanistic insights into the activation of oncogenic forms of EGF receptor." Nat Struct Mol Biol **18**(12): 1388-1393.

Webb, S. E. D., S. K. Roberts, S. R. Needham, C. J. Tynan, D. J. Rolfe, M. D. Winn, D. T. Clarke, R. Barraclough and M. L. Martin-Fernandez (2008). "Single-molecule imaging and fluorescence lifetime imaging microscopy show different structures for high- and low-affinity epidermal growth factor receptors in A431 cells." Biophysical Journal **94**(3): 803-819.

Weidemann, T. (2014). "Application of fluorescence correlation spectroscopy (FCS) to measure the dynamics of fluorescent proteins in living cells." Methods Mol Biol **1076**: 539-555.

Weiß, K., A. Neef, Q. Van, S. Kramer, I. Gregor and J. Enderlein (2013). "Quantifying the Diffusion of Membrane Proteins and Peptides in Black Lipid Membranes with 2-Focus Fluorescence Correlation Spectroscopy." Biophysical Journal **105**(2): 455-462.

Wells, A., J. B. Welsh, C. S. Lazar, H. S. Wiley, G. N. Gill and M. G. Rosenfeld (1990). "Ligand-induced transformation by a noninternalizing epidermal growth factor receptor." Science **247**(4945): 962-964.

Whitson, K. B., S. R. Whitson, M. L. Red-Brewer, A. J. McCoy, A. A. Vitali, F. Walker, T. G. Johns, A. H. Beth and J. V. Staros (2005). "Functional effects of glycosylation at Asn-579 of the epidermal growth factor receptor." Biochemistry **44**(45): 14920-14931.

Widengren, J. (2010). "Fluorescence-based transient state monitoring for biomolecular spectroscopy and imaging." Journal of the Royal Society Interface **7**(49): 1135-1144.

Wiedenmann, J., F. Oswald and G. U. Nienhaus (2009). "Fluorescent proteins for live cell imaging: opportunities, limitations, and challenges." IUBMB Life **61**(11): 1029-1042.

Wilson, K. J., J. L. Gilmore, J. Foley, M. A. Lemmon and D. J. Riese, 2nd (2009). "Functional selectivity of EGF family peptide growth factors: implications for cancer." Pharmacol Ther **122**(1): 1-8.

Wilson, K. J., C. Mill, S. Lambert, J. Buchman, T. R. Wilson, V. Hernandez-Gordillo, R. M. Gallo, L. M. Ades, J. Settleman and D. J. Riese, 2nd (2012). "EGFR ligands exhibit functional differences in models of paracrine and autocrine signaling." Growth Factors **30**(2): 107-116.

Yamashita, H., Y. Yano, K. Kawano and K. Matsuzaki (2015). "Oligomerization–function relationship of EGFR on living cells detected by the coiled-coil labeling and FRET microscopy." Biochimica et Biophysica Acta (BBA) - Biomembranes **1848**(6): 1359-1366.

Yang, T. T., L. Cheng and S. R. Kain (1996). "Optimized codon usage and chromophore mutations provide enhanced sensitivity with the green fluorescent protein." Nucleic Acids Res **24**(22): 4592-4593.

Yarden, Y. and J. Schlessinger (1987). "Self-phosphorylation of epidermal growth factor receptor: evidence for a model of intermolecular allosteric activation." Biochemistry **26**(5): 1434-1442.

Yarden, Y. and M. X. Sliwkowski (2001). "Untangling the ErbB signalling network." Nat Rev Mol Cell Biol **2**(2): 127-137.

Ye, S. X., Y. J. Luo, S. L. Qiao, L. Li, C. H. Liu, J. L. Shi and X. J. An (2016). "[Study of Reaction Dynamics between Bovine Serum Albumin and Folic Acid by Stopped-Flow/Fluorescence]." Guang Pu Xue Yu Guang Pu Fen Xi **36**(1): 134-139.

Yeow, E. K. and A. H. Clayton (2007). "Enumeration of oligomerization states of membrane proteins in living cells by homo-FRET spectroscopy and microscopy: theory and application." Biophys J **92**(9): 3098-3104.

Yu, X., K. D. Sharma, T. Takahashi, R. Iwamoto and E. Mekada (2002). "Ligand-independent dimer formation of epidermal growth factor receptor (EGFR) is a step separable from ligand-induced EGFR signaling." Mol Biol Cell **13**(7): 2547-2557.

Zanetti-Domingues, L. C., M. Hirsch, C. J. Tynan, D. J. Rolfe, T. V. Boyadzhiev, K. M. Scherer, D. T. Clarke, M. L. Martin-Fernandez and S. R. Needham (2015). "Determining the geometry of oligomers of the human epidermal growth factor family on cells with 7 nm resolution." Prog Biophys Mol Biol **118**(3): 139-152.

Zhang, H., A. Berezov, Q. Wang, G. Zhang, J. Drebin, R. Murali and M. I. Greene (2007). "ErbB receptors: from oncogenes to targeted cancer therapies." J Clin Invest **117**(8): 2051-2058.

Zhang, Q., E. Park, K. Kani and R. Landgraf (2012). "Functional isolation of activated and unilaterally phosphorylated heterodimers of ERBB2 and ERBB3 as scaffolds in ligand-dependent signaling." Proc Natl Acad Sci U S A **109**(33): 13237-13242.

Zhang, X., J. Gureasko, K. Shen, P. A. Cole and J. Kuriyan (2006). "An Allosteric Mechanism for Activation of the Kinase Domain of Epidermal Growth Factor Receptor." Cell **125**(6): 1137-1149.

Zhang, X., K. A. Pickin, R. Bose, N. Jura, P. A. Cole and J. Kuriyan (2007). "Inhibition of the EGF receptor by binding of MIG6 to an activating kinase domain interface." Nature **450**(7170): 741-744.

Zhang, Z. Y. and R. L. VanEtten (1991). "Pre-steady-state and steady-state kinetic analysis of the low molecular weight phosphotyrosyl protein phosphatase from bovine heart." J Biol Chem **266**(3): 1516-1525.

Zhu, H. J., J. Iaria, S. Orchard, F. Walker and A. W. Burgess (2003). "Epidermal growth factor receptor: association of extracellular domain negatively regulates intracellular kinase activation in the absence of ligand." Growth Factors **21**(1): 15-30.

Zhuang, L., J. Lin, M. L. Lu, K. R. Solomon and M. R. Freeman (2002). "Cholesterol-rich lipid rafts mediate akt-regulated survival in prostate cancer cells." Cancer Res **62**(8): 2227-2231.

Zwaal, R. F. and A. J. Schroit (1997). "Pathophysiologic implications of membrane phospholipid asymmetry in blood cells." Blood **89**(4): 1121-1132.